Dissertations and Theses

12-2019

Computational Model for Pedestrian Movement and Infectious Diseases Spread During Air Travel: A Molecular Dynamics-Like Numerical Approach

Pierrot Derjany

COMPUTATIONAL MODEL FOR PEDESTRIAN MOVEMENT AND

INFECTIOUS DISEASES SPREAD DURING AIR TRAVEL: A MOLECULAR

DYNAMICS-LIKE NUMERICAL APPROACH

A Dissertation

Submitted to the Faculty

of

Embry-Riddle Aeronautical University

by

Pierrot Derjany

In Partial Fulfillment of the

Requirements for the Degree

of

Doctor of Philosophy in Aerospace Engineering

December 2019

Embry-Riddle Aeronautical University

Daytona Beach, Florida

COMPUTATIONAL MODEL FOR PEDESTRIAN MOVEMENT AND INFECTIOUS DISEASES SPREAD DURING AIR TRAVEL: A MOLECULAR DYNAMICS-LIKE NUMERICAL APPROACH
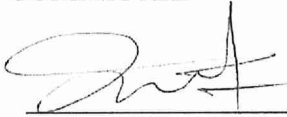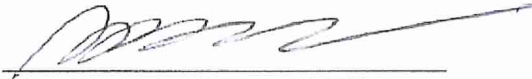
By

Pierrot Derjany

This Dissertation was prepared under the direction of the candidate's Dissertation Committee Chairman, Dr. Sirish Namilae, Department of Aerospace Engineering, and has been approved by the members of the dissertation committee. It was submitted to the Office of the Senior Vice President for Academic Affairs and Provost and was accepted in partial fulfillment of the requirements for the Degree of Doctor of Philosophy in Aerospace Engineering

DISSERTATION COMMITTEE

Chair, Dr. Sirish Namilae

Member, Dr. Virginie Rollin
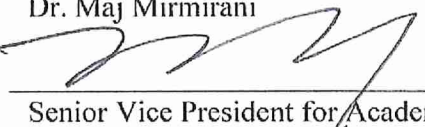
Graduate Program Coordinator,
Dr. Marwan Al-Haik

Dean, College of Engineering,
Dr. Maj Mirmirani

Senior Vice President for Academic
Affairs and Provost,
Dr. Lon D. Moeller

(For Dr. D. Liu)
Member, Dr. Dahai Liu

Member, Dr. Marwan Al-Haik

12-12-19
Date

12/12/2019
Date

12/16/19
Date

DEDICATION

I dedicate this thesis to my family – my wife Shannon Young who has encouraged and inspired me during the challenges of the graduate research –my dear son Patrick who has accompanied me through my last year of Ph.D., my parents Raymond Derjany and Kaly Kanaty for their endless, unconditional support, both morally and financially.

To our VIPRA team who shared their knowledge and advice to achieve this study.

ACKNOWLEDGMENTS

TABLE OF CONTENTS

LIST OF TABLES

LIST OF FIGURES

Figure   Page

Figure   Page

SYMBOLS

a_i	instantaneous acceleration
v_i	instantaneous speed
$\hat{e}_v$	motion direction
$\vec{F}_i$	net resulting force
$\vec{f}_i^{int}$	intention force
$\vec{f}_i^{ped}$	repulsive force
$\vec{f}_{j/i}$	force acting on the particle "i"
$\vec{r}_i$	position vector of particle "i"
$\vec{\nabla}$	gradient
i_c^0	initial infectives
P_a	aerosol exposure and inhalation probability
p_c	infectivity of individual as a function of age of infection
P_d	Coarse pathogen droplet inoculation probability
P_m	pathogen spread mechanism probability component
R_0	reproduction number
R_e	effective reproduction number
$V_{crowd_{min}}$	Crowd sedate footpath
v_{0i}	pedestrian desired free speed
v_A, v_B	speed constants
v_i	pedestrian actual walking speed
γ_i	random number between 0 and 1

ρ_{max}	highly packed crowd density
ρ_{min}	minimum surrounding crowd density
C_a	maximum initial concentration of contagion in aerosol suspension
P_{inf}	infection probability
S_A	exposed mucosa surfaces
S_C	circular area base of the cone
V_C	volume of cone in which droplet can fall
V_o	volume of infection envelope
w_i	frequency of mean
$\bar{x}$	statistical mean
ΔP	difference of momentum
Δt	time step
A	Area
c	days of infection
D	density
d	maximum number of days for virus incubation
m	total number of contact
N	total population size
Q	respiration rate of susceptibles
R	contact radius
s	Standard deviation
x	virus-specific contact radius

Φ	Lennard-Jones potential
β	Product of contact per person by the transmission probability
γ	transition (recovery) rate
$\delta, \delta_1, \delta_2$	minimum cut-off distance
ε	tolerance value
λ	mean of Poisson distribution
σ	van der Waals radius
τ	exposure time
ϵ	well depth
ϑ	potential energy

ABBREVIATIONS

CDC	Centers for Disease Control and Prevention
Comb	combination
Config	configuration
CRJ	Canadair Regional Jet
H1N1	Influenza type H1N1
HEP	high energy physics
LBS	location-based services
LDS	low discrepancy sequence
MD	Molecular Dynamics
QMC	Quasi-Monte Carlo
REU	Reticular-Erythematous-Ulcerative
RNA	ribonucleic acid
SARS	Severe acute respiratory syndrome
SI	Susceptible-Infected
SIR	Susceptible-infected-Recovered
SIS	Susceptible-infected-susceptible
VV	Verlet-Velocity

ABSTRACT

There is direct evidence of the transmission of fatal infectious pathogens in large human gatherings. Air transportation is no exception. The mixing of susceptible and infectious individuals in this high-density man-made environment involves pedestrian movement which is generally not taken into account in modeling studies of disease dynamics. This thesis addresses this problem through a multiscale model that combines pedestrian dynamics with stochastic infection spread models. This generic model is applicable to several directly transmitted diseases. Through this multiscale framework, the effectiveness of certain layouts and strategies in suppressing the disease spread in highly crowded locations such as airplanes, airports and waiting queues is quantified. Inherent variability in human behavior leads to a large parameter space. This large parameter space is addressed by using novel parallel algorithms for parameter sweep based on low discrepancy parameter sweep, compared to a default lattice-based sweep.

This dissertation shows that certain pedestrian movement strategies may be adopted during an outbreak to reduce pedestrian-to-pedestrian contacts. For instance, two-section boarding leads to lower infections whereas all deplaning strategies have a similar effect. Winding queues configurations at security checkpoints or theme parks have a major effect on pedestrians' interaction. A queue of two-zones with two inlets and outlets and vertically portioned short aisles is superior over the other assessed configurations in terms of reduced infection. In terms of parameter sweep of the large domain, a low discrepancy Halton sequence is used for uncertainty quantification. This method has proven to be efficient and less time consuming when applied to at least one model of the entire multidisciplinary model compared to the default lattice-based model.

1. Introduction

This introductory chapter discusses the motivation for investigating the spread of infectious disease in air travel, and the analytical approaches used herein. Within the general framework, the subject is analyzed by means of a multidisciplinary approach, dealt with in detail in the following chapters. Particle dynamics approach which is the basis for the computational model is introduced. The objectives of this research and the content of the dissertation are also described.

1.1   Motivation

Air transportation medium and facilities are evolving exponentially to meet the necessity of connection, exchange, and travel in an increasingly interconnected world. Air travel brings together people from different geographic regions with different levels of vulnerability and receptivity due to variations in immunity, ethnic background, and intervention usage across geographic areas (Wilson, 1995). There is direct evidence for spread of infection during commercial air-travel for many infectious diseases including influenza (Moser et al., 1979), SARS (Olsen et al., 2003), tuberculosis (Kenyon et al., 1996), measles (Nelson et al., 2013) and norovirus (Widdowson et al., 2005).

During the Ebola epidemic in 2014, models estimate that without travel restrictions, 7.17 infectious passengers per month would depart from the highly affected countries Liberia, Sierra-Leone and Guinea, to various destinations around the globe (Bogoch et al., 2015). Transmission of Severe Acute Respiratory Syndrome (SARS) virus via air travel has been recorded, in 2003, on three flights; Among 681 passengers, 23 tested positive for illness (Olsen et al., 2003). In 1994, an infective with multidrug-resistant tuberculosis was on-board flights from Honolulu to Baltimore, passing by Chicago,

transmitted the illness to passengers seated in the vicinity (Kenyon et al., 1996). Three

factors are known to influence the contagion spread: the infectivity of the index

infectious individual, the number of contacts within the critical radius of infection, and

the duration of exposure to contagion (Kenyon et al., 1996). The number of contacts is

critically dependent on the pedestrian movement path within airplanes and at airport

lounges.

Given the preponderance of infection spread through air travel, it is essential to

identify air-travel related policies that can mitigate infection spread. Airport terminal

security screening remains a controversial issue awaiting a definite solution. Bender

(2016) reported that travelers are delayed for more than an hour at screening checkpoints

costing airlines about $39.74 per passenger per hour. The screening procedure at

checkpoints only involves the passengers and their carry-on baggage. However, no

equipment is available for use to detect viral contagions during an outbreak.

Consequently, security checkpoints congregated winding queues are a potential, prime

location for pathogen and major pandemics spread by active pedestrians coming into

proximity of infective agents on site.

1.2   Particle Dynamics Modeling

Particle dynamics modeling is a mathematical technique used to simulate the behavior

of groups of interacting particles and study their dynamic, mechanical and rheological

properties by means of computer simulations (Satoh, 2010). This model provides an

overview of the interaction between particles (e.g. atoms, molecules, powders, etc.), and

enables to monitor the change of a system's bulk properties under varying

thermodynamic conditions of pressure, density and/or temperature. The evolution of

position distribution of particles can be recorded in the time domain and material properties at equilibrium conditions can be evaluated through this method. The most attractive feature of this model is its ability to simulate complex interactions by simple models (Espanol, 2004).

Particle simulations are often used to validate the theory and predict the findings of experiments in predefined conditions (Ceperley, 1999). These simulations are also useful when the experiments or the analysis are difficult to perform due to limitations associated with atomic-scale measurement (Sokolowski, 2011; Chevalier et al., 2017; Hou et al., 2010; Wang et al., 2015; Hollingsworth & Dror, 2018). On the other hand, when experimental data can be obtained, averaged properties from molecular simulations are used for comparison and correlation (Rahman, 1964; Feig et al., 2018, June; Dingreville et al., 2016; Sawyer & Tichy, 2001). Extensions of these methods in other application areas include particle dynamics models for traffic (Chopard et al., 2002; Nagel, 1996; Treiber et al., 1999) and for pedestrians (Bellomo & Dogbe, 2008; Helbing & Molnar, 1995; Helbing et al., 2000; Henderson, 1971).

The main families of particle dynamics techniques on different scales (micro, meso and macro scales) in materials science include Molecular Dynamics (Rapaport & Rapaport, 2004), Brownian Dynamics (Schuss, 2015), Lattice Boltzmann (Succi, 2001) and Dissipative Particle Dynamics (Baydin, 2008), Monte Carlo (MC) (Fishman, 2013), and Discrete element method (Cook & Jensen, 2002). The common feature of all these methods is to find the external forces given the motion of the particles and vice versa (Yang, 2005). The appropriate model is chosen based on the determined physical scale of the study and the corresponding outputs.

In this study, an approach similar to the Molecular dynamics simulation technique is used for simulating the movement of pedestrian particles. Molecular dynamics (MD) is an N-body method in which the evolution of the system's configuration, on the microscale level, is computationally simulated by numerically solving the Newton's equations of motion to obtain positions and velocities at each time step (Rapaport & Rapaport, 2004). MD has been utilized in many fields including materials science, physics, chemistry, pharmacology and nanotechnology to elucidate the happenings at atomic and molecular scales.

Here, the molecular dynamics method is borrowed from the field of computational materials science and applied to the movement of pedestrians using a social force model. The proposed algorithm utilizes the same numerical framework as MD for evolving the trajectories of moving pedestrians. However, the social force fields are used for human guidance and trajectory tracking, unlike MD which uses thermostat properties to evolve the particles. A numerical approach that is very similar to the molecular dynamics method is used to evolve pedestrians in time and spatial frames. The forces representing atomic attraction and repulsion in the conventional MD algorithm are replaced by social forces attracting pedestrians toward their goal while avoiding collision with stationary pedestrians and obstacles impeding their motion respectively. These balancing forces, summated under Newton's second law of motion, prevent vibration of the pedestrians represented by point mass particles in the simulations, unlike atoms that vibrate in a continuum medium.

1.3   Multidisciplinary Model

The MD-like pedestrian dynamics method is one of the components of the multidisciplinary model. The trajectories of the pedestrians are obtained using this approach, which enables mapping of the contact evolution between the individuals. The contact data is then combined with an individual-based stochastic epidemiological model to monitor the propagation of infection in the designated population.

Epidemiological models used to predict the emergence and evolution of diseases among a host population often do not account for social behavior. Disease systems are treated in isolation from social systems ignoring the connection and influence on each other. Understanding the dynamics of an emerging disease among a crowd inhibits its evolution and reduces its fatality. Comprehending the influence of social behavior on infectious diseases by utilizing available resources helps to raise preparedness (Pharaon & Bauch, 2018).

This thesis addresses the transmission and dispersion of potentially fatal infectious pathogens in locations, where large groups of people gather at high densities, through a multidisciplinary model that couples pedestrian dynamics with stochastic infection spread models. The pedestrian dynamics model uses a Molecular Dynamics (MD) based numerical approach called the social force method. The MD algorithm captures the step-by-step evolution of the system of particles tracing their trajectories and can be used to estimate the contact frequency between passengers during air travel. In addition, an infection transmission framework is proposed to assess the influence of pedestrian movement policies on the spread of infectious diseases. This information is incorporated

into a discrete-time stochastic Susceptible-Infected (SI) model with infection probability and contact radius as primary inputs.

This generic model is applicable to different scenarios of pedestrian movement and diseases. Pedestrians' behavior varies depending on the nature of their activities and their background. The parameters of the same social force model can be altered to account for instance for a line or group formation, emergency escape and bottleneck formation at exits, etc. Also, several directly transmitted diseases can be accounted for in the epidemiological model by varying the input parameters related to infectivity (probability of infection) and transmission mechanisms (radius of infection). Through this multidisciplinary framework, the effectiveness of certain pedestrian movement strategies in suppressing the disease spread during air travel and crowd formation is validated by quantifying the uncertainties of the multiscale model parameters through a parameter sweep.

1.4   Objectives

The overall objective of this research is to evaluate the effect of pedestrian movement during air-travel on the spread of infectious diseases. Another aim is to formulate pedestrian movement models that can be used to study pedestrian movement in crowded environments. This goal is accomplished by developing a pedestrian dynamics model similar to MD models and integrating it with stochastic infection dynamics models. The specific tasks in this thesis with a brief statement of the research innovation are listed below:

> ➢ Formulate a mathematical method to characterize the infection spread in airplanes and airport lounges. The pedestrian movement and stochastic infection dynamics

models are combined; the pedestrian trajectory information obtained from the pedestrian dynamics model is integrated with a discrete-time stochastic Susceptible-Infected (SI) model to achieve this target. Multiple directly transmitted diseases are incorporated in the model such as Ebola, SARS and H1N1.

➢ Generalize the proposed model to account for group formation between the moving agents. The model is extended to the movement of pedestrians within winding queues commonly observed in airports and theme parks. The effect of crowd density is also implemented in the individual's desired speed of motion.

➢ Analyze the uncertainty in the multidisciplinary model using novel algorithms on massively parallel computers. The inherent uncertainty in pedestrian dynamics and infection spread models necessitates a large parameter space. The use of novel algorithms based on low discrepancy sequences and parallel computers is established to traverse this large parameter space in a multi-model setting.

1.5 Content of the Dissertation

In this dissertation, the pedestrian movement is related to epidemic outbreak propagation among a population. Pedestrian movement strategies that can mitigate viral infection spread are investigated. A Molecular dynamics-based multiscale approach, formulated by integrating a pedestrian dynamics model with epidemiology, is used to analyze the effectiveness of alternative public policy choices in limiting the spread of infections. The multidisciplinary model is applied to air travel during various enplaning and deplaning scenarios for various air carriers' capacities to study the infection transmission within airplanes and airport lounges. The transmission of the Ebola, H1N1

and SARS viruses through casual contacts are studied. The model is then generalized to understand pedestrian behavior in crowded environments and winding queues. The effect of the waiting area geometry, aisles distributions and pedestrian arrangement during line forming is assessed. Several walking policy options that impact the disease spread are presented. Such a framework is usually neither feasible nor robust to predict the impact of walking strategies due to inherent behavioral uncertainties.

Due to the inherent stochasticity of the pedestrian and epidemic models, the sources of uncertainty are parametrized for further exploration and uncertainty quantification. Sequential computations are time consuming and limited. Parallelization of the algorithm to come up with results during a decision meeting is required. The computational effort increases exponentially with dimensionality and model refinement to account for more factors. Accordingly, a novel parameter sweep using low discrepancy sequence (LDS), that covers the entire large parameter space as efficiently as possible, is incorporated and carried out to identify the parameters' robustness under a variety of possible settings.

2. Scientific Background

In this chapter, related work corresponding to the different aspects of the thesis is described. Advances in pedestrian dynamics models, based on the molecular dynamics are described in section 2.1. The numerical aspects and similarities of this approach with MD are first discussed. The force fields implemented in the proposed MD-like algorithm are the social forces representing pedestrian dynamics, and are discussed in section 2.2. The contact data extracted from pedestrian trajectories is combined with an infection model to estimate the reproduction rate of infection. A review of susceptible-infected epidemiological models and contact analysis approaches is compiled in sections 2.3 and 2.4. Both the social force and the epidemiological models comprise uncertain parameters requiring a parameter sweep to quantify their uncertainties. The parameter sweep methods are reviewed in section 2.5.

2.1   Molecular Dynamics-like Numerical Approach

The Molecular Dynamics method is a mature classical simulation methodology that has been extensively used to understand the materials' dynamics on a microscopic level (Tadmor & Miller, 2011; Allen, 2004). While advanced techniques facilitate experiments at atomic scale to study motion of atoms in materials (Tadmor & Miller, 2011), such work is extremely challenging. From this perspective, Molecular Dynamics (MD) simulations can be extremely effective in explaining the atomic scale material behavior. This technique considers atoms as continuous Newtonian particles in motion; The MD algorithm analyses the evolution of the atoms' instantaneous positions and speeds resultant of interatomic actions and reactions. The interatomic forces are expressed by the gradient of potential energy ϑ for a specific three-dimensional arrangement of the

particles. Such potential breaks down into potentials due to internal (intramolecular) and external interactions (non-bonded); within the system, atoms interact between each other whereas interaction still exists between the particles and their external surroundings (Allen, 2004).

Molecular Dynamics simulations predict the trajectories of a collection of "N" particles constituting a system of second-order differential equations:

$$\frac{d^2\vec{r}_i}{dt^2} = \frac{\Sigma_{i \neq j} \vec{f}_{j/i}}{m_i} = \vec{a}_i \; ; \; 1 \leq i \leq N \tag{1}$$

The forces $\vec{f}_{j/i}$ acting by the neighboring particles on the particle "i" alter at each position update $\vec{r}_i$ or when other adjoining particles switch their positions leading to a continuous change in potential (Tadmor & Miller, 2011):

$$\vec{f}_{j/i} = -\vec{\nabla}v^{ij}(r_{ij}) = -\frac{\partial v^{ij}(r_{ij})}{\partial x}\hat{i} - \frac{\partial v^{ij}(r_{ij})}{\partial y}\hat{j} \tag{2}$$

where: $f_{j/i} = f_{i/j}$ (Newton's third law of action and reaction).

The atomistic simulation of materials relies on the interatomic bonding formulation represented in terms of potential energy gradients $\vec{\nabla}v^{ij}(r_{ij})$. These potential energies break down into attractive and repulsive terms:

$$v^{ij}(r_{ij}) = v_{attractive}(r_{ij}) + v_{repulsive}(r_{ij}) \tag{3}$$

Among the potentials cited in literature are pair potentials like Lennard-Jones pair potentials (Lennard-Jones, 1924) and multibody potentials like Abell-Tersoff bond order potentials for carbon-based materials (Abell, 1985; Tersoff, 1986; Tersoff, 1988a; Tersoff, 1988b; Tersoff, 1989, Brenner, 1990), short-range repulsive potentials (Ziegler & Biersack, 1985; Nordlund et al., 1997), the Stillinger-Weber potential (Stillinger & Weber, 1985) and embedded-atom method potential for metals (Daw & Baskes, 1984).

Calculating the gradient of these interatomic potential energies gives the net forces between neighboring atoms.

The Lennard-Jones potential is an important pair potential and is computationally expedient. It consists of steep repulsive and smooth attractive potential terms. The gradient of the attractive potential represents the London dispersion forces which are the weakest intermolecular temporary attractive forces (Lennard-Jones, 1924). The Lennard-Jones Potential is given by the equation:

$$v(r_{ij}) = 4\epsilon \left[\left(\frac{\sigma}{r_{ij}}\right)^{12} - \left(\frac{\sigma}{r_{ij}}\right)^{6} \right] \tag{4}$$

where ϵ is referred to as the well depth which is a measure of the attraction strength between two particles. σ, known as the van der Waals radius, is the minimum distance between two non-bonding particles measured between their centers.

In continuous potential models, the initial boundary value problem of Equation (1) cannot be solved by means of a simple integral. The integration is discretized and numerical techniques are used to derive the trajectories. The total integration time is sectioned into appropriate time steps Δt. The acceleration in equation (1) is directly obtained from calculating the interatomic forces $f_{j/i}$ acting on particle "i". Then, the instantaneous speed (v_i) and position (r_i) are computed using step-by-step numerical methods. MD second order differential equations are mainly integrated by finite difference or predictor-corrector methods that are developed based on the Taylor series expansion of position (r), speed (v), acceleration (a) and higher-order derivative terms (b) and (c) (Andrew, 2001). For instance, the Verlet-Velocity (VV) algorithm (Verlet, 1967) and the predictor-corrector (Beeman, 1976) method are mostly used. Comparing both

methods, the predictor-corrector strategy is of higher accuracy in narrow time steps when the VV method leads for wider temporal intervals (Andrew, 2001).

An approach (Figure 2.1-b) that is very similar to the Molecular Dynamics method (Figure 2.1-a) is used here to model pedestrian motion. This approach has been pioneered by Helbing and co-workers and is termed as social force model (Helbing, 1995). The forces of equation (2) representing atomic attraction and repulsion are replaced by social forces attracting pedestrians toward their goal while avoiding collision with stationary pedestrians and obstacles impeding their motion, respectively. The repulsive force chosen for the pedestrian model is a potential gradient of the repulsive term of the Lennard-Jones potential $4\epsilon\left(\frac{\sigma}{r_{ij}}\right)^{12}$. However, the values of ϵ and σ are substituted by valid values for pedestrians' behavior. The attraction term motivating the pedestrian toward his/her destination is represented by the rate of change of momentum $\left(\frac{\Delta P}{\tau}\right)$ between his desired free (v_{0i}) and actual walking speeds (v_i). The actual walking speed is a reduction of the free speed with respect to a minimum cut-off distance (δ) and depends on the distance with the most forward pedestrian in the queue. Namilae et al. (2017a) have performed massive parameter sweep on parallel computers and compared with experiments to obtain the model parameter values used here. The details of the pedestrian dynamics modeling approach are explained in chapter 3.

Pedestrian motion modeling is an important problem for transportation engineering and safety design. As shown in this work, it can have a far-reaching impact on applications like epidemic spread modeling. The focus is on pedestrian movement modeling in air transportation infrastructure using social force-based approaches.
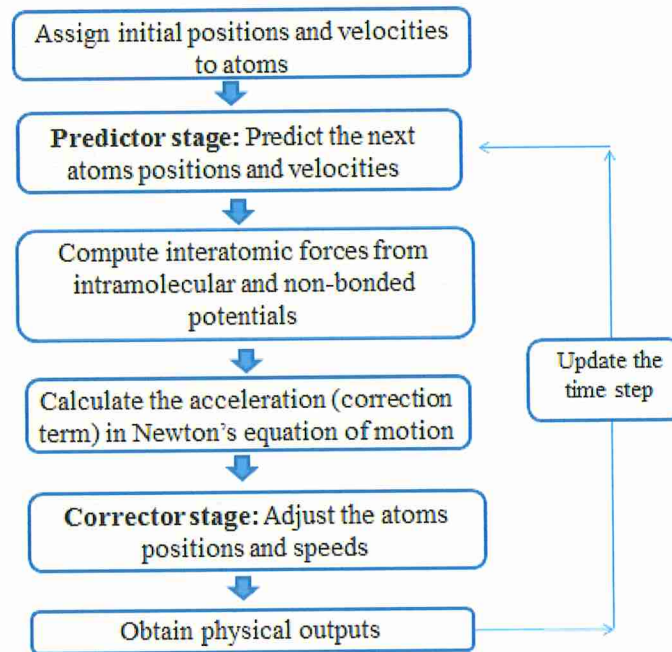
(a)
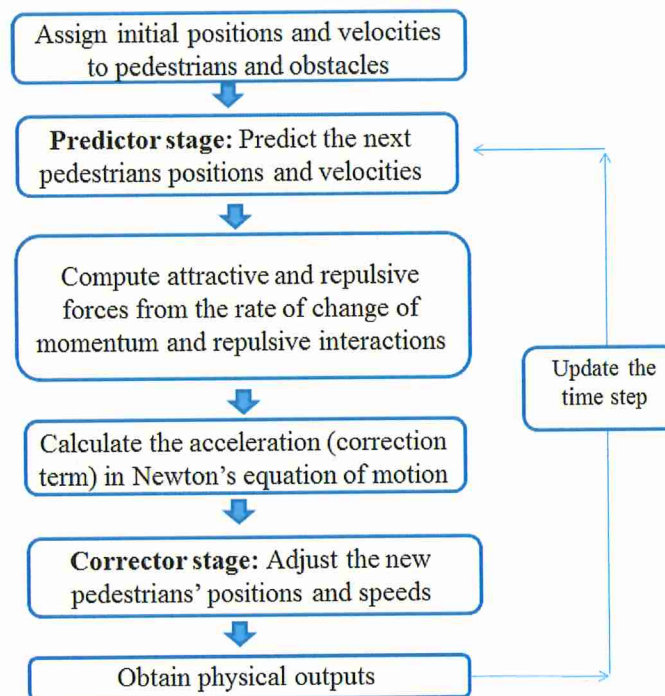
(b)

Figure 2.1. Flow chart of (a) molecular dynamics, (b) molecular dynamics-like approach for pedestrian dynamics model.

2.2 Pedestrian Dynamics Model

Pedestrian Dynamics has been addressed using several approaches such as particle dynamics or social force models (Helbing, 1995 & 2000), models based on cellular automata (Burstedde, 2001), fluid flow models (Henderson, 1971), and queuing based models (Van Landeghem, 2002). Social force models of pedestrian movement are essentially based on molecular dynamics. Social force models extend the concepts of molecular dynamics to pedestrian movement. Here, the forces are a measure of the internal motivation of individual pedestrians to move towards their destination in the presence of obstructions like other pedestrians and objects (e.g. walls and chairs). Social force models have been applied to crowd simulations in panic situations (Helbing et al., 2000), traffic dynamics (Treiber, 1999), evacuation (Wei-Guo, 2006) and animal herding (Li & Jiang, 2014). Algorithmic developments have included generation of force fields using visual analysis of crowd flows (Mehran et al., 2009), explicit collision prediction (Zanlungo, 2011), and collision avoidance (Lämmel & Plaue, 2014). Namilae et al. (2017a & 2017b) have used pedestrian dynamics described by social force model in a multiscale model to study the spread of epidemics during air travel.

Unlike other models, the social force model has specific advantages for studying passenger movement and contacts in airplanes as each traveler is modelled individually and moves continuously. This enables tracking the individuals' trajectories and estimation of the contacts between pedestrians. The social force model is discussed in more details, below because it is an important part of the future work plan.

Helbing and Molnar (1995) developed a microscopic particle-based social force approach to mimic the behavior of foot-travelers in their milieu of locomotion. Their

principle reflects the influence of the surrounding on the internal motivation of a pedestrian to reach his designated terminus. Founded on Newton's second law, repulsive and attractive forces are summated and equated to the acceleration to reach the desired velocity. The tendency to avoid collision with other individuals in high-density crowds and immobile obstacles in the walking path is represented by the repulsive term although there are no physically subjected forces on the pedestrian itself. Repulsive forces inhibit the walker's motion in close proximity with an obstruction. On the other hand, guided by his intention, a pedestrian self-propels to his targeted destination or one of the exits either individually or collectively by joining a formed group of walkers. Further, Helbing et al. (2002) establish a comparison between pedestrian behaviors in normal and evacuation situations. The social force model alters between these analyzed cases since the nervousness factor is implemented. In normal situation, the self-organization of pedestrians is emphasized through line formation along hallways and oscillations at bottlenecks. In panic circumstances, the situation is more chaotic. The tendency of herding, lane breakdown and clogging are observed, which in return reduces the chance of survival.

Lakoba et al. (2005) improve on the basic ideas of Helbing et al. (2000). Despite the accuracy of their theoretical model presented for a panic situation, the parameters within the repulsive terms are not realistic. They are not valid for a small crowd or an isolated pedestrian. In addition, the repulsive term used to model pedestrian-pedestrian and pedestrian-wall repulsion doesn't guarantee overlapping prevention. For this purpose, an optimized algorithm is set up to seek for the adequate parameters' values. The density effect is also taken into consideration and implemented in the force expression derivation

as it inversely affects the free speed of a pedestrian. Chraibi et al. (2010) suggest a theoretical improvement to the repulsive term in the social force model to prevent collision between individuals. In contrast to the standard circular representation of the pedestrian, a more realistic elliptical concept is introduced. The study restricts itself to crowd enclosed in corridors and a unique set of parameters for this investigation are chosen.

Mehran et al. (2009) utilize the principle of the social force model to localize abnormalities in a crowd. For this aim, a data set of crowd videos is interpreted. A grid of mobile points is placed over the screen and the floating particles are allowed to move with the stream of people. The estimation of the interactive forces between the pedestrian and his surroundings is indicative of distortions. Their method proved its capability to evaluate the crowd as a whole without need for identifying every single individual and identify the irregularities.

From a computer graphics perspective, Pelechano et al. (2007) suggest an improvement to the mathematical models previously proposed by implementing a high-density autonomous crowd model relying on psychological, physiological and geometrical rules for a more realistic simulation. This technique also eliminates the fluttering of the particles during the time step evolution occurring at high-density crowds.

Analyzing pedestrian motion in different circumstances is necessary for facilities with high people density to plan evacuation strategies in the case of emergencies. For instance, Von Sivers et al. (2016) modeled the emergency evacuation of the London train station when bombed in 2005 using a new approach combining a locomotion model combined with social identification and self-categorization theories. Mekkah is a city in Saudi

Arabia that receives millions of Muslims across the world for pilgrimage during the last month of the Muslim calendar. Deaths due to pushing in high-density crowds are recorded every year. Dridi (2015) simulated the pilgrimage situation using Pedflow. The software solves the differential equation of motion using a microscopic social force approach. The study also aimed to shed the light on the important role of the social and physical force model to plan and set up evacuation strategies in emergency conditions in highly congested zones.

Li and Jiang (2014) performed a computer simulation using the AnyLogic software to mimic the evacuation situation in case of an emergency in the Xizhimen Metro station in Beijing since it's difficult to perform actual experiments. Alonso-Marroquin et al. (2014) investigate the occurrence of the tragic incidence that took place in the Madrid Arena Pavilion in 2012 in Spain, where five girls were the victim of a crowd stampede. In contrast to conventional representation of pedestrians as single or three-circles for a comfortable or moderately crowded environment, the authors suggest a spheropolygons representation of pedestrians to simulate heavy crowd conditions. A counter-flow of pedestrians in a corridor is selected to reproduce the real incidence. Dong et al. (2014) simulated a crowd evacuation in Beijing south subway station to emphasize the role of crowd leaders, guiding the crowd to the nearest exits, in suppressing evacuation time and reduce injuries and lives loss.

Movement of pedestrians in airports and during emergencies studied in this thesis is a special case of a more general problem of pedestrian movement. Several researchers have studied the pedestrian movement at airports especially from the viewpoint of airport operations and reduction of the turnaround time of airplanes at terminals. For instance,

Schultz et al. (2006) model the intuitive behavior of airport travelers under an emergency situation by a cellular automaton model. In this model, the floor area is subdivided into small partitions where pedestrians may switch positions with neighboring spots based on a probabilistic distribution. Several other investigators used agent-based models to model pedestrian motion and passenger flow in airport terminals (Ma, 2013; Cheng, 2014). Other studies such as that by Lin and Chen (2013) study the flow of pedestrians to their destinations by optimizing the guiding signs.

Pedestrian movement in airports is peculiar because it involves a series of nondiscretionary as well as discretionary activities. For example, prior to their scheduled flights, travelers fulfill the trip requirements starting from check-in, security and boarding. Once these processing steps are completed, they are often involved in individual or collective discretionary activities such as dining and shopping at the departure terminal (Kraal et al., 2009; Popovic et al., 2010). The airport environment and building layout have a great influence on the passengers' movements, choice and perception of activities preference over a set of alternatives (Lin & Chen, 2013; Kalakou, 2015). This uncertainty creates additional challenges in modeling the pedestrian motion at airports.

Despite all the work done to simulate pedestrian motion in airports, no work focuses on the effect of pedestrian movement on airborne disease propagation among travelers. In this study, the social force model is used to generate the contact data among travelers coming into proximate contact in various travel stages such as enplaning, deplaning and progressing in winding queues for booking or security checking. The contact data is then

combined with an epidemiological model to assess the propagation of infection among the susceptible crowd of travelers coming to proximate contact.

2.3   Mathematical Epidemiological Models

There is evidence for the spread of many diseases through air travel. Airports and airplanes are fertile ground for disease propagation and transmission to large geographical areas throughout the world. After the Ebola outbreak of 2014, there were concerns that air transportation could play a major role in the transmission and dispersion of fatal infectious diseases. Potential pathogens spread speedily during air travel since passengers congregate in common spaces for extended hours and are in close proximity to each other in affordable air-carriers. Predicting the disease transmission rate is essential to set up preventive strategies to mitigate transmission during outbreaks. Mathematical modeling of diseases also referred as epidemiological models are effective tools to study the factors related to diseases dispersion and suggest possible control strategies based on the knowledge of the dynamics of an epidemic. In the following, the basics of epidemic modeling are discussed as applied to the current study.

An infectious disease is defined as an infectious agent transmitted through direct or indirect route from an infected person, vector, reservoir or environment to a susceptible host and causing illness (Last, 1988). Infectious diseases are classified by their transmission agent (virus, bacteria, protozoa and helminths) and mode (person-person, person-environment, reservoir-vector, vector-person and reservoir-person). Vectors are bloodsucking insects that transmit infectious diseases between humans or from animals to humans. Domestic and wild animals serve as reservoir for infestation. An infection occurs when an infectious agent enters a human or an animal's organism directly or

indirectly via various transmission routes. Upon contract of infection, it may or may not

develop into a disease (Barreto et al., 2006). The transition from infection to disease,

during the latent period, is unapparent and not always identifiable; its detection relies on

the diagnostic techniques able to spot the early signs of infection activity in the organism

causing disease (Thagard, 1998a &b). The disease keeps developing during the

incubation period defined as the period pre-onset of the symptoms. However, it can be

infectious and transmittable to a susceptible individual even when the virus is still

shading (Figure 2.2).
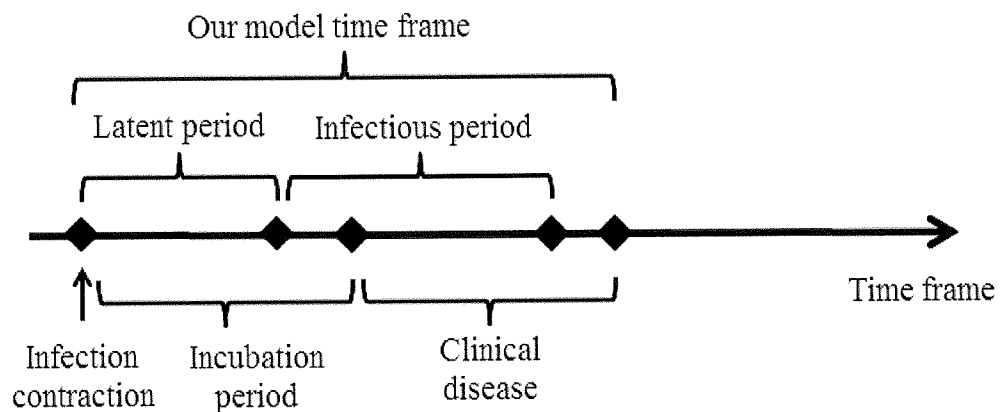
Figure 2.2. Schematic of the segments of viral evolution from contracting the infection to disease transmission.

Infectious diseases occurrence in human populations can take the form of an epidemic,

outbreak, endemic or pandemic. These nomenclatures define the nature of the

propagation of disease. An endemic is a continuous disease occurrence in a controlled

time and geographical frame where transmission occurs at an expected frequency within

a population. When the transmission exceeds the normal expectation, it is defined as an

epidemic. If limited in a certain localized geographical region, the term outbreak can be

used. However, when international boundaries are crossed and a larger population is

affected, a pandemic is happening (Last, 1988). Infectious diseases are complex due to

ethical issues, difficult and expensive to search in human populations. Instead, three main models are used to replicate infectious disease propagation in humans; those are the animal, mechanical (bead) and mathematical models.

Mathematical models, consisting of parameters linked by algebraic formulas are more favorable in terms of analysis and logical proofs compared to the other approaches (Vynnycky & White, 2010). The analysis of outbreak events, approached by mathematical and statistical techniques, allows a better understanding of the stochastic nature of their dynamics. These models are capable of producing accurate epidemiological information about disease propagation in order to develop disease-management policies. Mathematical and statistical models apply for large outbreaks among a population and predict the probable threat of disease outbreak at its early stage. The mathematical models are classified as deterministic (compartmental) and stochastic (Vynnycky & White, 2010).

Deterministic models offer an average insight of infection propagation in a population (Vynnycky & White, 2010). Deterministic models classify the population into categories or compartments. These compartments range between susceptible "S", pre-infectious (exposed) "E", infectious (or infected) "I", and recovered (removed or immune, not spreading the disease) "R" in an N size population. In a deterministic model, it is assumed that the population is homogeneous (all individuals have the same susceptibility to infection) and that there is a uniform mixture among the individuals (all individuals are exposed). The population is also fixed assuming no births or deaths. There is no latent period meaning that the infectious period is the same duration needed for contract of disease and recovered individuals are immune.

Such deterministic compartmental models are based on difference or differential equations in time domain. Difference equations use discrete-time steps to express the evolution of the number of individuals in a certain category in terms of the number at earlier time step. The selection of the time step is very critical to the accuracy of the results and it is difficult to predict. According to Vynnycky and White (2010), in difference equations, the time step should be chosen such that it is less than the lowest average duration spent by an individual in a certain compartment. To avoid the complexity related to the determination of the time step in difference equations models, differential equations in the continuous time domain are proposed.

Differential equations describe the rates of change in the number of individuals entering and leaving the categories. In person-to-person infectious disease spread, there are three basic types of initial value problem differential deterministic models, (1) The SIS Model, (2) The SIR model without vital dynamics, and (3) The SIR model with Vital Dynamics (Hethcote, 1989). In the SIS model, the susceptible population exposed to infection becomes infected and recovered individuals are susceptible again to infection. The SIR model assumes that after recovery, the individuals confer immunity; therefore, their immunity defends the infection if exposed again. In an epidemic with short outbreak duration (less than 1 year), the births and deaths within the population are not taken into consideration. Therefore, the SIR model doesn't account for vital dynamics. During an endemic lasting for a long period of time (more than 10 or 20 years), the vital dynamics are implemented in the model. The SIR system is expressed by the differential equations:

$$S+I+R = N$$

$$\frac{dS}{dt} = -\frac{\beta IS}{N}$$

(5)

$$\frac{dI}{dt} = \frac{\beta IS}{N} - \gamma I$$

$$\frac{dR}{dt} = \gamma I$$

Where γ is the transition (recovery) rate and β is the product of contact per person by the transmission probability.

Deterministic differential equations extensively contributed to the mathematical theory of epidemics (Anderson et al., 1992; Diekmann & Heesterbeek, 2000; Kermack & McKendrick, 1927; Mollison, 1977). Conventional deterministic methods offer an insight into the regeneration number of infected individuals, resultant from disease propagation without specifically determining the infected individuals' indices. Developments in deterministic methods focused on the network of dynamic contact (Sharkey et al., 2006; Van Baalen, 2000; Rand, 1999; Keeling, 1999; Satō et al., 1994; Matsuda et al., 1992). However, the application of deterministic models is mostly limited to idealized, homogeneous systems (Sharkey, 2008). Instead, stochastic epidemiological methods are applied in complicated situations to assess the effectiveness of methods for disease control and prevention (Sharkey, 2008; Allen, 2008). Stochastic models are more flexible than deterministic models (Ferguson et al., 2006; Keeling, 2005; Sharkey et al., 2007). More realistic models in a small population (Vynnycky & White, 2010) or large population (Britton, 2010) are also of a stochastic nature.

A stochastic model includes the effect of probability on the outcome (Anderson & Britton, 2012). The development of stochastic models arises for many reasons. Even if an infective individual is introduced in a susceptible population, infection spread may not occur. Stochastic models allow standard errors during parameter estimates from disease

data. Also, stochastic models better explain disease extinction (Britton, 2010). There are

several kinds of stochastic models; those are (1) individual-based models, (2) discrete-

time compartmental models and (3) continuous-time compartmental models (Vynnycky

& White, 2010).

In order to track each individual in the population represented by travelers, the

individual (agent) based approach is used. This method allows determining whether each

individual is only exposed or becomes infected based on the risk of infection. This

approach accurately quantifies disease transmissibility through proximate human-to-

human interaction (Bobashev et al., 2007, December; Burke et al., 2006; Rakowski et al.,

2010; Smieszek et al., 2011; Ajelli et al., 2010; Rocha & Masuda, 2016). Various

variables are involved in the dynamics of disease spread and urge for the development of

improved methods based on contact tracing for better data extraction and parameter

estimation (Matthews & Woolhouse, 2005). Advances in the analysis of outbreak lead

to the development of computational molecular-based techniques to trace contact in

the time frame. The same approach is applied in the following chapter to trace contact

using a molecular dynamics-based approach.

2.4 Integrated Contact Analysis in Individual-Based Infection Spread Model

In the mathematical epidemiological models, the contact between individuals leads to

infection although the contact is assumed to be random with an equal chance of contact

of the susceptible host population seen collectively. When investigating control strategies

to suppress disease propagation among a group or population, the contact pattern between

the interacting individuals should be considered and mapped. Computational contact-

based epidemiological models provide a better insight into the interaction between

individual and trace their motional behavior. Unlike general deterministic and stochastic models that evaluate the disease spread dynamics in demographic and environmental conditions, contact-based models significantly relate disease transmission to the contact network of the contagion host. The tailored network pattern of contact of the contagion host with the surrounding individuals consist the medium for disease dynamics (Bansal et al., 2010).

The integration of contact tracing in epidemiology also captures the heterogeneity in the transmission dynamics and the variability in the reproduction ratio of new infections. Smieszek (2009) proposed a "mechanistic" contact-based model assuming variation in the intensity and duration of potential contagious contact. Ignoring the heterogeneity and assuming a constant transmission-through-contact probability might grant inaccurate results in simulations (Smieszek, 2009). De Cao et al. (2014) proposed a survey data based epidemiological approach to measuring close contact leading to contagion, taking into consideration the frequency of contact and the long exposure duration sufficient for viral transmission. De Cao et al. (2014) correlated their theoretical findings to experimental data using Bayesian melding technique for two different viral strains.

Contact analysis is difficult to define especially among a large dynamic population (Mollison, 1977; Hyman et al., 2003; Perez & Dragicevic, 2009). The contributed to contact analysis is refelected by the use of the social force based pedestrian dynamics formulation to estimate the number of contacts as in Namilae et al. (2017a) and evaluate the disease spread in an airplane and at the airport waiting queues. The pedestrian dynamics model is integrated with a contact-based stochastic Susceptible-Infected

infection transmission approach. A homogeneous model is first applied assuming specific probability of infection and transmission mechanism, based on the evolution of the viral strain in time frame. Then, through a parameter sweep, the heterogeneity in the transmission dynamics is accounted for.

2.5 Parameter Sweep

The proposed multiscale model combining a social force based Molecular Dynamics approach with an epidemiological SI model comprises many parameters that lead to large parameter space. Pedestrian motion is stochastic and unpredictable by nature; pedestrians of different cultural backgrounds and ethnicity have different behavioral comportment (Chattaraj et al., 2009). The behavioral difference is reflected by the alteration of certain parameters in the model. Also, infection propagation depends on various environmental factors that facilitate its survival and transmissibility among a susceptible population, on the transmission mechanism and severity of infection of the index infective. Within the same population, the probability of disease contraction differs between individuals based on their immunization and exposure duration. Any change in these factors contributes to different infection scenarios.

Due to the inherent uncertainties in the proposed framework on the levels of the social force and epidemiological models, a large parameter space is created and each combination of these parameters in this space may lead to an estimation of infection regeneration rate. This large parameter space can be traversed by means of a parameter sweep using massive parallel simulations. Running these combinations in serial is highly time-consuming. Even on massively parallel computers, it is challenging to address the

entire parameter space using brute force methods. Accordingly, an efficient method for parameter sweep is necessary to reduce the time cost and computational efforts.

Parameter sweep is an important computational tool that employs massive computing resources to execute multiple computations having altered combinations of values of the same parameters. These parameters are defined over a range of values inputted in a form of sets or input files. Due to the multi-dimensionality of the parameters space, it is often necessary to test all the possible variations to find the accurate combination by means of a parameter sweep, also known as space meshing. Multiple computations are run independently for different combinations that cover the entire space of concern. Each task has the same executable with different input arguments and typically generates an appropriate output file dependent on the inputted data. The whole combined outcome set of tasks results in the parameter sweep experiment over the entire designated domain. Parameter sweep can be used to tune, estimate or evaluate the robustness of control parameters during uncertainty quantification. It is also used to localize a particular point in the multi-dimensional bounded mesh that verifies certain predetermined criteria.

Large-scale Parameter sweep runs have found extensive applications in the scientific and engineering fields (Youn & Kaiser, 2010). Electromagnetic cascade showers are simulated by means of parameter sweep Monte Carlo method (Ford & Nelson, 1978; Nelson et al., 1985). Abramson et al. (1994) modeled photochemical pollution using parallel and distributed computing platforms for parameters sweep. Stiles et al. (1998) used the parameter sweep Monte Carlo program (MCell) to simulate Neuro-Transmitter Release. Basney et al. (2000) developed two effective co-allocation mechanisms, the checkpoint domains and file system domains, for computational grids for high energy

physics (HEP) applications. Casanova et al. (2000a) use the Application-Level Scheduling (AppLeS) Template developed by Berman et al. (1996) for parameter sweep applications on Distributed Heterogeneous Networks. Naito et al. (2003) use parameter sweep to investigate the effects of the equatorial QBO on stratospheric sudden warming events. Kiss et al. (2010) model carbohydrate recognition using parameter sweep workflows. Mustapha et al. (2015) investigated a DC-DC boost converter circuit for low and high voltage range using parameter sweep.

Del Solar et al. (2015) optimize the energy management within an energetic island by means of several parameter search stages. In all these applications, the process of parameter sweep over a refined space may be time and computational effort consuming. Due to the extensive demand for parameter sweep, predictive algorithms for scheduling parameter sweep calculations in a cloud environment were developed by Bosmans et al. (2016). Recently, parameter sweep resources are available through cloud computing, an internet-based service using reliable virtual machines (Monge et al., 2018).

Instead of running each permutation of these variables in serial, a parameter sweep can be performed through parallel computing. One or more parameters can be swept by altering their values between simulation runs distributed on multiple processors. The independent output data of the runs are then compared and further analyzed. Multi-processor computational nodes are promising executive platforms for parameters sweep over a large range. However, the availability of the targeted resources is challenging due to the load, size and memory allocation requirements of the submitted jobs. Several scheduling algorithms such as "Max-min", "Min-min" and "Sufferage" were proposed to schedule and systemize the performance of clusters related to parameter sweep

independent tasks (Maheshwaran et al., 1999). Casanova et al. (2000a) suggest "an adaptive scheduling algorithm" related to parameter sweep on multi-processors (p.4). Casanova et al. (2000b) relate scheduling to inappropriate performance prediction. Casanova et al. (2000b) adjust the standard heuristics of assigning tasks to the host grid and extended the "Sufferage" environment into the so-called "XSufferage". The XSufferage algorithm has proven superiority and better efficiency over the conventional heuristics by means of simulations scheduling. Despite all the proposed scheduling algorithms to allow smooth access and execution on the cluster, choosing an accurate parameter sweep algorithm is an important preceding step in such computations.

A suitable parameter sweep algorithm reduces the required run time and gives the job priority over longer time-consuming tasks on a finely scheduled cluster. The aim of the parameter sweep algorithm is to efficiently cover the parameter space and account for every probable accurate combination of the parameters over their defined ranges. In an N-dimensional space (N parameters) of certain mesh size, if M designates the number of nodes that are possible solutions to the designated problem, then the margins bounded by these points are not accounted for. Refining the coarse mesh to a smaller mesh of K nodes (K>M) is a solution. However, the increase of nodes leads to an increase in processing time which is undesirable especially at higher dimension problems. Accordingly, a parameter sweep algorithm with optimum mesh size and execution time is highly recommended. Parameter sweep algorithms are classified under two main categories; those are the uniformly and the non-uniformly partitioned space methods. The lattice-based method is the conventional uniformly partitioned space method whereas

pseudo-random and quasi-random sequences fall under the category of non-uniformly partitioned method.

In a lattice-based method, assuming a two-dimensional (rectangular) space, the distribution of points in the horizontal and vertical directions is equally spaced (Figure 2.3). This scheme is inefficient in terms of domain coverage with a specific number of grid points and for the check of convergence (Chunduri et al. 2018). For simplicity, a d-dimensional space domain is meshed uniformly in every direction with R nodes. Therefore, the total number of nodes is obtained by $N = R^d$. In order to check for convergence, the space domain is refined by increasing the nodes (decreasing the increment between the nodes by half). Assume $R' = 2R$ the new number of nodes in each dimension doubled compared to its predecessor. Denote by N' the total number of nodes in the whole domain of d-dimension, $N' = R'^d = (2R)^d = 2^d R^d = 2^d N$. The large ratio $\Delta N = 2^d$ between the two consecutive lattice sizes is very large and does not allow to precisely determine at which total number of nodes, convergence has occurred between N and N'. Also, running a mesh of N' nodes, in this case, is computationally exhaustive and time-consuming. Instead, alternate non-uniform techniques are presented for better convergence and faster outcomes.

Non-uniform domain partition methods such as the pseudo-random and quasi-random (deterministic) sequences are promising algorithms for nodes sequence generation enabling faster convergence at a lower number of nodes compared to the lattice method. These methods are commonly used in Monte Carlo and quasi-Monte Carlo algorithms to solve numerical integration problems and particle simulations of transport processes (Goncu, 2009). In a Monte Carlo simulation, the accuracy of the results depends on the

generation of the pseudorandom sequence over a [0,1] interval. Using random sequence may prevent convergence especially that the parameter space is not efficiently covered by the random sequence. For instance, sparse and clustered regions are observed in the space domain. The Linear Congruential Generators (LCG) are common methods to generate pseudo-random sequences. Despite the simplicity of this method, LCGs do not qualify for some statistical and randomness tests (Goncu, 2009).
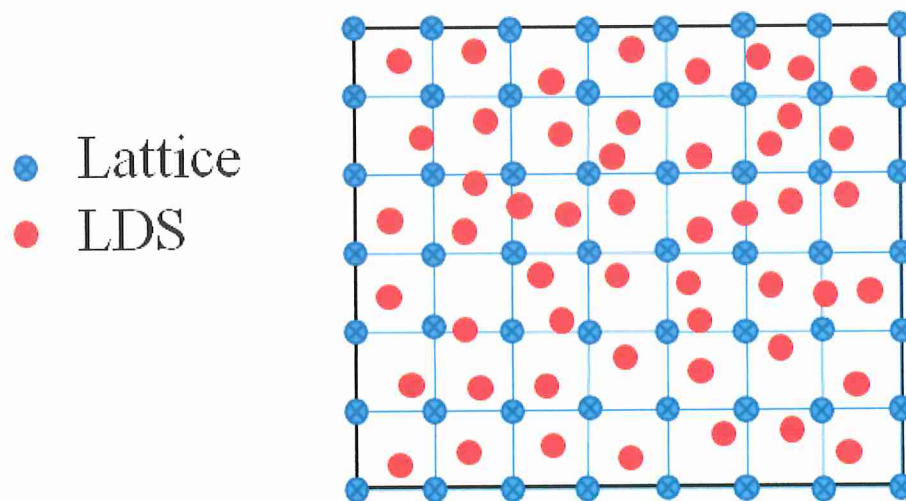
Figure 2.3. Two-dimensional space partition comparing Lattice and LDS parameter sweep algorithms.

Quasi-random sequences are deterministic alternatives to pseudo-random sequences. They are an infinite sequence of points, used in Quasi-Monte Carlo (QMC) simulations (Morokoff & Caflisch, 1994; Goncu, 2009). These sequences are referred as Low Discrepancy Sequences (LDS) since the points are more evenly distributed $[0, 1]^d$. Discrepancy measures the uniformity of the sequence. In other words, discrepancy is "the error in representation of the volume of subsets of the unit cube by the fraction of points in the subsets" (Morokoff & Caflisch, 1994). LDS permits efficiently to check for convergence. For Monte Carlo method, the convergence is of order $O(N^{-1/2})$ compared to

O(log^d (N)/N) for QMC because of the Koksma-Hlawka inequality (Goncu, 2009). Quasi-random sequences have different variants such as Halton, Scrambled (randomized) Halton and Hammersley sequences. The Halton sequence construction, defined via the radical inverse function, uses coprime numbers as their bases (Halton, 1964). Lack of correlations between the radical inverse functions of different bases, the two-dimensional projections are inadequately distributed in different space dimensions. The scrambled Halton sequence corrects the defect by redistributing more accurately the projections (Figure 2.3). Halton and Scrambled Halton sequences have advantages over other sequences in terms of extension of the domain's dimensionality. For instance, extending a d-dimensional domain to a d+1 – dimensional domain only requires adding an additional one-dimensional sequence. The first d coordinates in the d+1-dimensional domain remain the same as of the d-dimensional domain.

In the context of this thesis, it is proposed to use the Scrambled Halton LDS for a parameter sweep as in Chunduri et al. (2018) interchangeably for the pedestrian and infection models. The results are then compared to lattice to prove the efficiency of LDS in terms of faster convergence and execution time. Also, if additional variables are added later to the multi-scale model, the scrambled Halton sequence enables re-using previous output files.

3. Multiscale Model for Pedestrian and Infection Dynamics during Air Travel

In this chapter, a novel multiscale model combining social force-based pedestrian movement with a population level stochastic infection transmission dynamics framework is edeveloped. The model is applied to study the infection transmission within airplanes and airport gate, and the transmission of Ebola, H1N1 and SARS viruses through casual contacts. The computational model is used to evaluate the effects of passenger movement within airplanes and airport gate, and the air-travel policies on the geospatial spread of infectious diseases. The schematic in Figure 3.1 depicts the overall approach of this modeling study. Aggregated results indicate that passenger movement strategies and airplane size predicted through these network models can have a significant impact on an event like the 2014 Ebola epidemic. The methodology developed here is generic and can be readily modified to incorporate impact from outbreak of other directly transmitted infectious diseases.
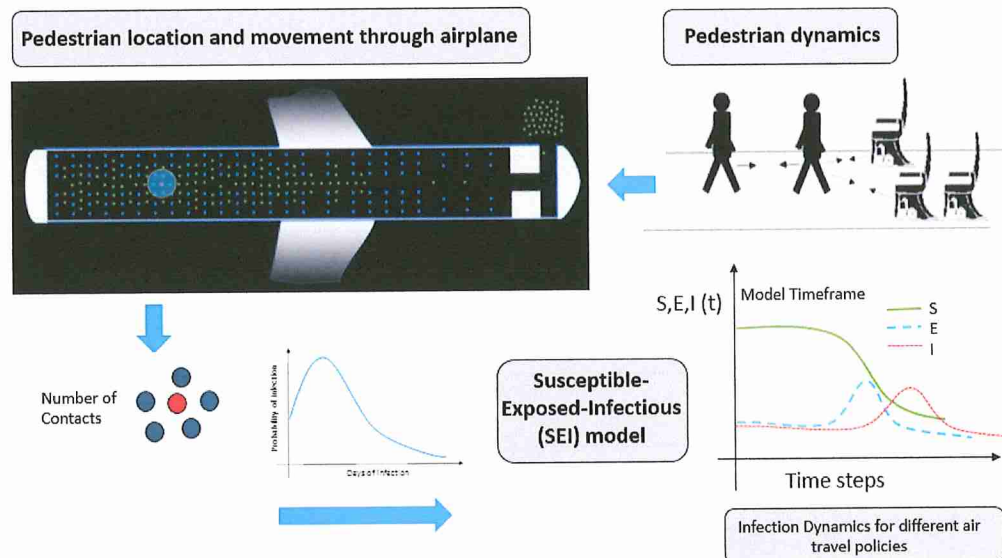
Figure 3.1. Schematic of the infection analysis during boarding from a gate.

3.1 Model Formulation of the Pedestrian Movement

In the problem setting, the model the motion of pedestrians is mdeled using a molecular dynamics approach based on the social force model proposed by Helbing and Molnar (1995) that captures the actual interaction of pedestrians with their environment in real-life situations. While heading towards his designated destination, the behavior of an individual is influenced by his inclination to navigate effectively towards his targeted terminus. However, delays are always expected due to impediments manifested with stationary crowds or physical barriers obstructing the course of motion.

Considering the self-propelled pedestrian P_i as a point mass m_i in a two-dimensional space, and applying Newton's second law of motion, the net resulting force $\vec{F}_i$ is expressed by:

$$\vec{F}_i = \sum \vec{f}_i = \vec{f}_i^{int} + \vec{f}_i^{ped} = m_i \vec{a}_i \tag{3}$$

Where $\vec{f}_i^{int}$ is the intention force motivating the pedestrian to pursue his track despite the fact that a resulting opposing force $\vec{f}_i^{ped}$ is exerted by the surroundings to delay his locomotion. Note that $\vec{a}_i$ is the acceleration vector of particle "i".

The force $\vec{f}_i^{int}$ in the motion direction $\hat{e}_v$ is the rate of change of momentum within a time interval (step) τ and is defined by:

$$\vec{f}_i^{int} = f_i^{int} \, \hat{e}_v = m_i \left(\frac{\overline{\Delta v}}{\tau} \right) = m_I \left(\frac{\vec{v}_{oi}(t) - \vec{v}_i(t)}{\tau} \right) = m_I \left(\frac{v_{oi}(t) - v_i(t)}{\tau} \right) \hat{e}_v \tag{4}$$

Here, $\vec{v}_i(t)$ designates the actual instantaneous velocity of the pedestrian P_i and is characterized by its magnitude and its anticipated orientation.

The desired speed $v_{oi}(t)$ is modified in the intention force expression, Equation (4), and introduced a term that adjusts the pedestrian speed depending on the proximity of its

local surroundings. During enplaning or deplaning, pedestrians form a line and the desired velocity of the self-propelling pedestrian is dependent on its distance with respect to the nearest forward pedestrian in the same direction of motion. In the designed model, the pedestrian can move in the direction of motion assigned to the hallway where he is located at. Let $\hat{e_1}$ and $\hat{e_v}$ denote the unit vectors of directions attributed to the hallway and the pedestrian respectively. Since the pedestrian P_i is not impeded by any obstruction, $\hat{e_1}$ is the same as $\hat{e_v}$. Therefore, in line forming, the desired speed at time t, $\vec{v}_{0i}(t)$, is obtained from the relation:

$$\vec{v}_{0i}(t) = v_{0i}(t).\hat{e_v} = v_{0i}(t).\hat{e_1} = (v_A + \gamma_i v_B)(1 - \frac{\delta}{\|\vec{r}_i - \vec{r}_j\|}) . \hat{e_1} \qquad (5)$$

The vector positions of pedestrian P_i and traveler P_j in his way are denoted by $\vec{r}_i$ and $\vec{r}_j$ respectively, and are issued from the origin of the coordinate system of the plane of motion. The pedestrian free speed is a cumulative frequency distribution that varies between individuals, the purpose of travel and the facility (Chandra & Bharti, 2013). In this model, this is accounted for in the ultimate desired speed term $(v_A + \gamma_i v_B)$ ranging between v_A and $(v_A + v_B)$. Here, γ_I is a positive random variable less than unity attributed to pedestrian "i" considering the factors that can affect his mobility such as age, sex, body type, health condition, etc. (Knoblauch et al., 1996; Zębala et al., 2012). However, this free speed is adjusted for the upcoming obstructions within a distance δ.

In particular, when traveler P_j is distant from traveler P_i in such a way that the latter's motion is not affected ($\|\vec{r}_i - \vec{r}_j\| \gg \delta$) then, equation (5) reduces to:

$$\vec{v}_{0i}(t) = v_{0i}(t).\hat{e_v} = v_{0i}(t).\hat{e_1} = (v_A + \gamma_i v_B).\hat{e_1} \qquad (6)$$

In the course of embarkation and deplaning, the impenetrability with other pedestrians and obstacles should be ensured. This is achieved by the repulsive force $\vec{f}_i^{ped}$. In

literature, power functions and monotonically varying exponential expressions are used

to evaluate the repulsion term (Helbing & Molnar, 1995; Helbing et al., 2000; Wei-Guo

et al., 2006; Li & Jiang, 2014; Zanlungo et al., 2011). In other studies, the repulsive force

is estimated from visual analyses as in Mehran et al. (2009). In this study, for the

repulsive term, the same Lennard-Jones potential used by Namilae et al. (2017a) is again

used. Thus, $\vec{f}_i^{ped}$ is obtained from the gradient of the higher-order term in Lennard-Jones'

potential as follows:

$$\vec{f}_i^{ped} = \sum_{i \neq l} \vec{\nabla} \, \varphi(r_{il}) = \sum_{i \neq l} \vec{\nabla} \left[\epsilon \left(\frac{\sigma}{r_{il}} \right)^{12} \right] \tag{7}$$

Where ϵ and σ are repulsive force field parameters ($\epsilon = 16$, $\sigma = 0.86m$) and r_{il} is the

distance between the ith and the lth pedestrian.

There are several parameters in the pedestrian dynamics model, such as maximum

walking speed $v_A + v_B$, random variation γ_i, distance parameter δ, two parameters for the

Lennard-Jones repulsive-force terms (ϵ and σ), and aisle delay for luggage. There is

experimental data available for some of the parameters such as the range of walking

speed (Knoblauch et al., 1996; Zębala et al., 2012). Also, the observed exit times and

passenger flow rate for some commercial airplanes are available in the literature (Marelli

et al., 1998; Wald et al., 2014).

In an earlier study, Namilae et al. (2017a) used a parameter sweep on 60,000

processors to determine the parameters that match the available observed data of

deplaning (Marelli et al., 1998; Wald et al., 2014). Namilae et al. (2017a) have been able

to match the pedestrian dynamics model with experimental data on flow rates and exit

times for five different airplane seating configurations for which test data are available. In

addition, Namilae et al. (2017a) have also been able to capture qualitative features such

as front to back unloading and hallway congestion. The pedestrian dynamics parameters

obtained through their work are used in the current model and are tabulated in Table 3.1.

In this thesis, a similar parallel computing approach is used to quantify the uncertainty in

model parameters related to infection spread over a large design space.

Table 3.1

Parameters ranges and values used in the suggested model.

Parameters	Definition	Estimate or range
$\bar{v}_{0i}$	free waking speed (no obstructions)	1.07-1.55 m/s
γ_i	random number	0-1
δ	distance parameter (distance between people in a stationary line)	0.405m
ϵ	repulsive-force field parameter	16
σ	repulsive-force field parameter	0.86m
P_c	Infectivity of individual as a function of age of infection (c days)	0.01-0.098
D	Maximum number of days for virus incubation	1-21 days
i_c^0	Number of infectives with an age of infection of c days	1

The theoretical approach, stated above, for modeling pedestrians in motion is

integrated by means of a Molecular Dynamics approach to generate the instantaneous

motion characteristics of pedestrians. At this level, the pedestrian motion is modeled

within aircraft and at an airport gate. The time evolution of pedestrian trajectories has

been displayed for both egress from an Airbus A320 carrier (Figure 3.2) and ingress from

a gate (Figure 3.3) for comparison of outputs. During the enplaning, the trajectories of

passengers, initially seated or standing in the departure lounge, heading to the passenger

boarding bridge and finding their assigned onboard seats, are modeled. In both scenarios,

the instantaneous position and speed of each walking individual are obtained from

solving equation (3) using a predictor-corrector numerical integration. Many qualitative

features of pedestrian movement are captured by the model. For instance, lane formation

is observed in the hallways, in addition to the reduced speed at bottlenecks where

passengers from different seating zones merge and head to the airplane (Figure 3.3).

Similar features are observed in egress when passengers walk out of their seats toward

the aisle (Figure 3.2).
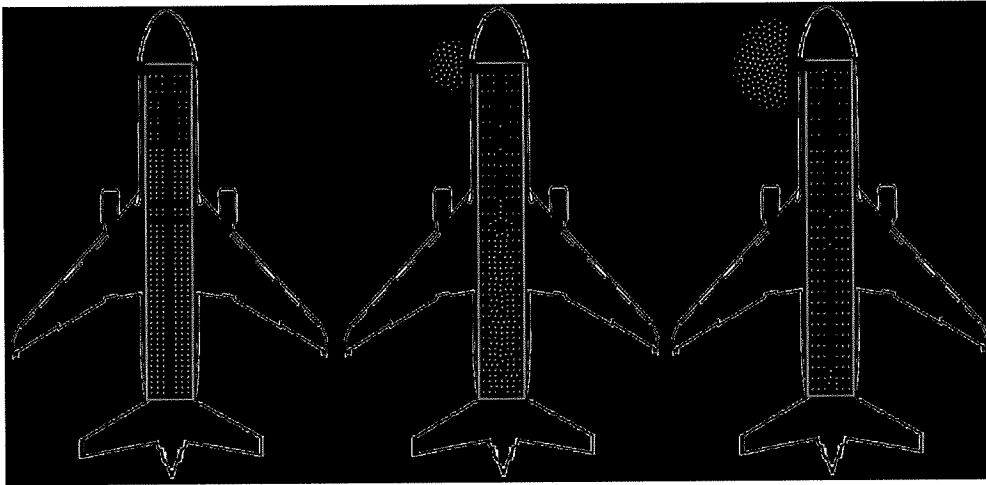
Figure 3.2. Simulation snapshot of Airbus A320 deplaning at different time steps.
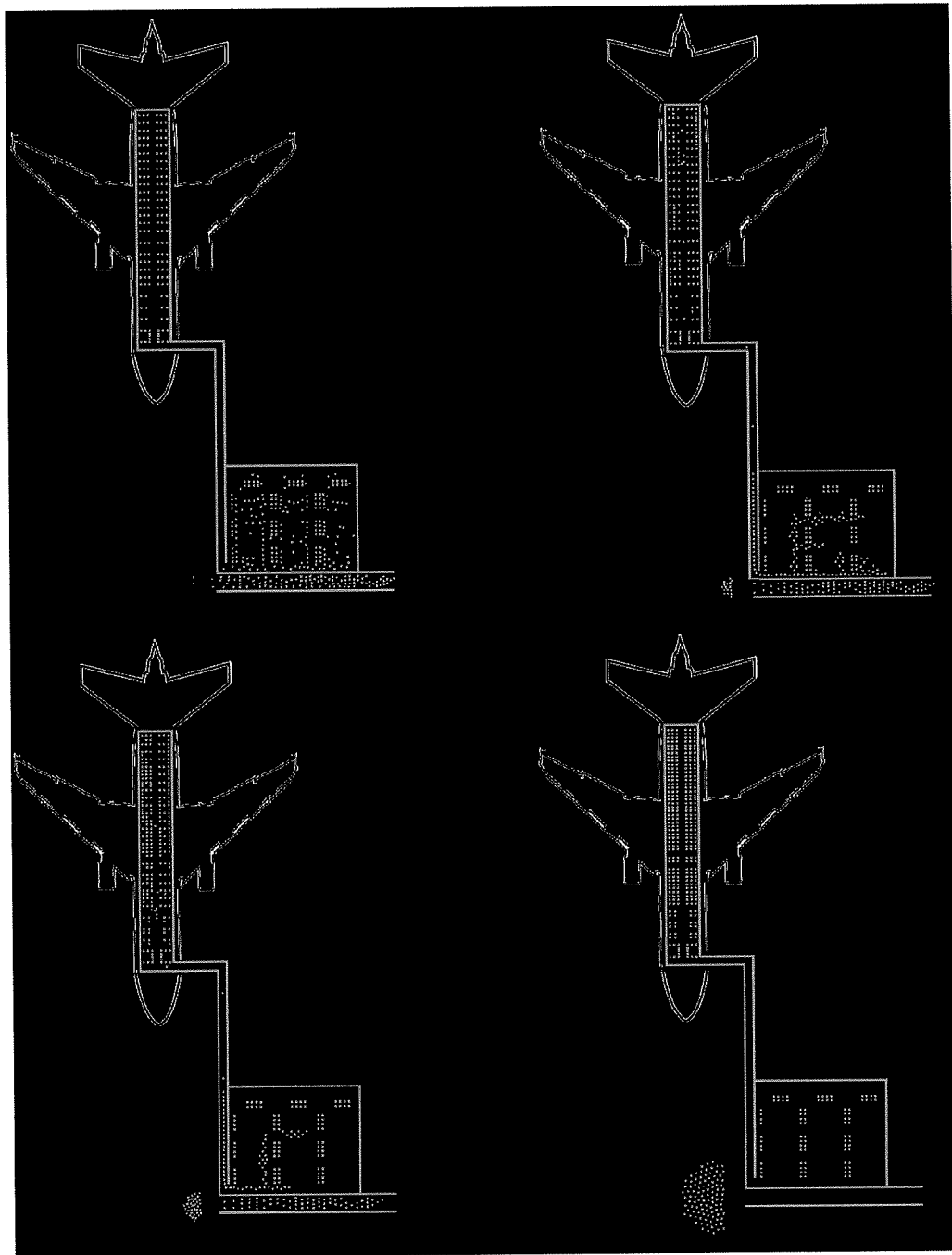
Figure 3.3. Simulation snapshot of embarkation of an Airbus A320 from a departure lounge at different time steps.

Once the pedestrian trajectory information from the above model is obtained, the data

is integrated with a discrete-time stochastic Susceptible-Infected (SI) model for infection

transmission discussed in the following section. Then, the overall multiscale model combining the pedestrian model with the infection stochastic model estimate the number of newly infected susceptible who came into proximate contact with the infective traveler within the gate or aboard the airplane.

3.2 Stochastic Infection Spread Model

The study of epidemics informs how disease propagates and what are the suitable policies to suppress or inhibit its spread. Therefore, the Susceptible-Infected (SI) dynamic model (Keeling & Rohani, 2008) of an epidemic is employed for the purpose. A population of size N consisting of I(t) infected and S(t) susceptibles at time t is assumed. A susceptible becomes infected when coming into direct contact with an infected. However, the newly infected cannot be infective during the start of the incubation period of the illness (there is no second reproduction of the illness). At time t, N, I(t) and S(t) are related by:

$$N = I(t) + S(t) \tag{8}$$

The infection spread initiates due to the insertion of i_c^0 infectives initially ($t_0 = 0$) at their "c" days of infection. Thus,

$$N = \sum_{c=1}^{d} i_c^0 + S(0) \tag{9}$$

where d is the extent of the illness post-onset of the symptoms at day one.

Let "m" be the total number of contacts per individual per time step and N the total population size. Assume the presence of a single infectious individual at c days of infection. The probability that this infective meets other individuals is m/N. Denote by P_c the probability that contact between a susceptible and an infective, whose age of infection is τ days, results in infection of the susceptible. The number of contacts s is estimated

using the pedestrian trajectories from the pedestrian dynamics model described in the previous section.

The axiom of the conditional probability (Bayes' theorem) is given by:

$$P \text{ (contact and infection)} = P \text{ (infection/contact)} \cdot P \text{ (contact)} = P_c \cdot \frac{m}{N} \qquad (10)$$

Therefore, the number of susceptibles infected by this infective is binomially distributed with parameters n= S(t-1), the number of susceptibles exposed to the contagion at time t, and $p = P_c \cdot \frac{m}{N}$. In this situation, n is large and p is very small (below 0.1). Accordingly, the Poisson distribution can be used to approximate the binomial distribution with mean $\lambda = n.p = S(t-1). P_c \cdot \frac{m}{N}$ and is written as:

$$I(t) \sim \text{Poisson} \left[m\frac{S(t-1)}{N} \sum_{c=1}^{d} p_c \right] \qquad (11)$$

Since an infective placed in a totally susceptible population would infect $m. p_c$ people on the cth day of infectivity, the total number of infections that an infective would produce at time t, that is the reproduction number R_0, is given by:

$$R_0 = m \sum_{c=1}^{d} p_c \qquad (12)$$

The reproduction number R_0 defines the average number of people infected by a typical individual over his/her infectivity period (in the model this represents the duration of enplaning and deplaning) in a totally susceptible population.

Let P_c be the ratio of the probability of infection at day "c" over the summation of the infectivity along the days of illness, thus:

$$P_c = \frac{p_c}{\sum_{c=1}^{d} p_c} \qquad (13)$$

Replacing Equation (12) and (13) in (11) yields:

$$I(t) \sim \text{Poisson} \left(R_e \sum_{c=1}^{d} P_c \right) \qquad (14)$$

where R_e is the effective reproduction number and is given by:

$$R_e = \left[\frac{S(t-1)}{N}\right] R_0 \tag{15}$$

For multiple infectious individuals at time $t_0=0$, the number of newly infected by an ith infective at time t, a discrete variable is a Poisson probability distribution, with mean m_i (t-1). $p_c.[S_i (t-1)/N]$. Therefore, the number of people infected at time t by all the infectives with an age of infection "c" is Poisson distributed with a mean $\sum_{i=1}^{i_c^0} \left[m_i(t-1). p_c .\left(S_I \frac{t-1}{N}\right)\right]$. Summing over all values of c, I(t) is given by:

$$I(t) \sim \text{Poisson} \left(\sum_{c=1}^{d} \left(\sum_{i=1}^{i_c^0} \left[m_i(t-1). p_c .\left(S_I \frac{t-1}{N}\right)\right] \right)\right) \tag{16}$$

where m_i is the number of contact of susceptibles with the ith infectious traveler and p_c the infection transmission probability.

Again, plugging Equations (12) and (13) in (16) gives the equation of the Poisson distribution in terms of the effective reproduction number and the probability ratio:

$$I(t) \sim \text{Poisson} \left\{\sum_{c=1}^{d} \left[m. p_c \sum_{i=1}^{i_c^0} S_I (t-1)/N\right] \right\}$$

$$= \text{Poisson} \left\{\sum_{c=1}^{d} \left[R_0. P_c \sum_{i=1}^{i_c^0} S_I (t-1)/N\right] \right\} \tag{17}$$

Once the travelers' trajectories have been generated, the pedestrian moment model, combined with the stochastic infection dynamics formulation, determine the extent of disease propagation among the travelers onboard. The probability of infection (p_c)has a major influence on the findings as it determines the total of newly infected passengers who were exposed to the contamination within a suitable environment for propagation. The probability profile p_c of the disease under investigation has to be obtained and implemented in Equation (17) to obtain the Poisson distribution of infected travelers.

The probability-distribution of infection transmission varies depending on the incubation periods and transmission rates for specific diseases. In the context of air-travel of a few hours, a newly infected passenger does not become infective but reduces the total susceptible population. When these infectives come into contact with susceptibles as determined by the pedestrian movement model, the newly infected at time t and the probability of their infection can be estimated as the Poisson approximation of binomial distribution. The use of Poisson distribution here accounts for demographic stochasticity and variations in susceptibility of the population. Inherent uncertainties in human behavior and stochasticity in infection spread make precise predictions of number of infections difficult. Instead, the pedestrian movement strategies are identified during air travel that generally lead to reducing the spread of infectious diseases.

3.3 Probability of Infection

During an epidemic outbreak, the prevalence of the disease in a large population relies on the ability of a pathogen to establish unrestrained reproductive infections. Consequently, disease control, suppression or prevention starts by determining the core of its initiation as well as the incidence, medium, range and probability of propagation. During the progression of the illness, the variation of antigens in the blood serum can be captured, and it determines the severity of the patient's situation. The probability-distribution of infection transmission varies depending on the incubation periods and transmission rates for specific diseases. For example, for the Ebola virus, the mean incubation period is 12.7 days (Eichner et al., 2011), with logarithmic increase in virus levels in blood and transmission probability during acute illness phase (Centers for Disease Control and Prevention, 2014).
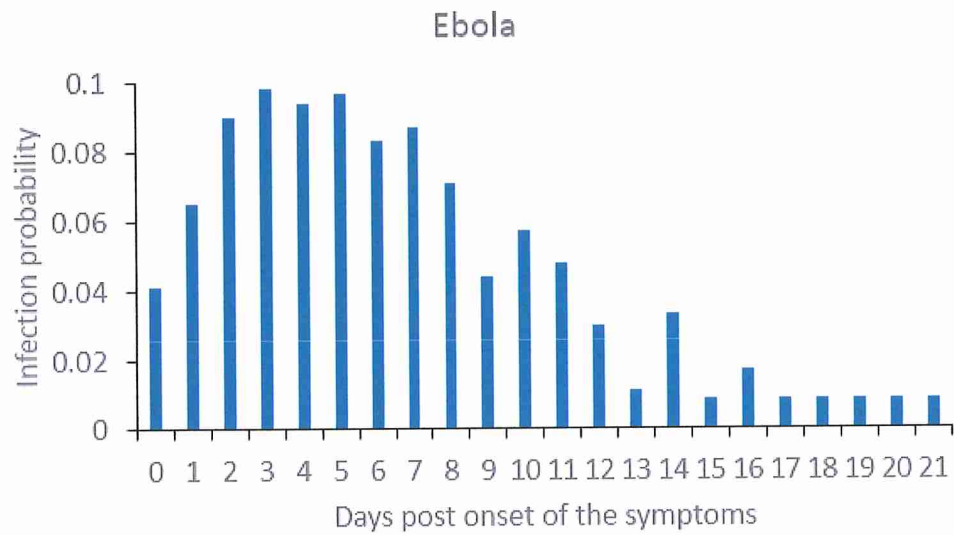
Ebola

Figure 3.4. Infectivity profile along the days after clinical signs of Ebola infection.
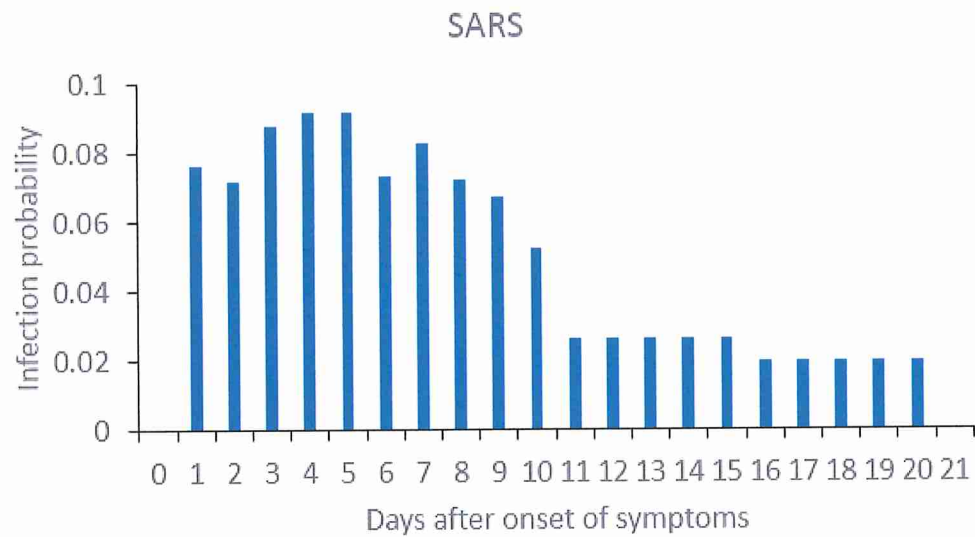
SARS

Figure 3.5. Infectivity profile along with the days post-onset of SARS symptoms.
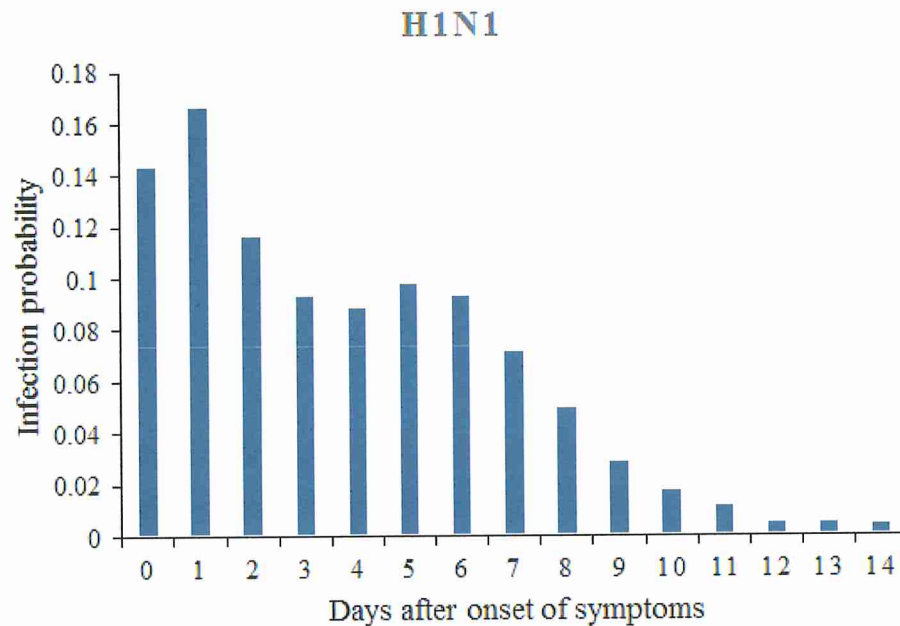
Figure 3.6. Infectivity profile along the days post-infection with H1N1 virus.

In this study, observations of the evolution of the antibodies are referred to within the incubation period of the virus to generate what is referred to as the infectivity profile. The simulations are carried out for Ebola, SARS and H1N1 Influenza viruses since these contagions were previously encountered in air travel (Baker et al., 2010). For Ebola, the infectivity profile is acquired by the amount of RNA (ribonucleic acid) virus copies above the detection threshold in the blood serum since the illness contraction (Towner et al., 2004). The daily logarithmic amounts of RNA for fatal and non-fatal contagion are averaged along the 21 days of illness period, then divided by the total to obtain the probability of infection at a designated day (Figure 3.4). For SARS pathogen, the viral gene expression of the nucleocapsid (N) protein (Figure 3.5), detected at different rates along the evolution of the virus from post-onset of the symptoms till convalescence is indicative of the possibility of transmission (Zhao, 2007).

For Influenza H1N1, sometimes the viral shedding and RNA are not detectable (especially until 5-6 days of onset of symptoms) in positively tested patients (Yu et al., 2010). The contraction of the influenza virus is also replicated in mammals. For instance, experimental investigations are conducted on pigs (Wiersma et al., 2015; Brookes et al., 2010), mice (Kim et al., 2015) and ferrets (Paquette et al., 2015) for better observation and understanding of the virus. The H1N1 nasal, oral or ocular shedding has been detected by determining the relative equivalent unit (REU) from viral RNA level (Brookes et al., 2010). In this model, it is assumed that the transmission of Influenza disease occurs through aerosols expelled during coughing, sneezing or talking thus via nasal route. Therefore, the infectivity profile for H1N1 virus is obtained from measuring the evolution rate of Reticular-Erythematous-Ulcerative (REU) in saliva from the first day of disease contraction. The infectivity profile is shown in Figure 3.6. The infectivity data for the three viruses under investigation is then combined with the number of contacts between pedestrians generated using the pedestrian movement model to assess the extent of disease propagation among the travelers onboard.

3.4   Results and Discussion

3.4.1   Enplaning and Deplaning Aboard an Airplane

The situation with one infected individual with Ebola traveling on a commercial airplane is considered. The infective passenger onboard is not identifiable; therefore, the seating position of the infected individual is varied through all the seats in the airplane. Due to the stochastic nature of the problem, it is assumed that the number of newly infected travelers by a single infectious chosen randomly among the airplane passengers is Poisson distributed with mean λ_i at every simulation. After performing all the

simulations in parallel, the effective probability of means is calculated. Then, using the Bayes' theorem the probabilities are combined to generate the probability distributions. This approach is used to evaluate air travel policies such as boarding and deplaning strategies, and airplane seating capacity that impact infectious disease spread.

The boarding and exiting strategies have been investigated with respect to minimizing the turn-around time of airplanes at boarding gates (Marelli et al., 1998; Wald, Harmon & Klabjan, 2014). Several passenger ingress strategies such as random, outside-in, back to front, column-wise, zone/section style enplanement have been studied. A few of the boarding strategies are compared with respect to spread of infections. In Figure 3.7, it is shown that the three-sections boarding method has the highest mean, thus represents the worst strategy for reducing spread of infection. Many current airlines use such a strategy with multiple zones or sections. In this method, passengers sitting in the front of the aircraft (e.g. first class) board first followed by a middle zone and then the back section of the airplane. Because of this pattern, the passage-way is filled with passengers waiting to get to their seats resulting in clustering and increased exposure with infected passengers, resulting in a higher number of newly infected passengers.

The column-wise method, used here, is the same as the outside-inside strategy in a front-to-back manner. This scheme also results in more infected members. A two-section strategy involves dividing the plane into two sections and the passengers are randomly boarded within these sections. For the random and two-sections boarding, passengers close together in a queue may be seated in seats that are wide apart. This leads to arbitrary movement of passengers along the cabin preventing clustering of a group of travelers around the infected passenger which in-turn reduces infection transmission. The

two-section and random boarding have the same mean value of two newly infected, although the infection transmission for two-section strategy results in a lower probability of infection at the mean. This model suggests that this approach may be a good choice to minimize infection transmissions during boarding. A similar pattern of results is found for 144-seat Airbus A320 seating configuration as well as 182-seat Boeing 757-200 seating configuration (see Figure 3.7 a & b). In all these simulations the airplanes contain a single Ebola-infected passenger with infectivity corresponding to one day of infection in an unidentified seating location with a contact radius of 1.2 m.
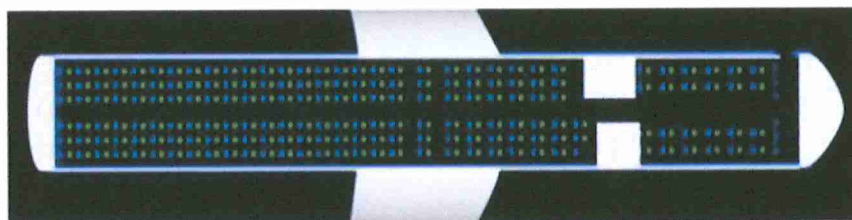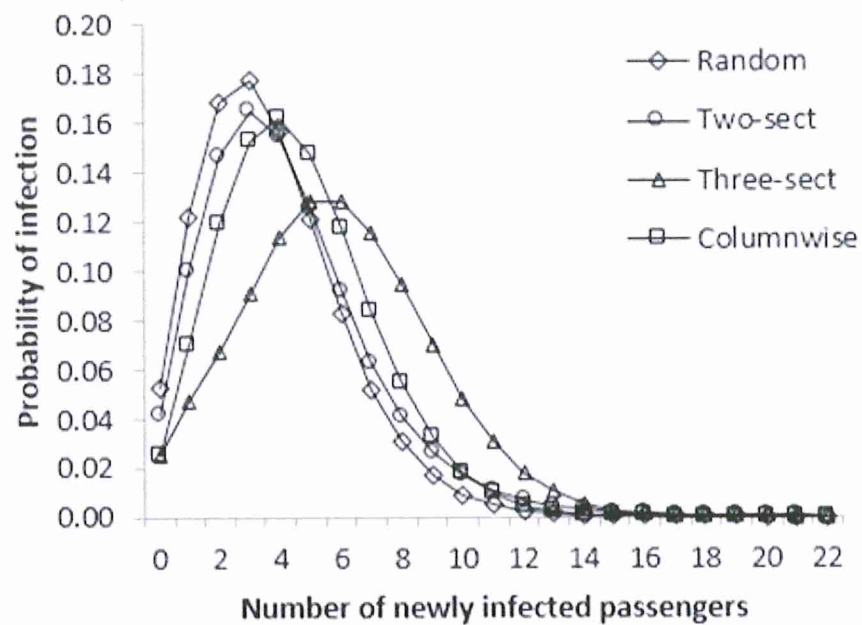
(a)
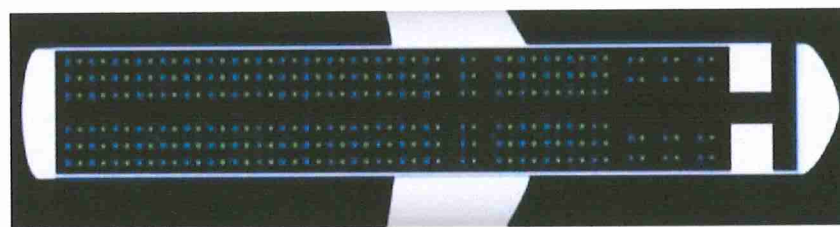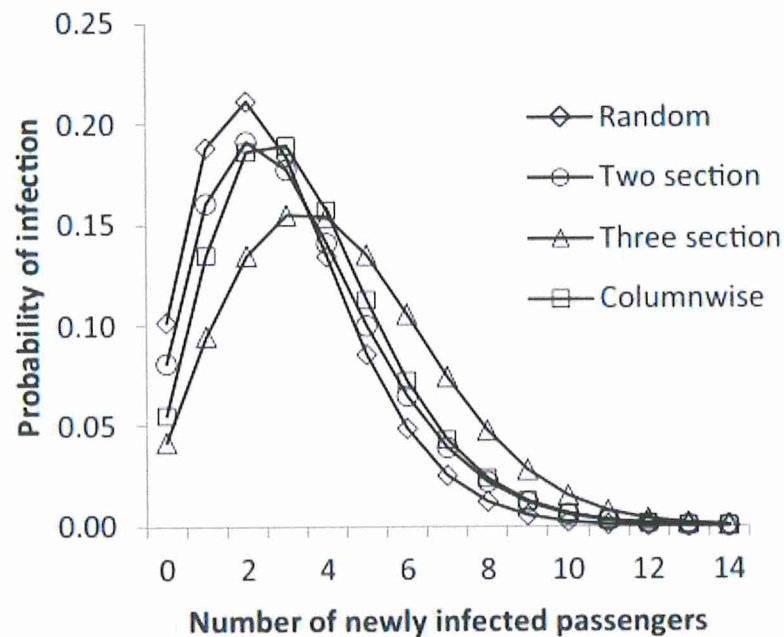
(b)

Figure 3.7. Infection distribution profile at different boarding strategies for (a) Boeing 757-200 capable of 182 passengers, (b) Airbus A320 capable of 144 passengers. The pictures on the bottom show the corresponding aircraft seating configurations with seats (b) Airbus A320 capable of 144 passengers. The pictures on the bottom show the corresponding aircraft seating configurations with seats (blue dots) and pedestrians (green dots).

A similar approach is followed for deplaning strategies. It is found that deplaning had a smaller impact on infection dynamics because of the lower number of new contacts and lower time of exposure during the comparatively faster process. Figure 3.8 shows a comparison of deplaning strategies for the Boeing 757 182-seating configuration. The different deplaning strategies such as alternating columns, alternating rows, zone wise

and baseline (closest to exit-out first) result in similar number of mean infectives. When

comparing the probabilities, alternate rows and baseline strategies are marginally better.

In Figure 3.9, the mean infectives is computed by combining the egress, ingress, and in-

plane movement. It is apparent that other pedestrian movement strategies can be better

than boarding using multiple zones. It is shown that the worst-case situation where an

infected individual with peak infectivity is seated at a location that results in the highest

number of contacts.
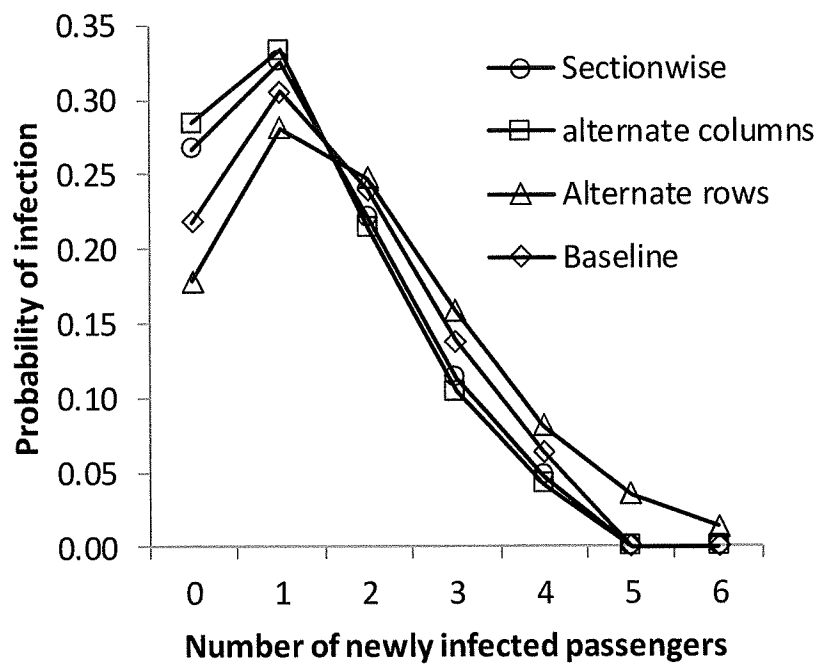
Figure 3.8. Infection distribution profile for different deplaning strategies for 182 seat
Boeing 757.
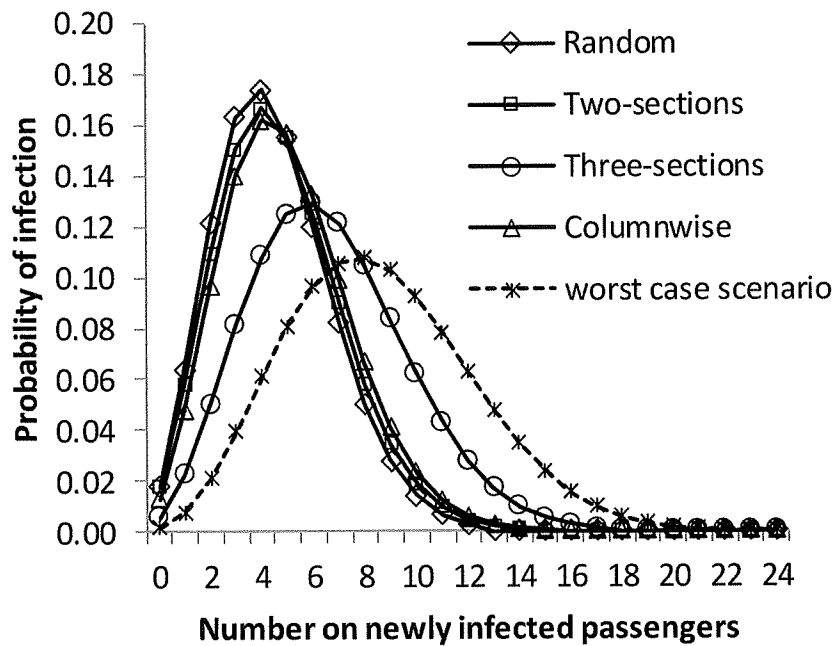
Figure 3.9. Infection distribution profile for different deplaning strategies for 182-seat Boeing 757.

There is inherent uncertainty in the human movement behavior as well as the stochasticity in the infection model. Many parameters affect the simulations including airplane size and seating arrangement, the number of infective passengers, the infectivity characterized by days post-onset of symptoms, the radius of infection which in turn depends on transmission mechanics (e.g. coughing, talking, etc.), and the susceptibility of population. It is necessary to assign values for some of these parameters for deterministic analysis. However, the uncertainty in these parameters needs to be quantified to assess effective air travel policies under a broad set of conditions. The variations in some of those parameters is studied.

According to CDC data, a nonfatal Ebola infection lasts for 21 days post-onset of symptoms, with highest virus shedding rates and correspondingly highest infectivity in

days 3-5 of disease development (Centers for Disease Control and Prevention, 2014). The three-zone boarding simulations are repeated by varying the number of days of infection for an infective person as shown in Figure 3.10. The number of mean newly infected passengers clearly varies with the infectivity of the index passenger.
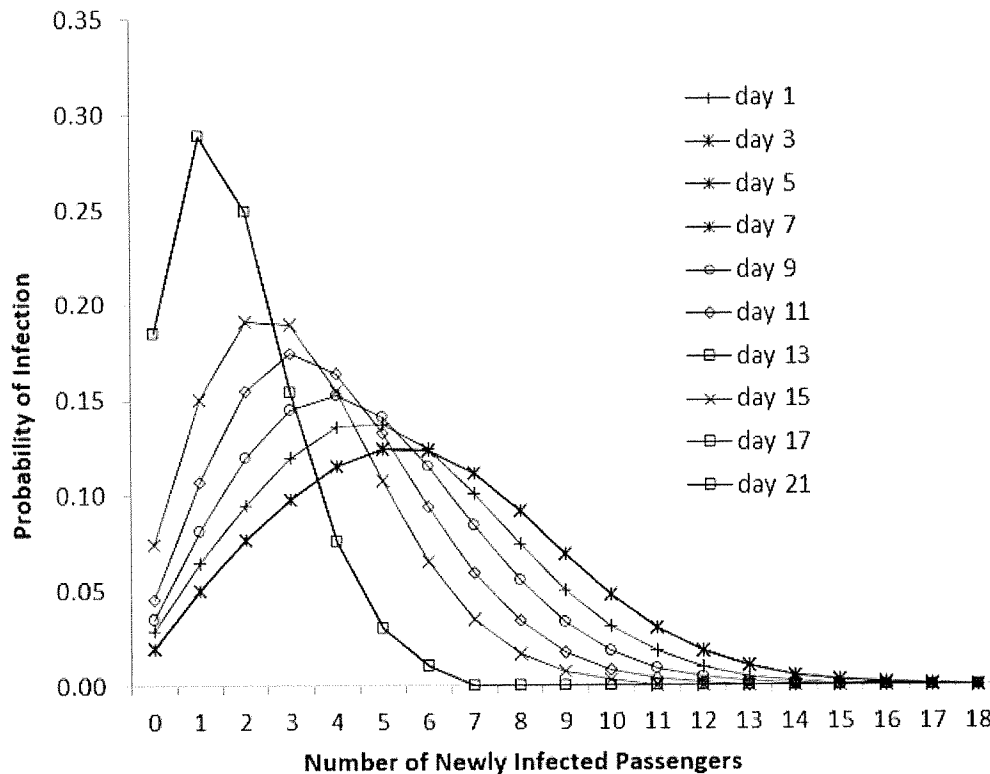
Figure 3.10. Infection distribution profile varying the days of infection for the index case. Three-zone boarding strategy for 182 passenger seating configuration is used for these simulations.

During a known outbreak, reported infected passengers will most likely be grounded for further monitoring, but there have been cases of newly infected passengers traveling through commercial airplanes (Regan et al., 2015; Sky Talk, 2014; Shuaib, 2014). One such example is the case of the medical professional, who was on Frontier Airlines flight from Cleveland to Dallas on October 13, 2014 (Regan et al., 2015). Contact tracing indicated that the case did not lead to further infections. According to the simulations, the

probability of zero new infected cases is around 7% with a fully loaded flight. However, the flight capacity is 168 passengers and the CDC reported that 132 passengers shared the flight (Sky Talk, 2014). The vacant seats in the flight may have further helped in mitigating further spread.

Another critical model parameter is the contact radius which is the minimum distance at which a susceptible passenger in the proximity of the infective can be potentially infected. The distance to which particles travel depends on the particle size and associated fluid mechanics in expiratory events like coughing and talking (Bourouiba et al., 2014). Experimental investigations measure particle size in these expiratory events to be in the range of 0.1 to 10 μm (Morawska et al., 2009; Papineni & Rosenthal, 1997) and have been estimated to travel over 2 m (Bourouiba et al., 2014; Gupta et al., 2009). The transmission distance also depends on specific disease, for example, SARS has been transmitted by short-range droplet-based as well as longer-range airborne mechanisms (Clark & de Calcina-Goff, 2009). The primary mode of transmission for Ebola is through contact droplets, but studies on monkeys indicate possible transfer through aerosols (Jaax et al., 1995). Mangili and Gendreau (2005) indicate that large droplets and airborne mechanisms are possibly highest risk transmission mechanisms during air travel.
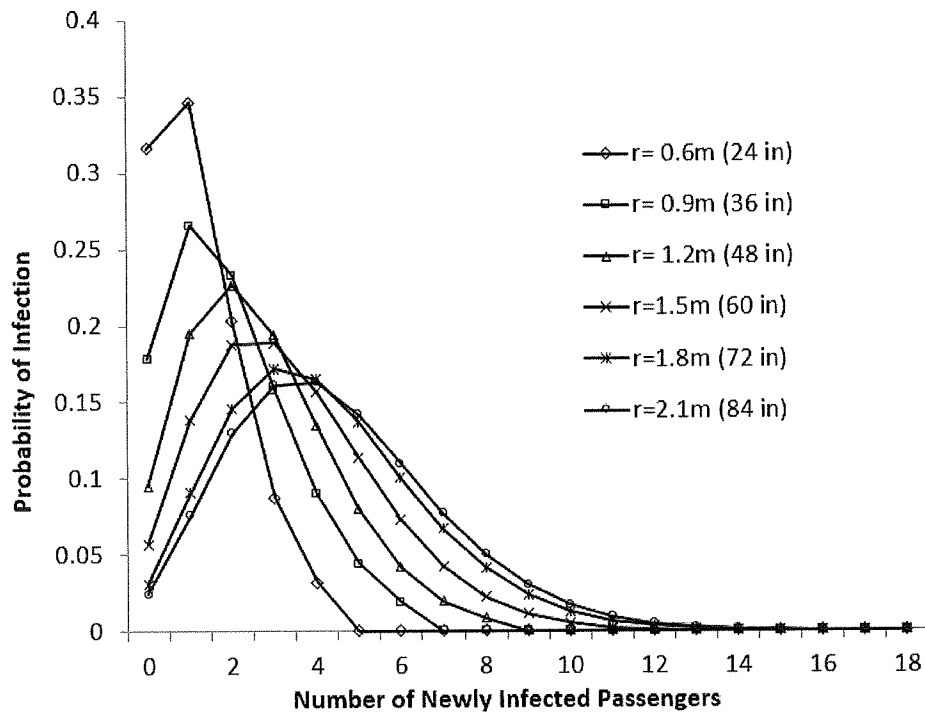
Figure 3.11. Infection distribution profile varying the contact radius for infection transmission. Three-zone boarding strategy for 182 passenger seating configuration is used for these simulations.

The effect of environmental variation and transmission methods on the contact radius is account for by varying it from 0.6 m (24 inches) to 2.1 m (84 inches) as shown in Figure 3.11. The typical seat width on airplanes is 18 inches (0.45 m). A distance between passenger particles of 24 inches (0.61m) is considered as a touching distance. The lower end of the range in Figure 3.11 signifies a contact-based and large droplet mechanism while a larger contact radius may be more relevant for aerosol-based mechanisms. As expected, the number of newly infected passengers is lower when the contact radius is lower.

In the model, the effect of the size and seating capacity of the airplane on infection propagation is considered. For instance, consider the case of transporting 1000

passengers aboard different capacity air-carriers. Different numbers of flights are required based on the selected cabin configuration. Small air-carriers require a greater number of flights compared to larger cabin configurations. It is also assumed that a single infective is onboard every flight so that the passengers on each flight are exposed to the infection by means of an infective passenger. Figure 3.12 shows the effect of airplane size with a random boarding strategy. It is shown that smaller airplanes such as CRJ-200 are better in reducing the spread of infection compared to larger capacity airplanes; however, the advantage with smaller seating capacity of airplanes quickly vanishes as the number of seats increases beyond 150. The smaller size of the susceptible population, the lower number of susceptibles within a given contact radius and the reduced time of in-plane movement are some of the factors that benefit smaller airplanes.
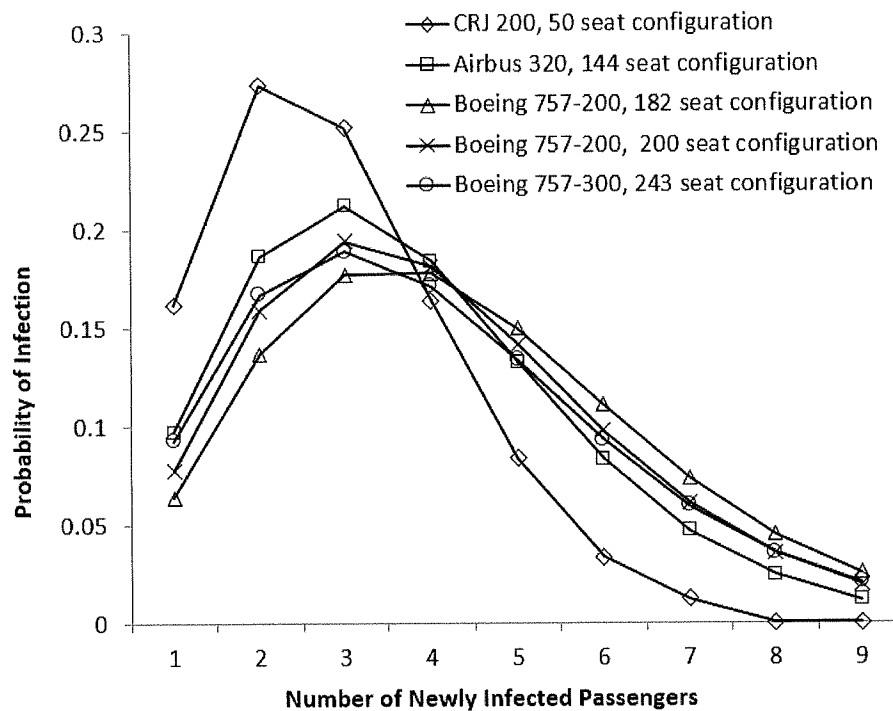
Figure 3.12. Infection distribution profile for random boarding strategy.

3.4.2 Comparison between Multiple Diseases

The plots (Figures 3.13 and 3.14) represent the probabilistic distribution of infected passengers who were closely exposed to Ebola, Influenza H1N1 and SARS viruses. These viral organisms are transmitted through direct contact or dispersion of particles exhaled from an infectious member by talking, coughing or sneezing, and remain sustained in the environment for a certain time before depositing and contaminating contiguous surfaces (Jones & Brosseau, 2014; Wang, 2005).

Mangili and Gendreau (2005) indicate large droplets and airborne mechanisms are possibly highest risk transmission mechanisms during air travel. The transmission distance also depends on the specific disease. For example, SARS has been transmitted by short-range droplet-based as well as longer-range airborne mechanisms (Clark & Calcina-Goff, 2009; Li et al., 2004). The primary mode of transmission for Ebola is through contact droplets (Centers for Disease Control and Prevention, 2014), but studies with monkeys indicate possible transfer through aerosols (Jones & Brosseau, 2014; Jaax et al., 1995). Likewise, the influenza virus may be transmitted through coarse droplets or microscale bioaerosols being respired into the respiratory tract of a susceptible member (Wong & Yuen, 2005). There's a debate on the nature of transmission of Influenza virus. Wong and Yuen (2005) suggest that transmission occurs when the virus particles are suspended in air and inhaled by a susceptible individual or when that individual touches a contaminated surface with deposited droplets and then touches their eyes, nose or mouth.

The size of these particles as well as the environmental condition play an important role in contagion dispersion. Small particles dispersed in aerosols transmit over large distances, for example, experiments indicate micrometer-sized aerosol clouds generated

during cough traveling over 2 m (Bourouiba et al., 2014; Gupta et al., 2009). Smaller aerosols can be driven farther by ventilation or a freestream flowing from a high static pressure location to a lower pressure zone (Tang et al., 2006). Based on primary modes of transmission, coarse droplets for Ebola and aerosol for SARS and H1N1, radii of infection of 1.2m (48 in) and 2.1m (84 in) are assumed respectively. Note that the infectivity profiles for both Ebola and SARS are quite close in values and less than 0.1, so the selection of radii of infection makes a noticeable difference in the number of contacts and transmission. For Influenza virus, the infectivity is at a higher rate compared to Ebola and SARS. This can be reflected by the reproduction number R_0. For instance, an infectious agent with SARS can reproduce 2-3 newly infected individuals, but this range increases considerably to an upper limit of 20 for H1N1 (Tang et al., 2006).

In Figure 3.13, an infectious passenger is considered on his first day is onboard among the susceptible population. Ebola and H1N1 record a peak of 2 newly infected passengers exposed to the virus, whereas this number increases to 5 for SARS due to the wider range of infectivity. Shifting the infectivity to its highest (day 3 for Ebola, day 5 for H1N1 and day 4 or 5 for SARS), the means of the Poisson distribution increases by one unit for Ebola and SARS but expands tremendously for H1N1 since the infectivity reaches its peak of 30% at the fifth day of H1N1 infection.

From the results for deplaning under similar conditions, shown in Figure 3.14, it can be noticed that the distribution of newly infected individuals behaves in the same way as that of Figure 3.13. However, the mean number of infected reduces to 1 for H1N1 and Ebola and to 2 to SARS on day 1. The egress phase is of a shorter period of time compared to boarding, therefore, there are fewer contacts and lower number of infected.
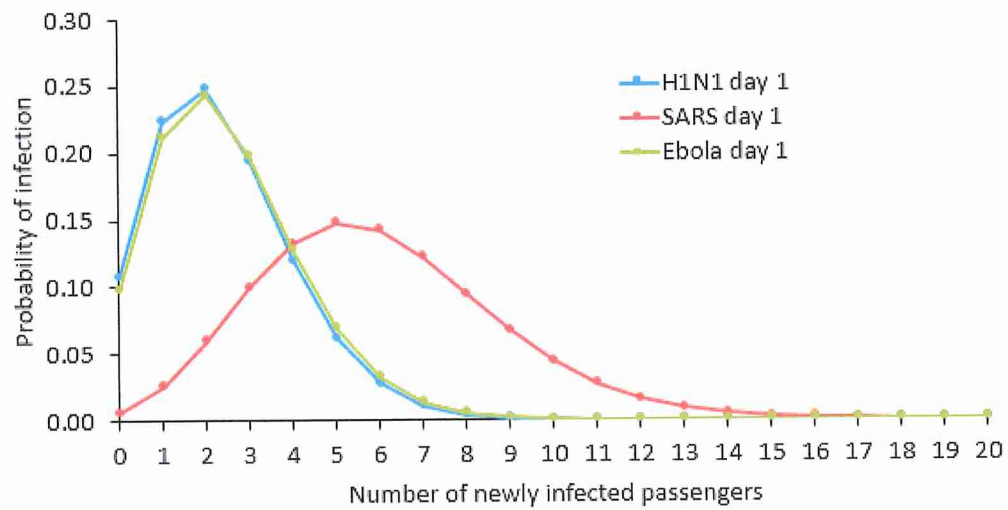
(a)
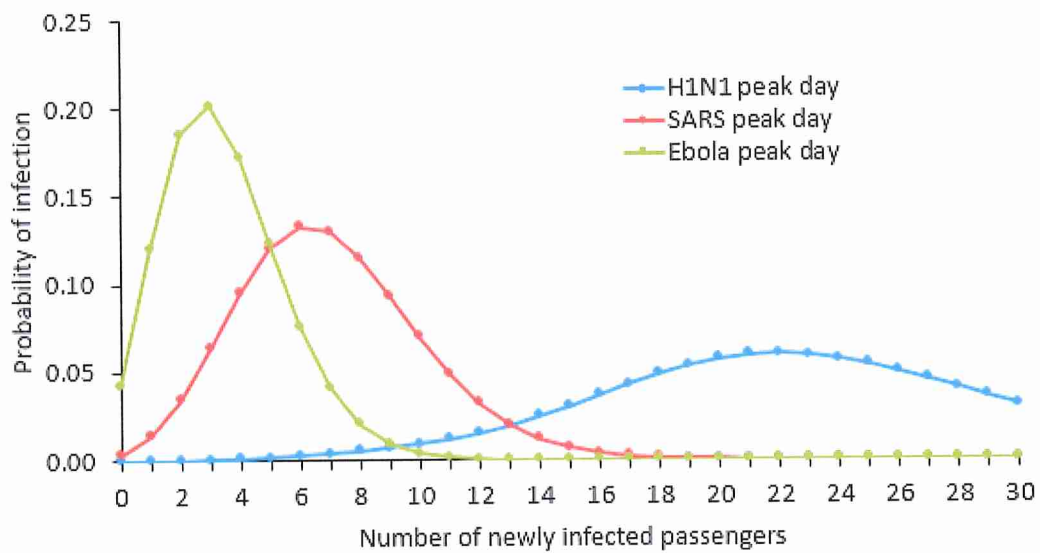
(b)

Figure 3.13. Infection profile at (a) the first and (b) peak days respectively post-onset of symptoms during a random ingress to an Airbus A320 (144pax) for Ebola, Influenza H1N1 and SARS contagions.
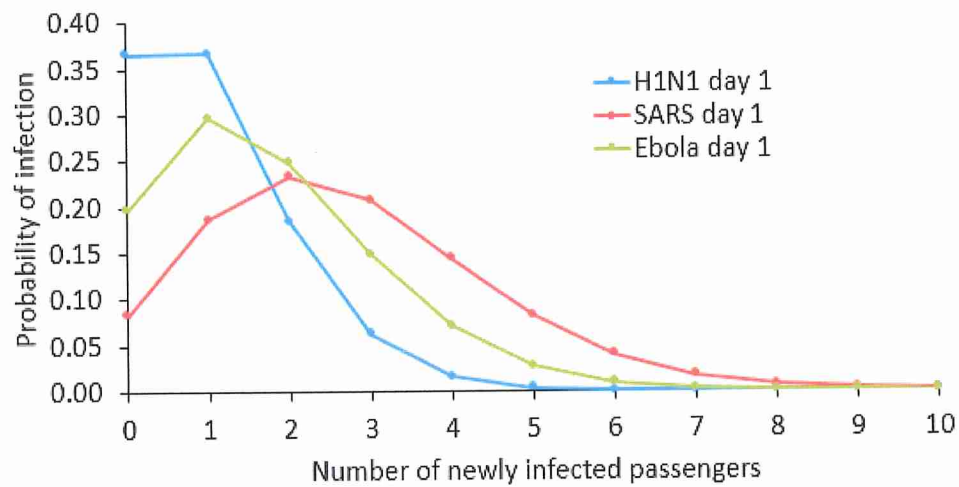
(a)
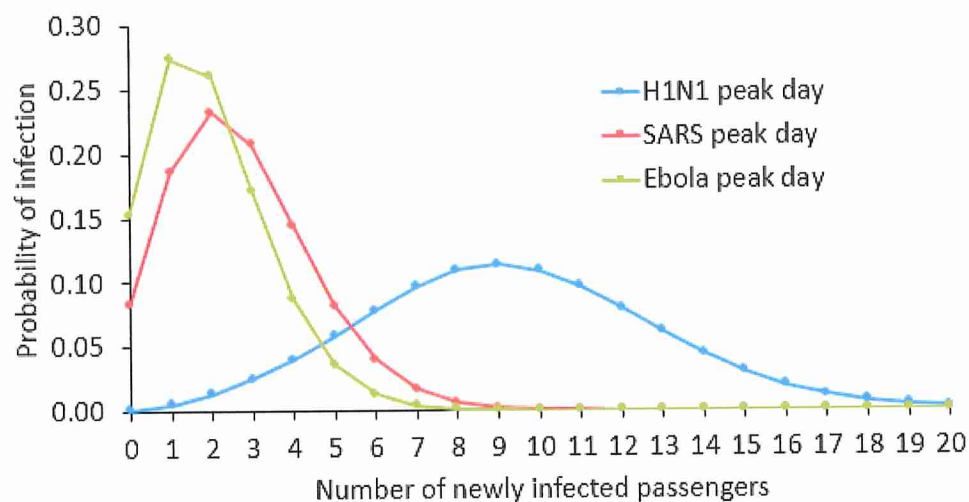
(b)

Figure 3.14. Infection profile at (a) the first and (b) peak days post-onset of symptoms during deplaning from an Airbus A320 for Ebola, Influenza H1N1 and SARS contagions.

3.5   Summary and Conclusions

A multiscale model combining social force based pedestrian dynamics and

metapopulation stochastic infection dynamics model has been formulated. The model is

used to study the dynamics of Ebola virus infection on airplanes specifically during

pedestrian movement related to boarding and disembarkation. Specific air travel-related policies that potentially mitigate diseases spread are identified.

Using the model, the transmission probability is estimated based on passengers' trajectories. The three pathological contagions Ebola, H1N1 and SARS are evaluated. Droplet- and aerosol-based simulations were performed to recognize the influence of these viral particles suspended in the air on the transmission of the contagion. The study highlights the potential gains that can be achieved through strategically integrated infection control with social force pedestrian movement model. For instance, two-section boarding leads to lower infections whereas all deplaning strategies have similar effects. The modeling approach developed here is generic and can be readily modified to other directly transmitted infectious diseases and dense pedestrian spaces.

4. Multiscale Model for Optimal Design of Pedestrian Queues to Mitigate Infectious Disease Spread

There is direct evidence for the spread of infectious diseases such as influenza, SARS, measles, and norovirus in locations where large groups of people gather at high densities e.g. theme parks, airports, etc. The mixing of susceptible and infectious individuals in these high people density man-made environments involves pedestrian movement which is generally not taken into account in modeling studies of disease dynamics. This problem is addressed through a multiscale model that combines pedestrian dynamics with stochastic infection spread models. The pedestrian dynamics model is utilized to generate the trajectories of motion and contacts between infected and susceptible individuals.

This information is incorporated into a stochastic infection dynamics model with infection probability and contact radius as primary inputs. This generic model is applicable for several directly transmitted diseases by varying the input parameters related to infectivity and transmission mechanisms. Through this multiscale framework, The aggregate numbers and probabilities of newly infected people are estimated for different winding queue configurations. It is found that the queue configuration has a significant impact on disease spread for a range of infection radii and transmission probabilities. The effectiveness of wall separators in suppressing the disease spread compared to rope separators is quantified. Further, it is found that configurations with short aisles lower the infection spread when rope separators are used.

4.1 Background

Pedestrian crowds are commonly observed in all public locations offering entertainment, transportation, social or religious activities. The mass gathering of people

congregated in limited space often elevates the risk of infectious disease spread due to the increased contacts between susceptible and infectious individuals. Further, individuals with different levels of vulnerability and receptivity due to variations in genetic background and intervention usage often congregate in touristic sites (Wilson, 1995). There is direct evidence for the occurrence of multiple epidemic outbreaks in high pedestrian density locations such as transportation hubs, entertainment venues, (e.g. theme parks, stadiums) and mass gatherings (Gautret & Steffen, 2016; Centers for Disease Control, 1983; Olsen et al., 2003; Mangili & Gendreau, 2005; Gundlapalli et al., 2006; McCarthy, 2015; Pfaff et al., 2010; Verhoef et al., 2008; Zieliński, 2009; Foo et al., 2009; Botelho-Nevers et al., 2010; Evans et al., 2002).

Gautret and Steffen (2016) report that sixty-eight cited instances of outbreaks among crowds occurred between 1980 and 2016. Numerous reports deal with the spread of diseases like influenza, SARS, and measles during air travel (Centers for Disease Control, 1983; Mangili & Gendreau, 2005). Examples of epidemics in entertainment venues include the influenza outbreak in 2002 during the winter Olympiad (Gundlapalli et al., 2006) and the measles outbreak in Disney World in 2016 resulting in 125 cases (McCarthy, 2015). Several outbreaks of directly transmitted gastrointestinal and respiratory diseases have been reported in religious and social outdoor mass gatherings (Pfaff et al., 2010; Verhoef et al., 2008; Zieliński, 2009), international meetings (Foo et al., 2009; Botelho-Nevers et al., 2010) and concert halls (Evans et al., 2002).

Disease spread in high pedestrian density locations is inherently a multidisciplinary and multiscale problem involving epidemiology and crowd dynamics. Deterministic (Brauer & Castillo-Chavez, 1995) and stochastic (Andersson & Britton, 2012)

epidemiological models including Susceptible-Infected-Recovered (SIR) models are effective tools for understanding epidemic spread. However, such models do not account for discrete human interactions in pedestrian crowds. Computationally intensive agent-based models *e.g.* EpiSimdemics (Barrett et al., 2008), and stochastic models (Germann et al., 2006) include human interactions through behavioral rules but are targeted at modeling simple interactions over large populations and geographical areas (Barrett et al., 2008; Germann et al., 2006), rather than evaluating the impact of fine-scale interactions. Instances mentioned above involve a high density of pedestrians over relatively small areas. Modeling non-uniform mixing in such instances and designing strategies for mitigation can only be achieved through multiscale modeling involving the combination of epidemic modeling with pedestrian crowd dynamics.

Understanding pedestrian dynamics and efficient crowd management practices are essential to enable effective flow of pedestrians, and for meeting safety standards in high pedestrian density environments noted above. Pedestrian crowd management often involves the combination of crowd psychology (Sime, 1995) and engineering methods for assessing the capacities of corridors, ramps, stairs, and other bottlenecks (Fruin, 1993). While several approaches including cellular automata (Burstedde et al., 2001), fluid flow models (Henderson, 1971) have been used for modeling pedestrian dynamics, social force models (Helbing & Molnar, 1995; Helbing et al., 2000) have the advantage of evaluating the complete individual trajectories necessary for contact estimation in epidemic studies. Since its conception, there have been several advances in social force models involving force field estimations (Mehran et al., 2009), algorithmic developments (Zanlungo et al., 2011; Lämmel & Plaue, 2012) and applications in situations like panic

(Treiber et al., 1999), traffic dynamics (Wei-Guo et al., 2006) and evacuation (Li & Jiang, 2014). Namilae et al. (2017a; 2017 b) have used pedestrian dynamics described by the social force model in a multiscale model to study the spread of epidemics during air travel.

Despite separate developments in pedestrian dynamics and epidemiology, there is a paucity of epidemiological models that utilize detailed information from pedestrian dynamics for contact estimation. There is a strong correlation between contact and infection rates in several disease epidemics such as SARS (Lipsitch et al., 2003) and Ebola (Rivers et al., 2014). Given the preponderance of epidemic outbreaks in high pedestrian density locations, a model that accounts for pedestrian dynamics in contact estimation can be a design tool for developing mitigation strategies. In this thesis, such a multiscale model is developed and utilized it to study disease spread in pedestrian queues.

Winding queue formation is a ubiquitous crowd control procedure. Consequently, individuals in crowded gatherings often spend a significant amount of time in waiting queue lines. In the multiscale model, pedestrian dynamics is used to generate trajectories of pedestrian motion and estimate the rate of contact between infected and susceptible individuals. This information is incorporated into a stochastic infection dynamics model with infection transmission probability and contact radius as primary inputs. This generic model is applicable for several directly transmitted diseases like Ebola, SARS, and H1N1 influenza by varying the input parameters related to infection probabilities and transmission mechanisms. This multiscale model is utilized to analyze disease spread in various pedestrian queue configurations, suggest preferred layouts, and design strategies that would reduce contacts and consequently mitigate the overall disease spread.

4.2 Modeling Methodology

4.2.1 Pedestrian Dynamics

To first estimate the number of contacts between susceptible and infectious

individuals, each mobile pedestrian is modeled as a particle and immobile objects like

walls or barriers as groups of stationary particles. The evolution of pedestrian particles

and their interaction with other pedestrians and stationary particles are described by

molecular dynamics like the social force model (Helbing et al., 2000). The net force $\bar{f}_i$

acting on an ith pedestrian (or particle) can be defined as:

$$\bar{f}_i = \frac{m_i}{\tau}\left(\bar{v}_0^i(t) - \bar{v}^i(t)\right) + \sum_{j \neq i}\bar{f}_{ij}(t) = m_i\frac{dv_i}{dt} \tag{18}$$

With the pedestrian position at a given time obtained by integration as $\bar{r}^i(t) =$

$\int \bar{v}^i(t)dt$. Here $\bar{v}_o^i(t)$ refers to the desired velocity of the pedestrian, and $\bar{v}^i(t)$ is the

actual velocity, m_i is the particle's mass and τ is the time constant. The momentum

generated by a pedestrian's intention, denoted by $\frac{m_i}{\tau}\left(\bar{v}_0^i(t) - \bar{v}^i(t)\right)$, results in a self-

propulsion force that is balanced by a repulsion force $\bar{f}_{ij}(t)$ to obstacles in the direction of

motion. In this study, the Lennard –Jones type repulsion term used earlier by Namilae et

al. (2017a; 2017b) is used again.

While equation (18) describes the general motion of pedestrians, modifications needs

to be introduced to this equation to account for slow-moving pedestrian queues.

Pedestrians in a queue move at the speed of the nearest person ahead in the line. To

model this scenario, location dependence is introduced to the desired velocity in the self-

propulsion term as:

$$v_0^i(t)\,\hat{e}_1 =$$

$$\begin{cases} \left(v_A + \gamma_i v_B\right)\left(1 - \dfrac{\delta}{\min\{r_{ij|front}\,;\,i \neq j\}}\right)\hat{e}_1;\ \delta = \begin{cases} \delta_1\,;if\ i\,\&\,j\ of\ same\ group \\ \delta_2\,;if\ i\,\&\,j\ of\ different\ groups \end{cases} \\ 0\,;if\ r_{ij|front} < \delta \end{cases} \quad (19)$$

Where $\hat{e}_1$ is the desired direction of motion. v_A and $\gamma_i v_B$ are the deterministic and stochastic components of the desired velocity, respectively. The values of walking speed terms (v_A and $\gamma_i v_B$) can be varied to obtain a given distribution of age groups and gender of travelers (Zębala et al., 2012). δ is the cut-off distance constant between the ith and j^{th} pedestrians at which the desired velocity of the ith pedestrian reduces to zero velocity (stationary condition).

To mimic real-life scenarios, the formation of groups of pedestrians ia also accounted for. The groups' formation is controlled by adjusting the distance (δ) in equation (19). The empirical observations on a theme park queue and comparisons with the literature (Moussaïd et al., 2010) indicate that δ separation values are different between pedestrians belonging to a group (e.g. family or friends in the queue) and other pedestrians. Based on this, an average distance of $\delta_1 = 0.46$ m is chosen for pedestrian particles within the same group, while this distance between independent pedestrians is given a value of $\delta_2 = 0.64$ m.

4.2.2 Contact Estimation and Infection Model

Consider a population of size N consisting of I(t) infected and S(t) susceptibles at time t. The pedestrian's position ($r_i(t)$) evolves through the pedestrian dynamics model. A susceptible can become infected when coming into direct contact with an infected individual in the course of motion. Given the trajectory of pedestrians over time, the

number of contacts m_i can be evaluated by counting the instances when the distance between the ith and j^{th} pedestrians (r_{ij}) is less than a virus-specific contact radius (x). This transmission distance (x) used to define the contact is dependent on the type of pathogen and mechanisms for its spread. For diseases like Ebola, studies indicate that the primary mode of transmission is through contact droplets (Osterholm et al., 2015; Judson et al., 2015). Consequently, a distance that enables direct touch needs to be used for estimating contact for such diseases. Other infectious diseases like SARS and influenza are known to be transmitted by both shorter and longer range airborne mechanisms (Clark & de Calcina-Goff, 2009; Yuen & Wong, 2005). Studies show that micrometer-sized aerosol clouds generated during cough can travel over 2 m (Bourouiba et al., 2014; Gupta et al., 2009). The contact radius is varied between these distances to account for the various infection spread mechanisms.

Next, consider the probability (P_{inf}) that contact between a susceptible and an infective results in successful infection transmission. This input parameter can be dividex into two components: a viral shedding probability distribution (P_c) which is a function of time since acquiring infection for the specific virus in question, and a pathogen spread mechanism component (P_m). This includes contributions of several independent mechanisms comprising (a) aerosol exposure and inhalation probability (P_a) common in infections such as SARS and influenza (Clark & de Calcina-Goff, 2009; Yuen & Wong, 2005), (b) Coarse pathogen droplet inoculation (P_d) common in infectious diseases like Ebola (Osterholm et al., 2015). Other mechanisms including fomite mechanism, which involves contaminated surface-to-hand transfer, would contribute to the infection spread,

but such mechanisms do not involve human-to-human contacts in this context and are not considered here. The infection probability would then be defined as:

$$P_{\text{inf}} = P_c . P_m = P_c \left(P_a + P_d \right)$$

(20)

First, consider the viral shedding probability distribution (P_c). Studies indicate that the amount of viral shedding is typically dependent on the length of the incubation period and the number of days since the appearance of symptoms. In a previous study for Namilae et al. (2017b), the CDC data is used on the amount of RNA (ribonucleic acid) virus copies in the blood serum since the illness contraction to generate this probability distribution for Ebola (Towner et al., 2004). A similar approach can be used for other diseases, for example, for SARS pathogen, the viral gene expression of the nucleocapsid (N) protein, detected at different rates along with the evolution of the virus from post-onset of the symptoms until convalescence is indicative of viral shedding (Zhao, 2007). For influenza, nasal, oral or ocular shedding of the H1N1 virus has been detected by determining the relative equivalent unit from viral RNA level (Paquette et al., 2015). Such data can be used to generate the P_c distribution. Figure 4.1 shows the viral shedding distributions generated based on Zhao (2007) and Paquette et al. (2015) for SARS and H1N1 influenza respectively.

H1N1

(a)
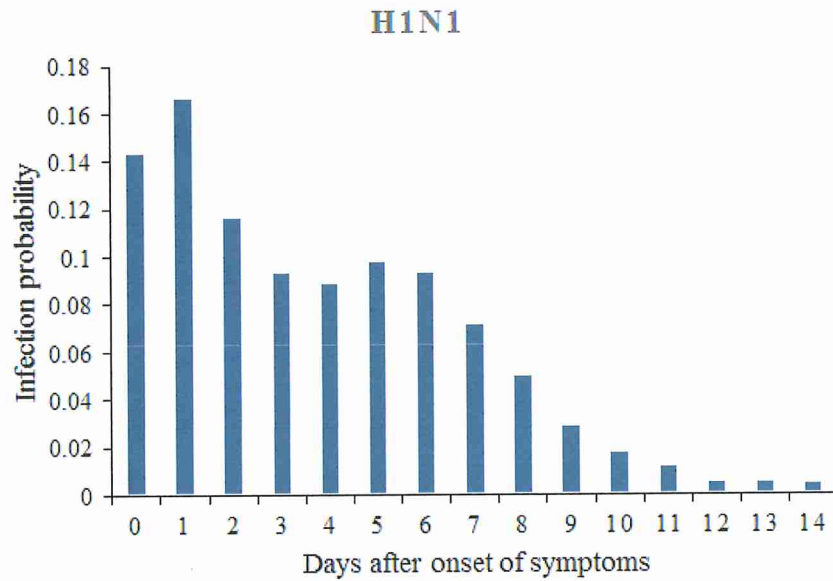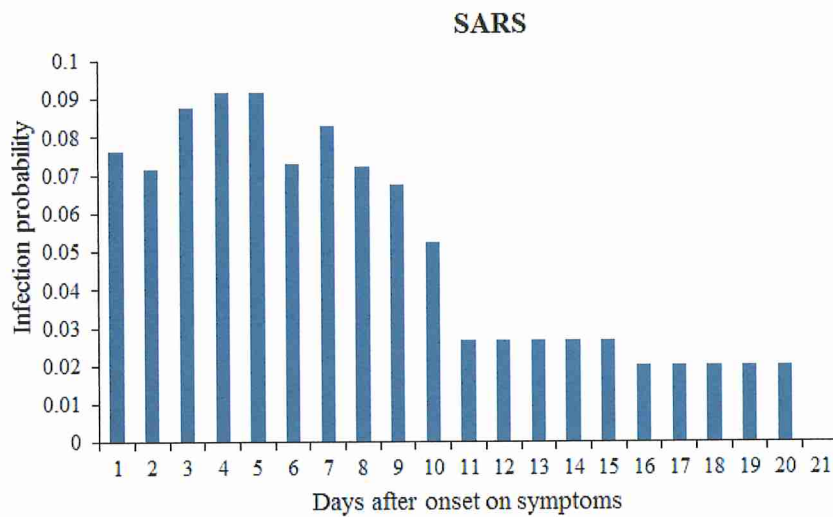
SARS

(b)

Figure 4.1. Viral shedding probability distributions (Pc) for (a) H1N1 influenza and (b) SARS.

There are many formulations in the literature to compute the mechanism-specific probability of transmission. Table 4.1 lists the details of the popular mechanisms for aerosol and coarse droplet mechanisms. The functional form of the aerosol inhalation

probability is described in the data-driven modeling framework in Teunis et al. (2008),

which in turn is based on Riley's Dose-response model (Riley & O'Grady, 1961). The

probability of coarse droplet inoculation mechanism considers the droplet cone emitted

during expiratory events like coughing (Teunis et al., 2010).

Table 4.1

Formulations for generating mechanism-specific probability distributions.

Mechanism	Equations	Notes	References
Aerosols mechanism	$P_a = \left(1 - e^{-\frac{QC_a\tau}{V_o}}\right)$	Data-driven model framework based on dose-response model C_a - maximum initial concentration of contagion in aerosol suspension τ - exposure time Q - respiration rate of susceptibles V_o - volume of infection envelope	Teunis et al. (2008) Riley & O'Grady (1961)
Coarse droplet inoculation	$P_d = \frac{S_A}{S_C} \cdot \frac{V_C}{V_o}$	Model based on expiratory droplet cone V_C - volume of cone in which droplet can fall V_o - room or exposure volume S_A - exposed mucosa surfaces S_C - circular area base of the cone	Teunis et al. (2010)

The probability that an infectious individual "i" in the crowd comes into contact with

other individuals is m_i/N, where m_i is the number of contacts. Using Bayes' theorem of

conditional probability, *P(contact and infection) = P (infection |contact) . P (contact) =*

$P_{inf} \cdot \frac{m_i}{N}$. To account for the demographic stochasticity of the susceptible individuals, the

number of newly infected by this infective "i" is estimated by a binomial distribution I_i

(t)~B(n$_i$,p$_i$) with parameters n$_i$= S$_i$ (t-1), the number of susceptibles exposed to the

contagion at time t, and $p_i = P_{inf} \cdot \frac{m_i}{N}$. Equation (20) is used for estimating P$_{inf}$.

For each infective individual, all the possible permutations are considered, i.e. the

infective is considered to be in all possible positions in the queue. Binomial distributions

are obtained to estimate a range of newly infected pedestrians with variations in the

position and infectivity of the infective pedestrian. Denote by the variable λ the possible

number of newly infected pedestrians ranging from zero to the maximum obtained

number N$_{inf}$ (λ= 0,...,λ_i,...,N$_{inf}$). The mean binomial distribution of the number of people

infected at time t by all the possible permutations is computed using Equation (21) below.

Here *Comb* denotes the number of combinations of infective positions and w_i is the

frequency of obtaining λ_i newly infected in the computations. The day post-onset of

symptoms that defines the infectivity (see Figure 4.1) is denoted by c. The probability

distributions are combined and averaged as given by:

$$I(t) \sim \sum_{c=1}^{d} \sum_{i=1}^{i_c^0} \{Binomial \; [S_i(t-1), P_m \cdot P_c \; \frac{m_i(t-1)}{N}]\} * w_i \; (\lambda_i) \; / \; Comb \qquad (21)$$

Note that the contacts between the infective and susceptibles are defined when the

susceptible pedestrians are within a specific transmission distance (dependent on the

transmission mechanism) from the infective and exposure duration. The exposure

duration is chosen as the time sufficient to complete one inhalation and bring the virus to

the respiratory tract. Acknowledging the alteration between pedestrians' breathing

process, an average time of 4 seconds is assumed as the exposure duration. Once a

susceptible individual is within the contact radius from the infective members for an

interval greater or equal the exposure duration required contracting the disease, then

contact occurs. During the contact the susceptible member contracts the infection.

However, inoculation (immunization) and the amount of the inhaled virus decide whether infection will turn to a disease or not. This is represented by the transmittance probability factor.

Instead of using fixed parameters for defining contact, the contact distance and transmission probability are treated as parameters in assessing epidemic spread. These parameters are varied over a broad range to model the different scenarios (diseases and transmission mechanisms) for several pedestrian queue configurations. Expelled fine aerosols travel farther and remain suspended for a longer time than coarse droplets (Bourouiba et al., 2014; Gupta et al., 2009). Coarse droplets and aerosols transmission mechanisms are accounted for by varying the contact radius parameter between 0.9 and 2.1 meters (36-84 inches). The transmittance probability (P_{inf}) is varied between 0.025 and 0.2 to account for the variation in the infectivity of different diseases.

4.2.3 Model Application to a Pedestrian Queue

Pedestrian winding queues are an essential component of crowd management. These queues are often unidirectional and have different widths and configurations to fit the available area. The queues are often separated by rope stanchions for their ease of use. However, temporary walls could also be used for this purpose. Examples of such queues usage include airport security, waiting areas at theme parks and other crowded places. Within the same line and among adjacent lines, many susceptibles are often within the contact radius and viral infection may propagate if an infectious pedestrian is present.

The role of motion pattern and contact creation between neighboring pedestrians are evaluated, for different queue configurations. The aisles' geometry, orientation and the number of inlets and exits are altered between the different configurations. To model

queue configurations that are used in practice, a real-life queue is evaluated at a theme park attraction as shown in Figure 4.2, and used those dimensions as a basis for the different configurations modeled in the study. In addition to dimensions, empirical data on contacts and groups was collected to guide the simulations. While progressing through the queue, two of the team members recorded the number of nearby individuals within a 1m radius, at 25 seconds time interval. The data was collected by two observers independently at two different times of the day. The approximate distance between pedestrians, while differentiating between individuals of the same group and different groups was also recorded. Table 4.2 compares the empirical data and the corresponding simulation data regarding the average number of contacts in the corners, inner and outer aisles.

This queue layout is utilized as the basis for evaluating the effect of the layout and shape of the queue configurations. The aisles' length and orientation are altered between the configurations of the same area and aisle width. The relationship between the layout shape and the contact evolution is also investigated, by modeling four square floor plans of the same area.
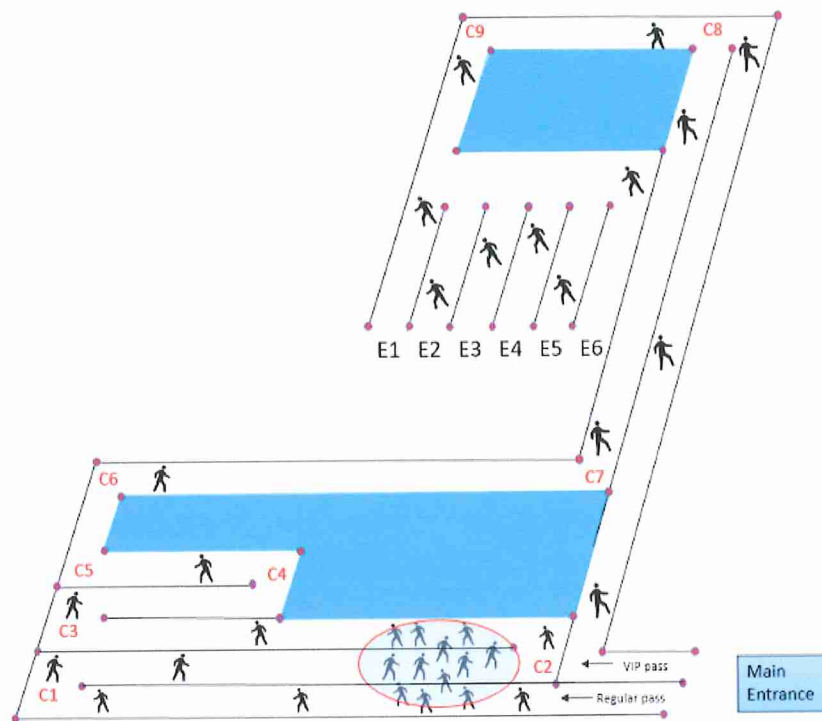
(a)
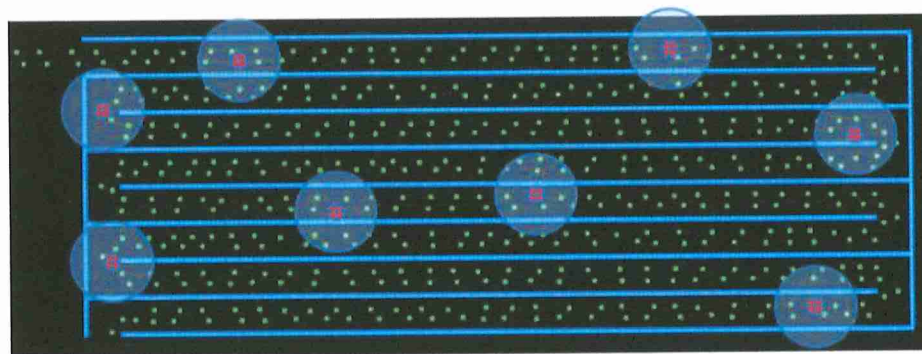
(b)

Figure 4.2. Replication of real-life pedestrian motion in queues using simulations.
(a) Schematic representation of an actual pedestrian queue in an entertainment venue.
(b) Simulation snapshot of a corresponding model.

Table 4.2

Evaluation of the number of contact within 1m radius from empirical and simulation data of a side-by-side (double) pedestrian queue in an entertainment venue waiting line.

Contact	Empirical data		Data from simulation	
	range	Mean	range	mean
at corners	[4-14]	9	[8-12]	10
in outer aisles	[3-7]	5	[5-9]	7
in inner aisles	[5-13]	9	[10-12]	11

4.3　Results and Discussion

The role of motion pattern in contact creation between neighboring pedestrians is evaluated, within a fixed control area, for four different queues configurations. The aisles' geometry and orientation are altered between the configurations. The walking aisles are distributed either in a vertical or horizontal manner. In some configurations, the control area is also taken as one entity with a single inlet and exit. In others, it is disseminated into left and right zones with independent inlet and exit to each zone. The aisle width are always constant. The aisle width are matched with the observations in an airport waiting lines and theme parks, and assume an aisle width of 1m which is greater than the minimum required dimension of 0.9 meters, stated by the regulations (Security Checkpoint Layout Design and Reconfiguration Guide, 2006).

The relationship between the layout shape and the contact evolution is also investigated, by modeling four square floor plans of the same area as above configurations. In all the simulations, a total of 600 pedestrians are distributed within the waiting area and in front of the inlet either in a single file or abreast queue. With time evolution, the pedestrians move forward in the sequence to reach the exit. It is expected that the aisle's length, direction and structure within the control area, and the distribution of turn corners, as well as the queue shape, have an effect on the contact between

pedestrians. Table 4.3 below provides a summary of the geometrical aspect of the investigated configurations.

In all the mentioned scenarios, the number of contact between pedestrians is calculated where rope separators or temporary walls are placed between the aisles. In the simulations, it is assumed that contact occurs if the infective and susceptible pedestrians are in continuous proximity for 3.75s or more time. For rope separators, contact extends to pedestrians in the neighboring aisles, whereas for temporary walls, transmission due to contact is limited only between the pedestrians within the same aisle. The possibility of pedestrian groups arranging side-by-side or the formation of a single file is also taken into account. The movement of pedestrians is simulated and examined for contact estimation. The data of pedestrian contact is then combined with the infection model mentioned in section 4.2 to prioritize certain appropriate preventive walking strategies, for every scenario, that help suppress infection spread by reducing contact rate.

Table 4.3

Geometric aspects of the different evaluated configurations.

	Rectangular layout				Square layout			
	C1	C2	C3	C4	C1	C2	C3	C4
Number of zone(s)	1	1	2	2	1		2	2
Number of inlet(s)	1	1	2	2	1		2	2
Number of exit(s)	1	1	2	2	1		2	2
Number of corners per zone	7	21	10	7	13	3	10	7
Number of aisles per zone	8	22	11	8	14	4	6	14
Aisle width (a_l) [m]	1	1	1	1	1		1	1
Aisle length	$22.a_l$	$8.a_l$	$8.a_l$	$11.a_l$	$14.a_l$	$14.a_l$	$14.a_l$	$7.a_l$

The situation of a single infective in the queue is considered. The infectious individual is unidentifiable; his rank in the queue is not known a priori. Therefore, all permutations of the infectious individual's position are simulated to determine the average number of contacts for a given queue configuration. Also, the infectivity of pathogens is characterized by the transmittance mechanism and probability. Airborne viral nuclei vary in size. Expelled fine aerosols travel farther and remain suspended for a longer period of time than coarse droplets. Coarse droplets and aerosols transmission mechanisms are accounted for by varying the contact radius parameter between 0.9 and 2.1 meters (36-84 inches). The transmittance probability is varied between 0.025 and 0.2 to account for the vulnerability and receptivity of the exposed infective to the infection.

4.3.1 Two Abreast (Side-By-Side) Pedestrian Queue

Based on the observations of common queues, the situations when two pedestrians belonging to the same group can move abreast or side-by-side are considered in the four configurations. As initial conditions, the pedestrians are distributed side-by-side inside the aisle and in front of the inlet. The spacing between the pedestrian particles is varied to differentiate between individuals of the same groups and others from different groups as mentioned earlier. As time evolves, the abreast queues turn into a single file in the exit aisles where the pedestrian speed increases (See Figure 4.3). The waiting time at the exit is not considered to decrease the computational effort.

4.3.1.1 Rectangular Floor Plan

Four different rectangular configurations are investigated with the same shape and area as shown in Figure 4.3. The four configurations are split vertically (configurations in Figures 4.3(b) and 4.3(c)) or horizontally (Figures 4.3(a) and 4.3(d)). Configurations in

Figures 4.3(a) and 4.3(b) have one inlet and one exit whereas configurations in Figures 4.3(c) and 4.3(d) have two inlets and two exits due to the existence of separated zones. The width of the pedestrian lanes remains 1 m, which allows some pedestrians belonging to the same group to form a double line. The four configurations are termed Configurations 1, 2, 3 and 4 respectively.
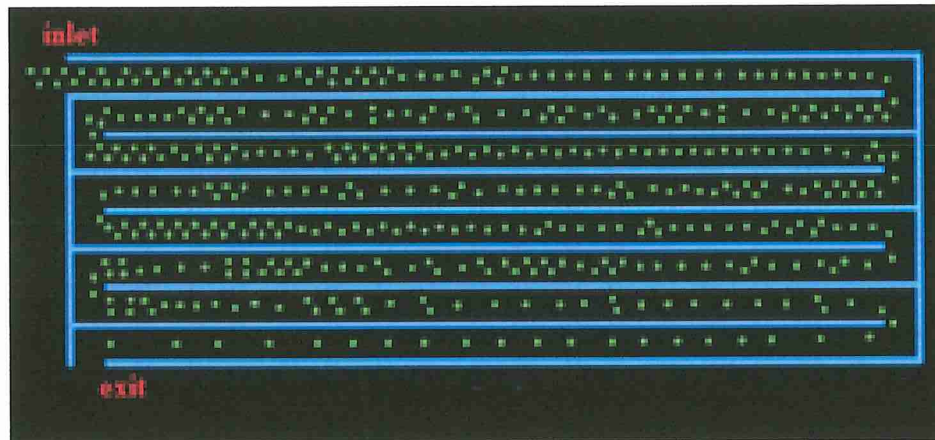
(a)
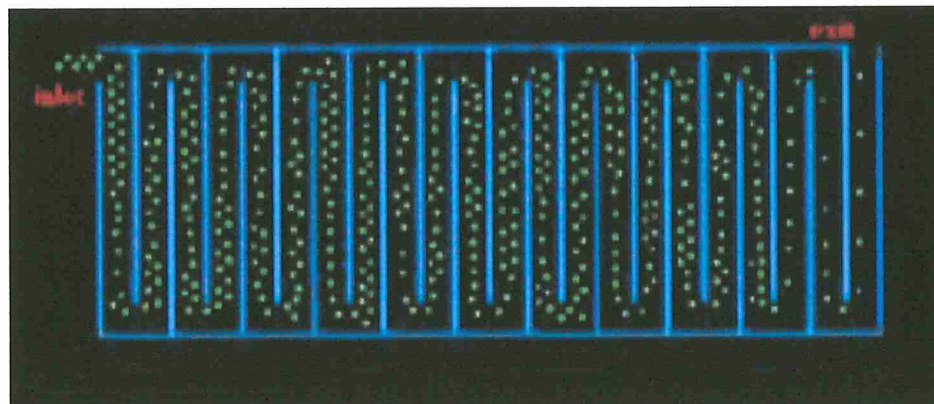
(b)
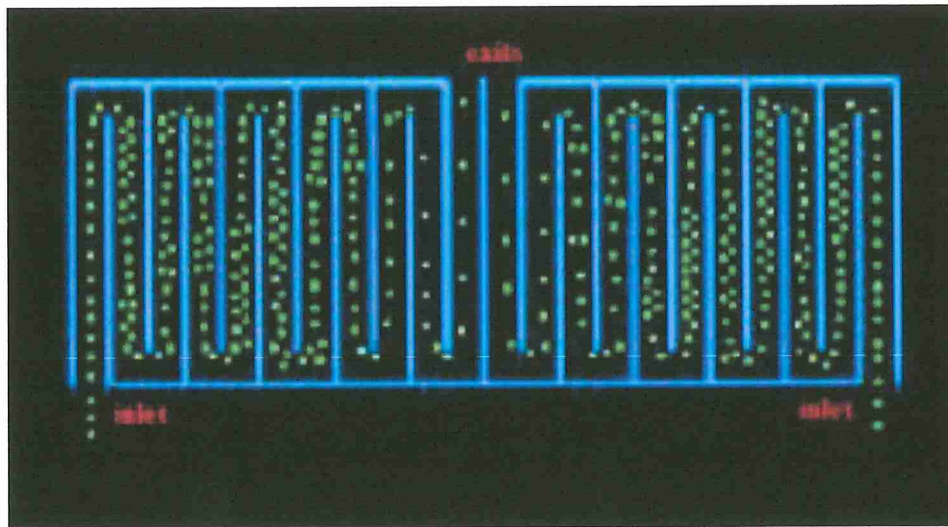
(c)
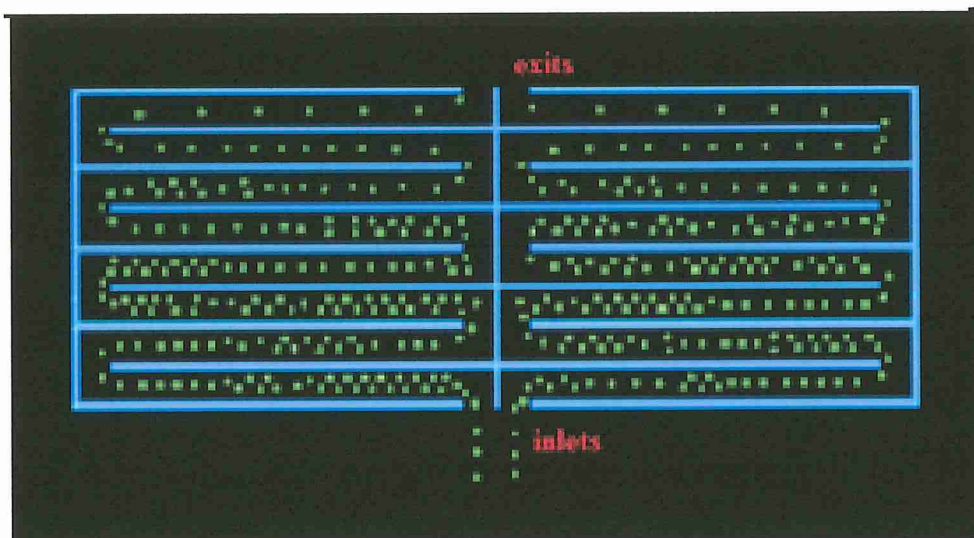
(d)

Figure 4.3. Evolution of pedestrians (t=125s) from simulation of abreast (double) queue rectangular layouts: (a) Configuration 1, (b) Configuration 2, (c) Configuration 3, (d) Configuration 4.

For a given configuration and a set of infection parameters, the mean number of newly infected pedestrians is binomially distributed to account for the demographic stochasticity in the immunity and receptivity of the susceptible population. For instance, Figure 4.4 represents the distribution of newly infected individuals for the four configurations at an

infection probability of 0.025 and a proximate contact radius of 1.2 meters for aisles separated by ropes. While such distributions are computed for the entire parameter space, for ease of representation in subsequent analysis, only the mean of the distributions is plotted as a function of pedestrian and infection parameters.
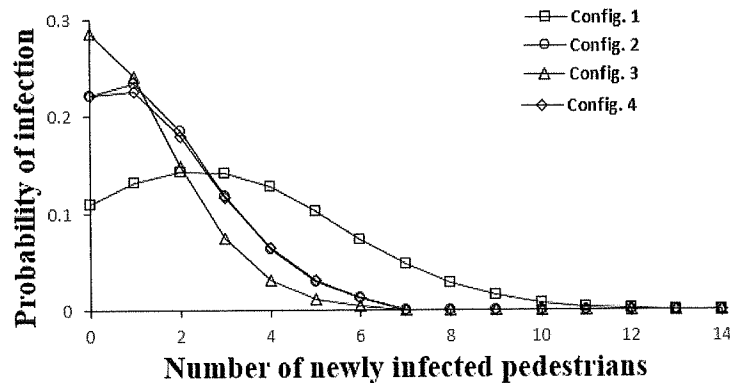
Figure 4.4. Infection distribution profile for the different configurations at Pinf =0.025 and R=1.2m with rope separation.

With the commonly used rope separators and an infection radius less than 1.2m, which corresponds to coarse droplet mechanisms, the infective has an influence on the directly adjacent aisles on both sides. The bar chart in Figure 4.5(a) estimates the total number of contacts between the infective and the susceptible population. However, a given contact will lead to infection based on the transmission probability. Combining the contact data of the bar chart with the infection model leads to the mean distribution of infection over the probability range like in Figure 4.4.

In Figure 4.5, the corresponding mean of the binomial distribution is plotted for the different configurations and transmission probabilities. Configuration 3 is the best layout for all transmission probabilities, followed by configuration 2 (Figure 4.5(a)). In configuration 2, the vertical aisles are short with fewer pedestrians. Configuration 3 has the same aisle geometry as configuration 2; however, the pedestrian will exit the queue

earlier (halfway) compared to that of configuration 2 which results in lower exposure time and consequently fewer contacts. Configurations 1 and 4 result in a higher mean number of infections. These configurations have long open aisles compared to configurations 2 and 3 with the lower aisle length, therefore more pedestrians are involved, and interaction occurs more frequently with pedestrians from neighboring aisles in these two configurations. Configuration 1 is the least favorable layout because diverse pedestrians from both sides come into proximity more frequently than in configuration 4 with comparatively shorter aisles. Configuration 4 is worse than configuration 2 because, at the common corners between the left and right zones, the infective comes into contact with additional pedestrians from the neighboring zones.

(a)

(b)

Figure 4.5. Infection distribution profile for different double queue configurations at a contact radius of 1.2m. (a) The rope is used for separation between the rows, (b) The temporary shading walls are used for separation between the rows.

The use of temporary (or permanent) walls in the place of ropes limits the mixing of pedestrians within the same aisle and reduces the impact of common corners between aisles. In this case, it is assumed that the contagion cannot cross over to the adjacent aisles due to the solid wall barrier; therefore it results in a lower number of contacts. Figure 4.5(b) shows the mean number of infections when walls are used for crowd control. Overall, the mean number of new infections is significantly lower than when using rope separators. It can be inferred from Figure 4.5(b) that configuration 3 still results in the lowest number of infections at all transmission probabilities, and configuration 1 with long lines results in the highest number of infections in this case too. The primary difference between using rope separators and walls is for configurations 2 and 4. Configuration 2 resulted in a lower number of infections compared to 4 when using rope separators while this is reversed with walls. In configurations 3 and 4, the exit time is again shorter than that of configurations 1 and 2 resulting in lower overall contacts. Also, at 1.2m radius of infection, the configurations with long aisles and high pedestrian density corners result in higher contacts when using wall separators. This is explained by the fact that the same group of pedestrians remains in contact for a prolonged time.

(a)

(b)

Figure 4.6. Infection distribution profile for different double queue configurations at a contact radius of 2.1 m. (a) The rope is used for separation between the rows, (b) The temporary shading walls are used for separation between the rows.

Figure 4.6 shows the results of repeating the transmission probability variation over the same range, but assuming the aerosol transmission mechanism with a longer contact radius of 2.1 m. Configuration 3 still results in the lowest number of contacts for both rope and wall separators. For rope separator, the same pattern of results is observed as with the lower contact radius, but with increased infection spread (Figure 4.6(a)). The differences between the configurations reduce at low transmission probabilities, therefore, the results for configurations 2 and 3, and for configurations 1 and 4 overlap. At 2.1 m contact radius, the dispersion of the fine contagion laden particles crosses the aisle boundaries to two adjacent aisles on each side. Here, the findings of configurations 2 and 3 are nearly identical since the aisles are distributed in the same manner except that configuration 3 has two separated zones.

When the transmission radius expands to many neighboring aisles, pedestrians of one zone in configuration 3 come into contact not only with other pedestrians within the same zone, but with those in the adjacent zone. Accordingly, configurations 2 and 3 have the same behavior. Here, the separation of these two groups has no effective role in reducing

contact. The same principle applies to configurations 1 and 4; the offset between the data

of configurations 1 and 4 is reduced compared to that of the coarse droplet transmission

mechanism for the same reason. Configuration 1 remains the worst layout, especially at

higher probabilities, due to the elongated, abundant contact between pedestrians from

adjacent aisles.

Previously, when the coarse droplet transmission with wall separator was evaluated

(Figure 4.5(b)), the maximum number of contacts for configurations 1 and 2 was highest,

followed by configuration 4. With aerosol transmission mechanism (R=2.1 m) as in

Figure 4.6(b), configuration 2 remains the greatest in terms of contacts generated,

followed by configuration 4, and the resultant number of contacts of configuration 1

drops. At a low contact radius (R=1.2m), pedestrian density within the circle of infection

is greater in aisles than at corners. Therefore, long aisles allow greater contact time.

However, an infection circle with a 2.1m radius of contact will include more pedestrians

at the corners rather than the aisles. Configuration 2 has the shortest aisles, with the

greatest number of corners (21 corners), which leads to a higher number of contacts.

The contacts generated between pedestrians in the four configurations are explored

assuming different infection mechanisms represented by the radius variation.

Configurations 2 and 3 result in a lower number of infections for rope separators, across

the range of infection radii from 0.9 to 2.1 m as shown in Figure 4.7(a). As explained

earlier, for aisles separated with ropes, shorter aisles lead to lower exposure of an

infective resulting in this behavior. For walls, the combination of the radius of infection,

as well as the interaction time within the aisles and at the corners alter the results as

shown in Figure 4.7(b). Each combination of infection radius and queue layout generates

a different number of mean newly infected individuals. At low infection radii, short-aisle and low exit time configurations are favorable. At higher radii, configurations with less turning corners are better.
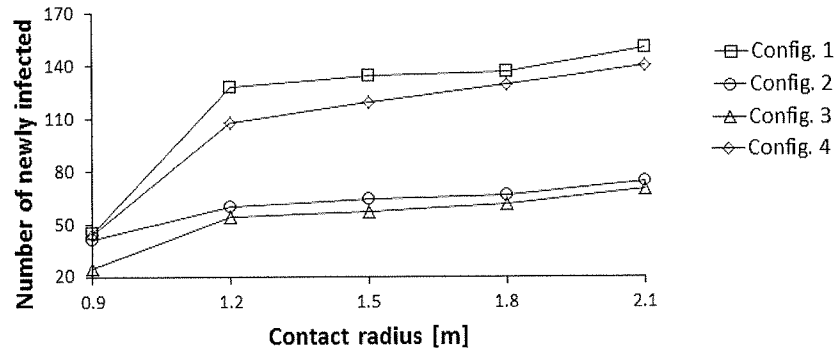
(a)
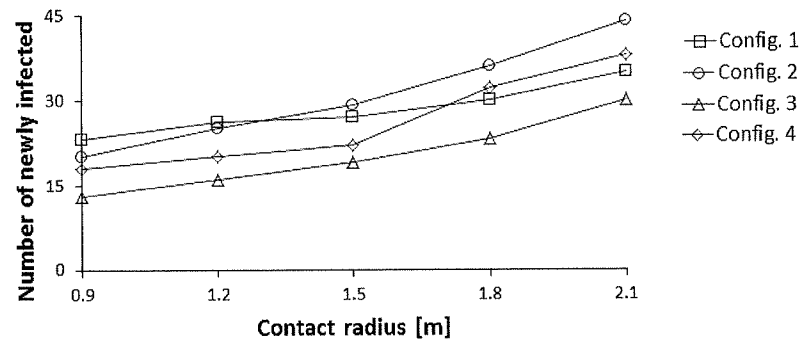
(b)

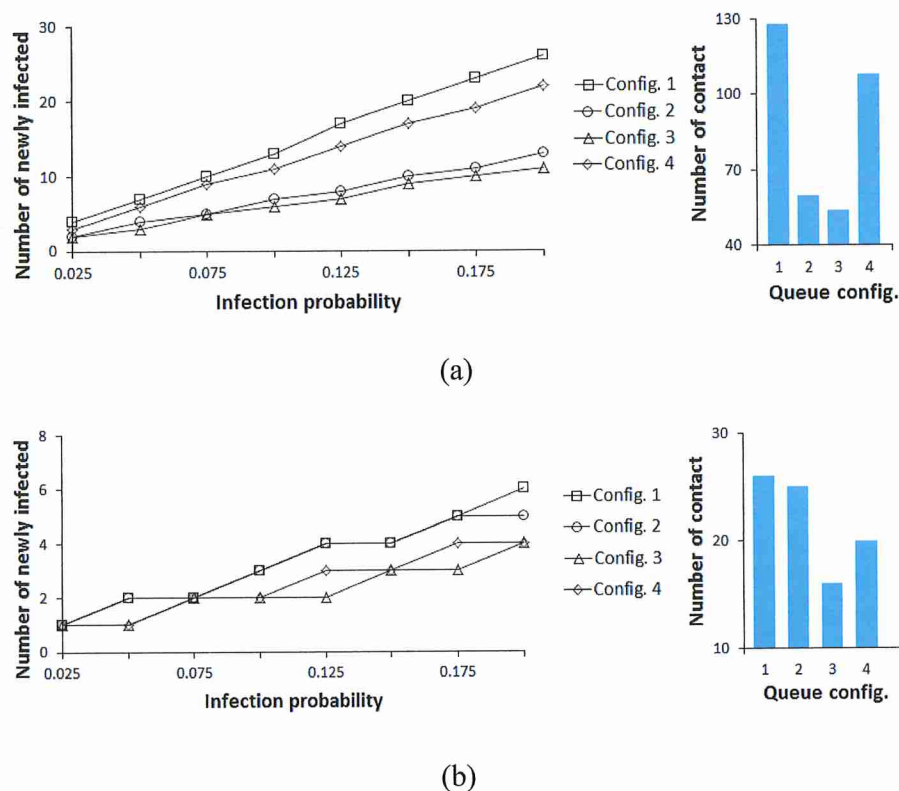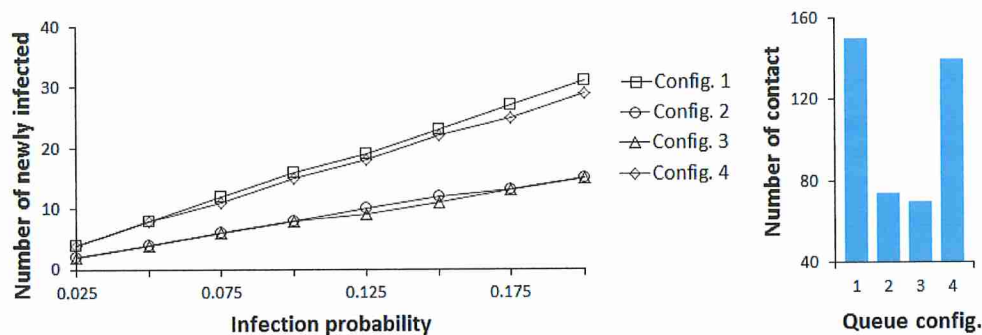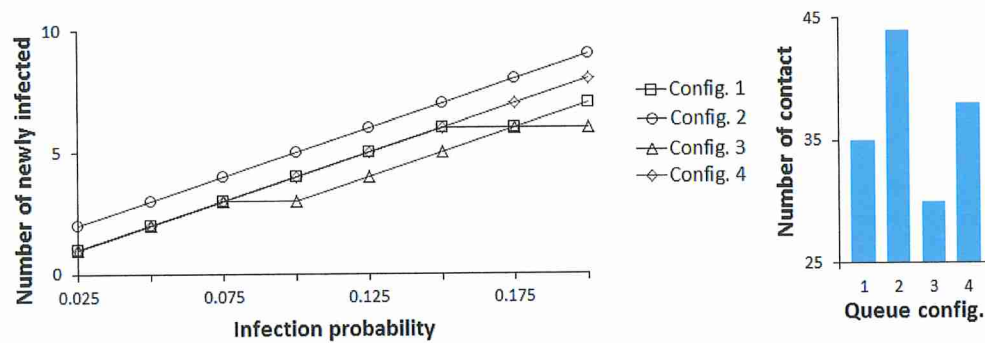*Figure 4.7.* Contact distribution for different double queue configurations. The contact radius is varied. (a) The rope is used for separation between the rows, (b) The temporary shading walls are used for separation between the rows.

4.3.1.2 Square Floor Plan

Square layouts are now considered with the same area as the rectangular layouts discussed previously. Since the aspect ratio of the square configuration changes from that of a rectangle, the number of aisles and their dimensions vary as shown in Figure 4.8.

Note that configurations 1 and 2, in Figures 4.8(a) and 4.8(b), are the same except for rotation, therefore, they are not discuss separately.
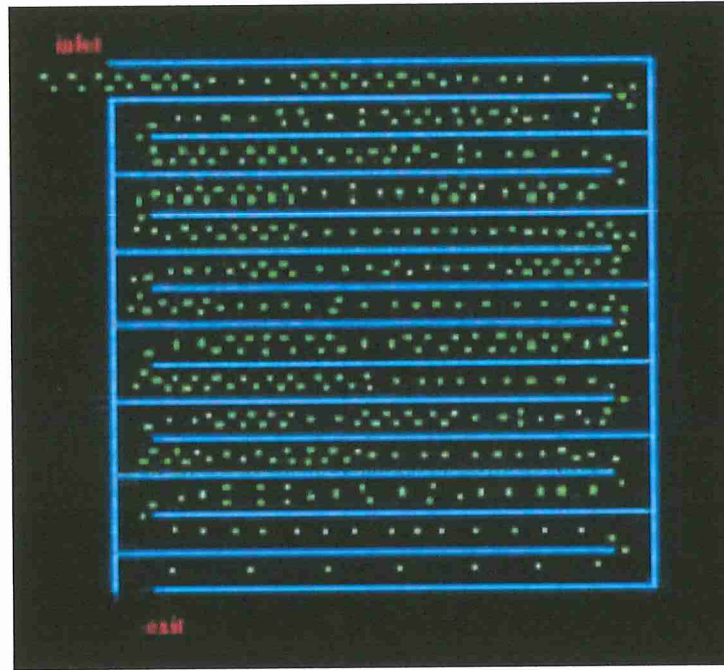
(a)
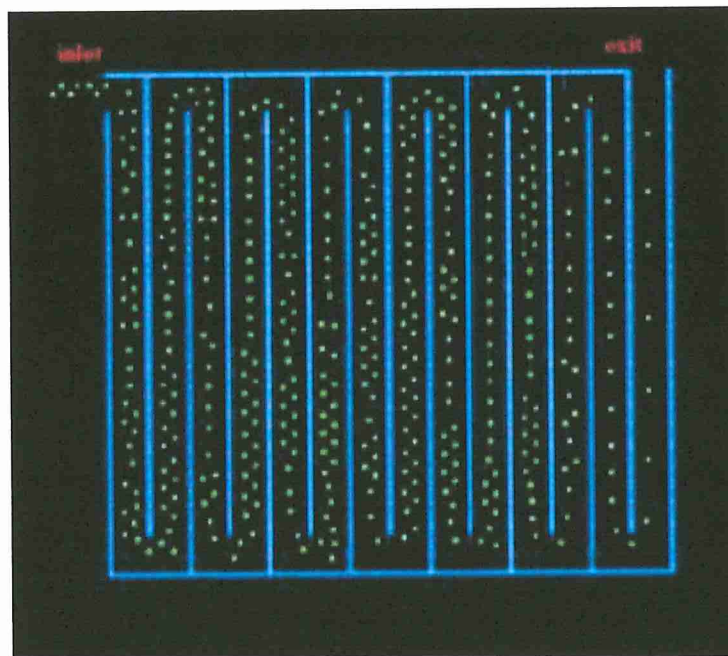
(b)
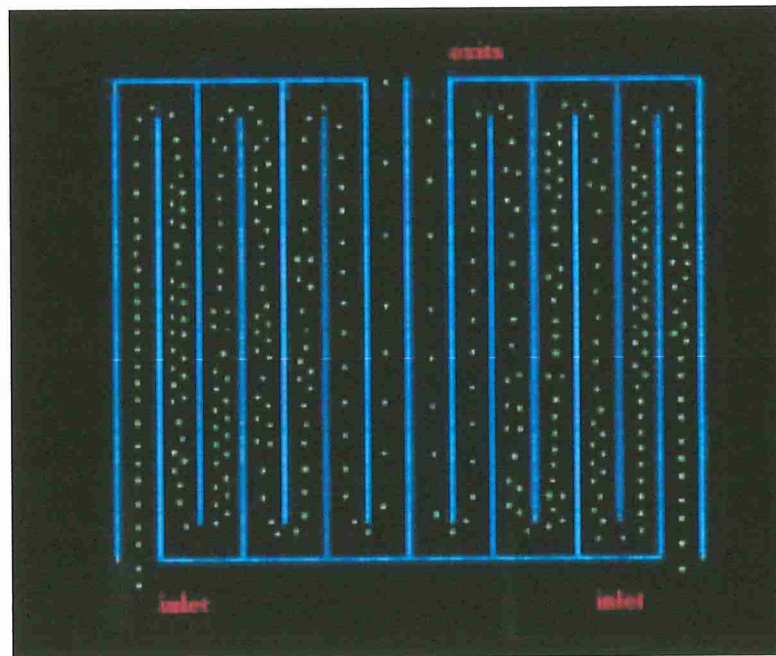
(c)
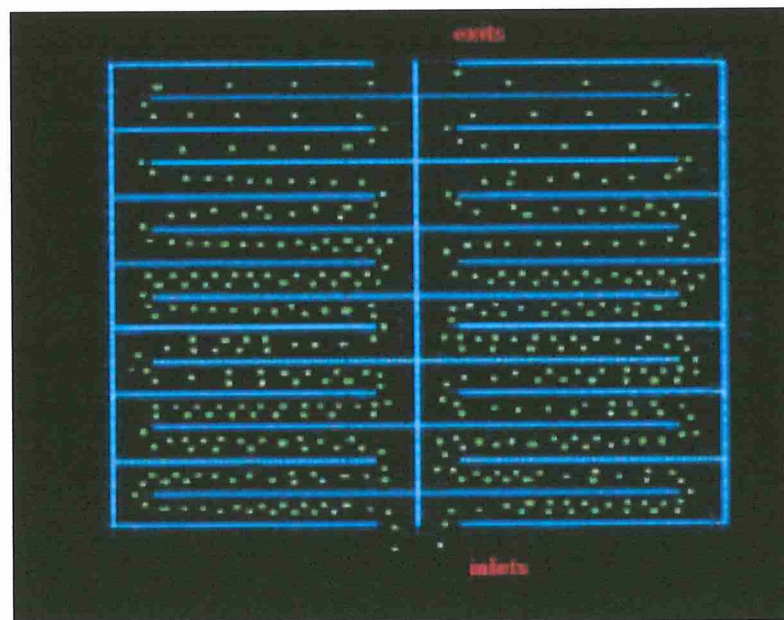
(d)

Figure 4.8. Evolution of pedestrians (t=125s) from a simulation of abreast queue square layouts: (a) Configuration 1, (b) Configuration 2, (c) Configuration 3, (d) Configuration 4.

The results shown in Figures 4.9-11 for these configurations are aggregate of those observed for configurations 1 and 2. Here, the best configuration is again investigated by monitoring the variation of the number of newly infected individuals in terms of infection probability and radius sweep. Looking at the four configurations, by varying the infection probability range, configuration 3 is again the most favorable, whereas the other three configurations result in a similar number of infections when using rope separators (Figure 4.9(a)). Configuration 3 only differs from configurations 1 and 2 by the two left and right zones, enabling faster flow at the inlets and exits. In contrast to configurations 1 and 2 where pedestrians remain in the queue for a longer duration, pedestrians in configuration 3 are exiting halfway with less elapsed time in the waiting line, thus, resulting in less interaction during the shorter wait. Although configuration 4 also possesses two inlets and exits (short exit time), the number of common corners where pedestrians from both zones are at proximate contact is more than that of a rectangular layout.

Also, the square configuration 4 here retains the shortest aisle length among all the configurations of the same square layout and even the rectangular ones. Although short aisles with rope separators allow less interaction as mentioned previously, shorter aisles lead to congestions at the corners where pedestrians reduce their walking speed while changing the direction of motion. Therefore, even with a shorter waiting time than the other configurations, configuration 4 allowed more frequent interactions between pedestrians of both zones resulting in a similar number of newly infected members as configurations 1 and 2, for lower contact radius (Figure 4.9(a)). Thus, the long elapsed time in the queue (aisle and corner) and the abundancy of turning corners have the same effect in increasing infection for rope separators in a rectangular floor layout. For the

same configuration geometries, if the floor layout is increased, i.e. wider and longer aisles, configuration 4 will have a better performance as the interaction at the corners and in the aisles as well as the time elapsed in the queue are lower than those of configurations 1 and 2.

With temporary walls used as aisle separators, the order of the configurations alters as shown in Figure 4.9(b). In this case, only the waiting time within the same line and congestion at the corners play an important role. Referring to Figure 4.8, it can be noticed that the pedestrians' density along the aisles is almost the same between all the configurations. However, at the corners of configuration 4, pedestrians are congregated at higher density than the other layouts leading to an increase in the number of infections for Configuration 4 (Figure 4.9(b)). This is explained by the shorter aisles and the necessity to keep changing velocity direction, thus the reduction in the magnitude of the velocity components. This phenomenon also applies to the rope separator scenario. However, with ropes, the maximum interaction with pedestrians in neighboring aisles and corners is of greater importance and frequency than that within the same line. Configuration 3 remains the most favorable as it comprises a combination of moderate aisle length and less waiting time at corners.
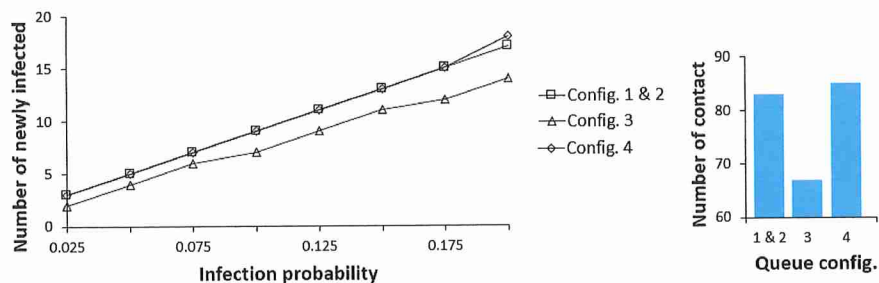
(a)
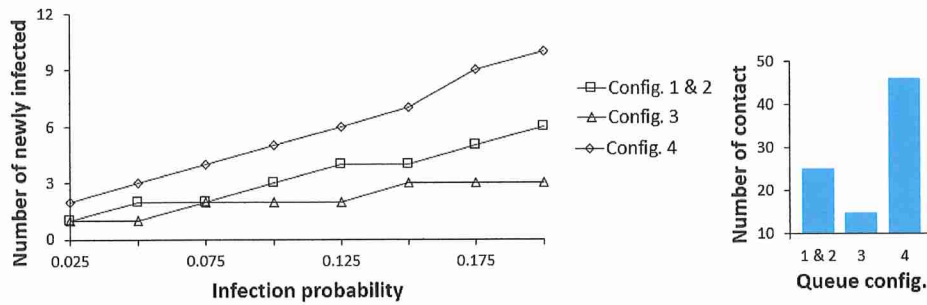
(b)

Figure 4.9. Infection distribution profile for different double queue configurations at a contact radius of 1.2 m. (a) Rope stanchions are used for separation between the rows. (b) Wall separators are used for separation between the rows.

(a)

(b)

Figure 4.10. Infection distribution profile for different double queue configurations at a contact radius of 2.1 m. (a) Rope stanchions are used for separation between the rows. (b) Wall separators are used for separation between the rows.

Expanding the contact radius to 2.1 m assuming aerosol transmission mechanism, all

configurations behave in the same manner for rope separators as shown in Figure 4.10(a).

Here, the infective's influence crosses multiple surrounding aisles and separation zones,

therefore, the number of corners and aisles do not have any effect. For walls, the pedestrians' distribution at the corners alters the results with minor differences (Figure 4.10(b)). Configuration 4 has the most congested corners and highest number of contacts. Figure 4.11 summarizes these results. At a low infection radius, for a rope separator, configuration 3 results in fewer contacts, whereas, with higher contact radii, the differences between the different configurations are reduced. For walls, pedestrians' density at the corners leads to higher contacts for configuration 4. The short waiting time of configuration 3 makes it competitive in all conditions.
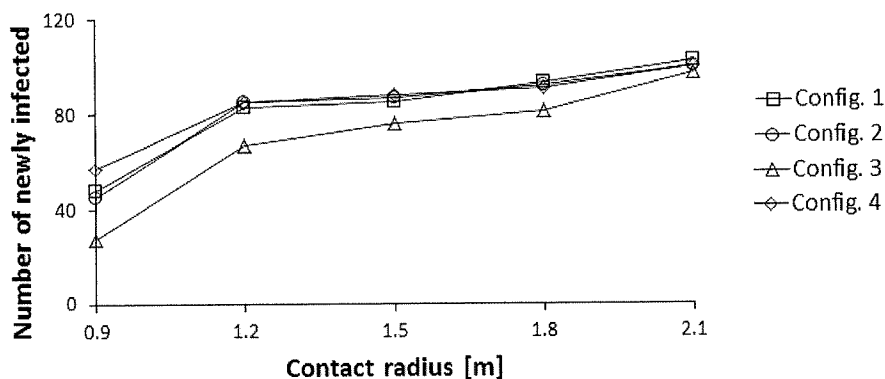
(a)
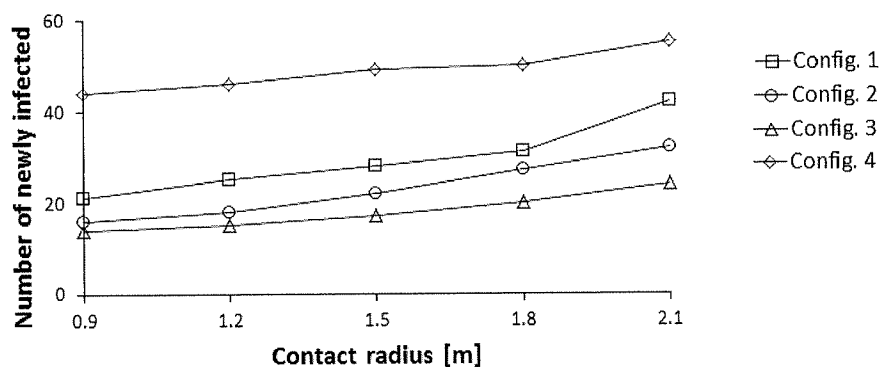
(b)

Figure 4.11. Contact distribution profile for different queue configurations with varying contact radii. (A) Rope separators used between the rows. (B) Walls used for separation between the rows.

4.3.2 Single-File Pedestrian Queue

The single-file pedestrian queues, which are found in many locations, such as ticketing at entertainment locations, airport booking and security checks, etc is now considered. Pedestrian movement is simulated for the four rectangular configurations discussed earlier as shown in Figure 4.12. Here, the pedestrians are initially distributed in a single-file manner. Since no waiting time is assumed at the exit, the single lanes are preserved as time evolves. However, the spacing distance between these pedestrians increases within the last aisle prior to exit as no obstructions delay their motion. Also, pedestrian distributions in aisles and at corners vary between the configurations, which cause some differences in the infection results. This variation results from the difference in aisle length, and corners, zones, inlets and exits distributions.
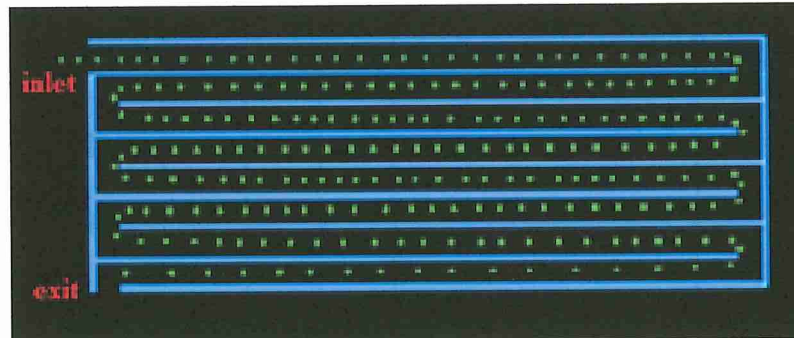
(a)
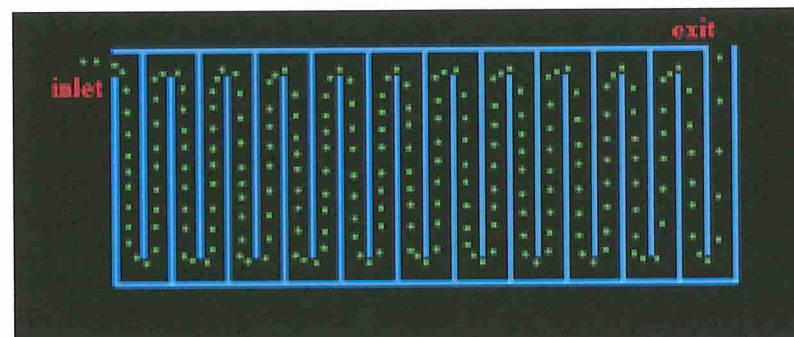
(b)
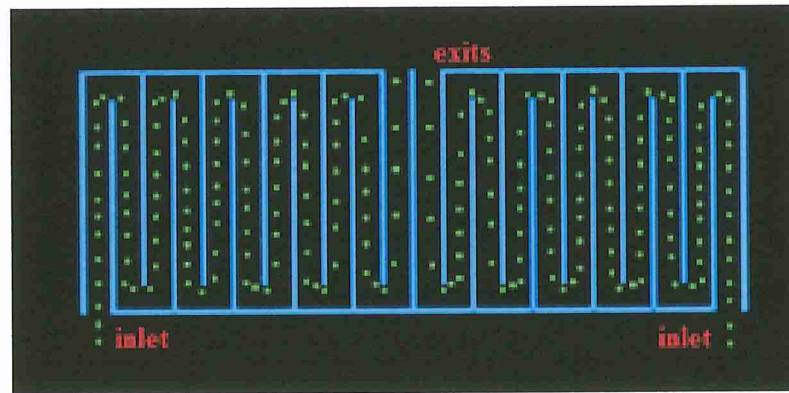
(c)
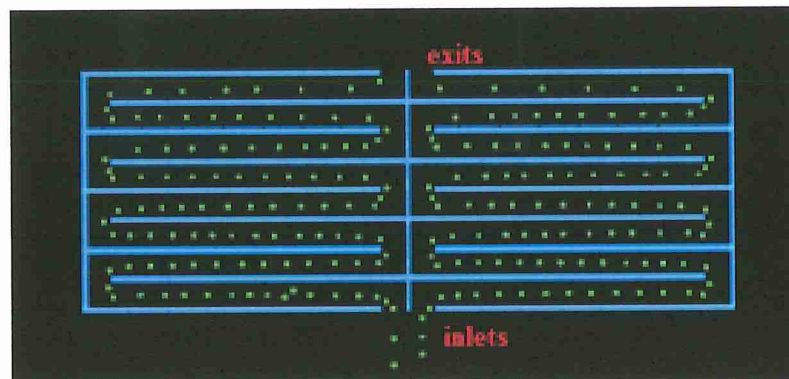
(d)

Figure 4.12. Evolution of pedestrians (t=125s) in single queue layouts of horizontal and vertical patterns for single and double accesses with the same geometric area: (a) Configuration 1, (b) Configuration 2, (c) Configuration 3, (d) Configuration 4.

Evaluating the probability range sweep, it is observed that the results of coarse droplets and aerosols transmission mechanisms are almost identical for rope separators as in Figure 4.13(a) and Figure 4.14(a). The vertical configurations (2 and 3) occupy the lowest mean whereas the horizontal configurations (1 and 4) are of higher values with maximum reached at configuration 1. This independence of the results from the transmission mechanism, with rope separator, is explained by the lower pedestrian density distribution. Despite the short exit time of configuration 3 over configuration 2, the susceptible population in the next-adjacent aisles does not come into critical contact

with the infective causing disease transmission. Only the forward and backward

pedestrians in the line, within the same or straight adjacent aisle, are mostly exposed.

Also, in all the configurations the pedestrian-to-pedestrian distance is larger in a single

queue since they are free to move at a higher degree of freedom as of an abreast queue.

With the solid walls placed, the density of pedestrians at the corners makes the difference

between the configurations for high transmission range, whereas aisles have greater effect

in low infection range. Configuration 1 proves to be the most efficient in reducing contact

for a single file formation (Figure 4.13(b) and Figure 4.14(b)).
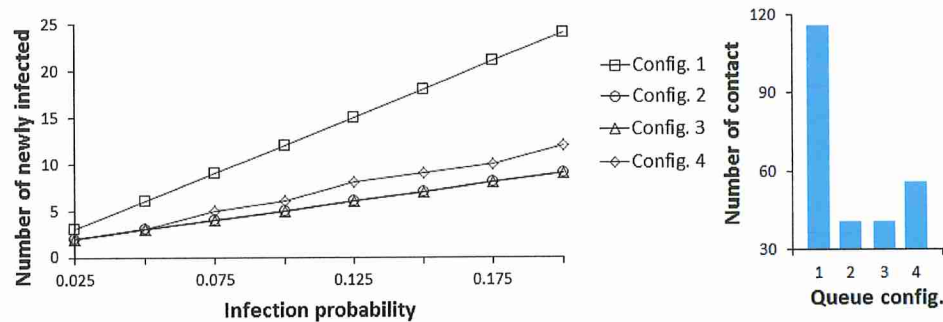
(a)
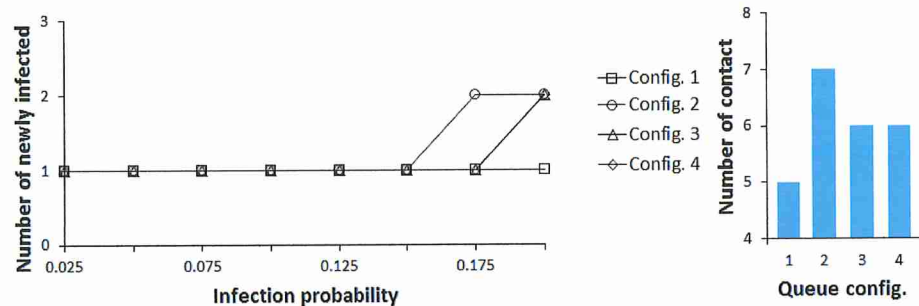
(b)

Figure 4.13. Infection distribution profile for different single queue configurations at a
contact radius of 1.2m. (a) The rope is used for separation between the rows, (b) The
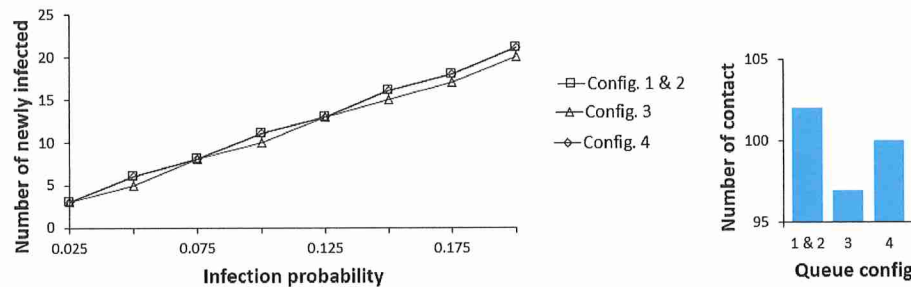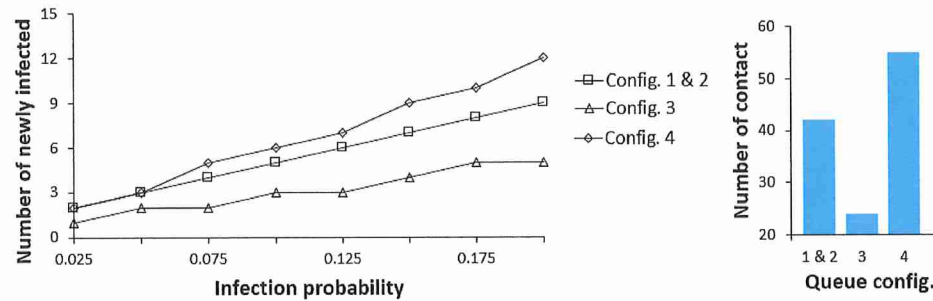temporary shading walls are used for separation between the rows.
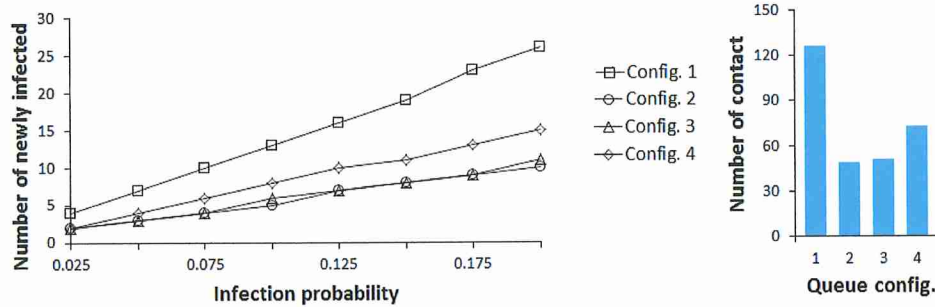
(a)
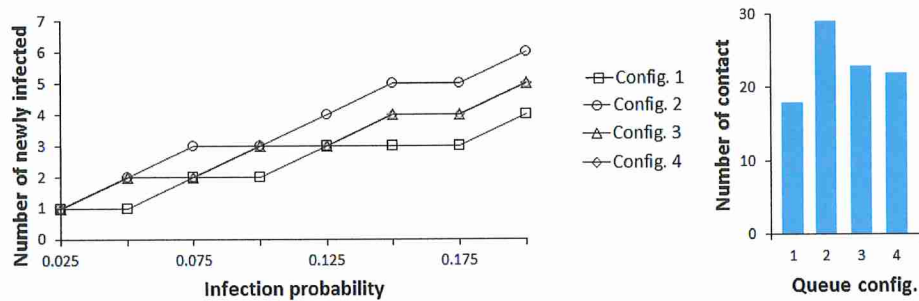
(b)

Figure 4.14. Infection distribution profile for different single queue configurations at a contact radius of 2.1 m. (a) The rope is used for separation between the rows, (b) The temporary shading walls are used for separation between the rows.
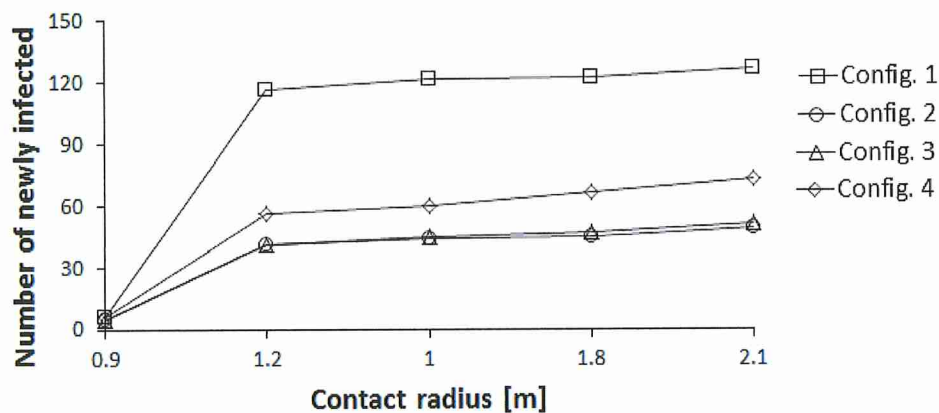
(a)
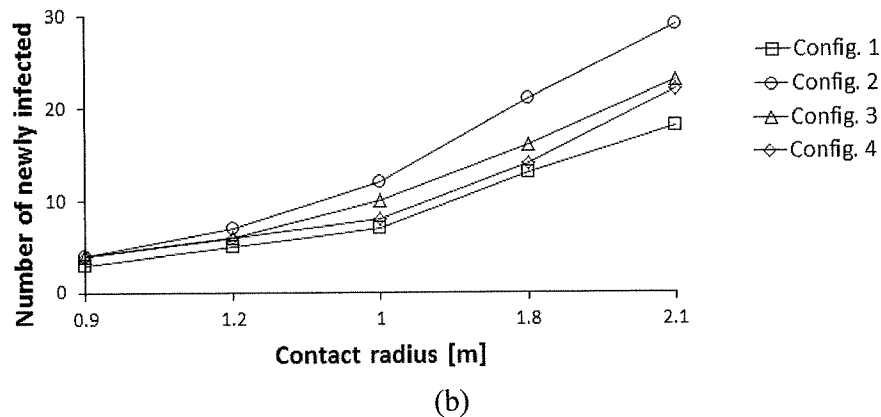
(b)

Figure 4.15. Contact distribution profile for different single queue configurations. The contact radius is varied. (a) The rope is used for separation between the rows, (b) The temporary shading walls are used for separation between the rows.

On the other hand, the variation of the transmission mechanism represented by the radius sweep also impacts the results. With a contact radius smaller than the aisle width, all configurations behave in the same manner (Figure 4.15(a)). Here, the contact occurs only within the same aisle, whether walls or ropes are used for separation. When the contact radius crosses to the neighboring aisles, the single-zone and double-zone vertical, short aisles allow short mixing (low-time exposure), therefore, are favorable to suppression of disease propagation (Figure 4.15(a)). The inverse phenomenon is observed when wall separators that isolate each aisle from its surrounding aisles are used. Here, the configurations with higher congestion at the turning corners like configuration 2, result in a higher mean number of infections (Figure 4.15(b)).

4.4 Discussion

The modeling approach developed in this study provides a unique approach to combine pedestrian movement models and infectious disease spread models. By tracing the trajectory of each pedestrian in the time frame, the data of contacts between susceptible and infective pedestrians is obtained. Then, applying a stochastic susceptible-infected model to the contact data determines the number of newly infected individuals

who are in critical contact with the infectives. This model has applications in the design

of high pedestrian density locations which are often associated with infectious disease

spread (Gautret & Steffen, 2016; Centers for Disease Control, 1983; Olsen et al., 2003;

Mangili & Gendreau, 2005; Gundlapalli et al., 2006; McCarthy, 2015; Pfaff et al., 2010;

Verhoef et al., 2008; Zieliński, 2009; Foo et al., 2009; Botelho-Nevers et al., 2010; Evans

et al., 2002). The approach for layout design is demonstrated by applying the model to

various configurations of pedestrian queues and assessing the contact and infection

spread dynamics as a function of various parameters.

Another aspect of the model deals with addressing the inherent uncertainty in this

problem. Human movement is often guided by discretionary behaviors with respect to

route and destination choices, intrinsic variability in pedestrian speed and inter-pedestrian

interactions, which results in a high level of uncertainty. This aleatory uncertainty is

further compounded by the combination with the infectious disease spread model, which

introduces variables like transmission probability and contact radius. The sources of

uncertainty are parametrized, thereby assessing the conditions under which certain

configurations or strategies are effective in mitigating disease spread. To account for the

various transmission likelihoods and transmission mechanisms, the transmission

probability and contact radius is varied in the parameter sweep. This approach can

identify the effectiveness and vulnerability of a given mitigation strategy. For example,

Figures 4.5 to 4.11 indicate that configuration 3 is the more effective configuration in

reducing the number of contacts across different parameter combinations. Further

analysis suggests that the difference between queue configurations is highest at low

contact radii (e.g. 1.2 m) compared to high contact radius (2.1 m), and also for higher

transmission probabilities. Such information can be useful for designing queue layouts with the objective of minimizing contact for a specific outbreak.

Three main methods are identified to reduce the number of contacts when pedestrians are waiting in queues. The shape and configuration of the layout affect the number of contacts. A longer rectangular queue with pedestrian movement aligned along the short side like in configurations 2 and 3 reduces the number of contacts. Another simple way of reducing the number of contacts in waiting queues is if temporary walls are used in place of rope separators. Such walls would potentially limit the contacts within the row, which would reduce the number of contacts from up to 55% to 75% compared to rope separators (see Figure 4.16(a)). Another approach is to reduce the aisle width to create a single file queue. Figure 16(b) compares the number of contacts between the default case and when a single file is enforced. The overall number of contacts reduces by 8 - 25% in the considered queue configurations when a single file queue is considered.
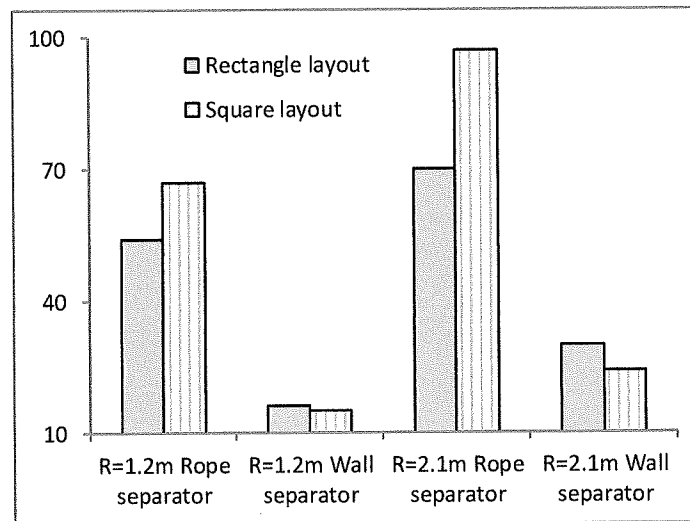
(a)
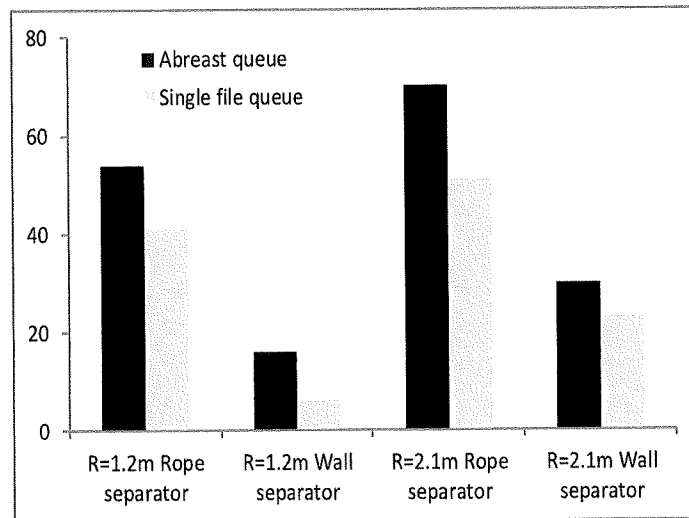
(b)

Figure 4.16. Comparison of the number of contacts between different configurations and queue arrangements. (a) Rope separators and walls for rectangular and square layout for configuration 3 with a contact radius of 1.2 m. (b) A similar comparison for the rectangular layout between the default and a single file queue setup.

4.5   Summary and Conclusions

There is a strong correlation between contact rates and infection rates in disease epidemics. The movement and interaction of people in high pedestrian density environments affect the number of contacts and thereby impact infectious disease spread. The mixing of susceptible and infectious individuals in these high people density environments involves pedestrian movement which is often not taken into account in the modeling studies of disease dynamics. In this thesis, a multiscale model is developed for incorporating input from pedestrian dynamics models into a stochastic infection spread model. The model is applied to a ubiquitous problem of contact evolution and infectious disease spread in pedestrian waiting queues.

The effect of queue configurations on generating contacts between neighboring pedestrians is evaluated. Four distinct queues are evaluated with vertical and horizontal

aisle patterns, one or two waiting zones, rectangular and square floor plans, and single-file or abreast pedestrian distributions within the control area. In these various geometrical scenarios, a comparison is made between the rope and wall separators and their effect on pedestrian interactions. With rope separators, pedestrians are allowed to interact with other pedestrians from neighboring aisles in addition to the forward and backward members in the queue within the same aisle. However, for wall separators, the interaction between pedestrians is restricted to those only within the same aisle.

The wall separators are found to be very effective in reducing the number of contacts and disease spread. In some cases, replacing ropes by wall separators results in a reduction in number of contacts by more than 75%. Among the different queue configurations considered in the study, configurations with motion along short aisles lead to lower number of contacts and disease spread when rope separators are used. Also, for the same area of the queue layout, it is found that rectangular configurations lead to lower number of contacts than square configurations. While the model is applied to the specific case of pedestrian queues in this paper, the general principles can be used for analysis of infectious disease spread in any high pedestrian density location.

5. Parameter Space Exploration and Uncertainty Quantification of Viral Outbreak

In chapters 3 and 4 multiscale models are developed to include the effect of pedestrian movement and behavior in the evolution of the contact network and the spread of infectious diseases. Pedestrians' movements were modeled during enplaning, deplaning and progressing in waiting queues. Due to the inherent stochasticity in pedestrian behavior and in disease propagation, especially at the early stage of epidemics, several uncertainties arise in the multiscale framework. The sources of uncertainty are parametrized and a parameter sweep is carried out to identify the accurate ranges of these parameters and assess the effect of the parameter variation on the eventual outcome. A conventional lattice-based parameter sweep that repartitions equally the one-dimensional domain of each parameter is first used for the purpose. However, this method has imposed two main challenges on the level of the simulations elapsed time and detection of convergence. During decision making for preventive strategies that can mitigate the disease spread among a population, the conventional parameter sweep method is impractical especially as the number of parameters increases. Instead, a novel approach using a low discrepancy sequence (LDS) is proposed here.

In this chapter, the importance of parameter sweep is first emphasized and its necessity in the multiscale model comprising a high degree of stochasticity. Then, LDS is applied separately for the pedestrian algorithm as well as the infection contact-based model. It is shown that LDS algorithm converges at coarser mesh compared to a lattice parameter sweep when applied to the queue configuration 3 of the previous chapter. Here, the pedestrian dynamics and infection model parameters are swept over large

parameter space. A total of five parameters are considered between the two models resulting in a 5D parameter space. Four different mesh types are evaluated; those are 5D lattice, 3D pedestrian lattice combined with 2D infection LDS, 3D pedestrian LDS combined with 2D lattice and 5D LDS. The convergence is evaluated in terms of the mean, standard deviation, kurtosis and skewness. LDS is more effective with dimensionality increase of the domain of definition of the parameters used. Also, with the increase of dimensionality, the parameter space should be meshed finer for both the Lattice and LDS methods (more simulations are required) to attain convergence. Comparing 5D lattice to 5D LDS, the number of required simulations has drastically decreased down to less than 1% of the initial effort required during conventional parameter sweep.

5.1   Necessity for Massive Parameter Sweep

Airborne diseases are caused by pathogens suspended in the air including bacteria, fungi or viruses. These organic particles, secreted by the nasal tracts and throat of an infected individual are dispersed to the environment through breathing, talking, sneezing or coughing. Contraction of airborne diseases may occur by directly inhaling pathogenic organisms by nose or touching a contaminated surface then transmitting the virus by contact with the mouth or eyes. As these viral particles are able to remain suspended in the air and navigate for long distances, there is a high risk of disease outbreak in a local area among a population. Two main factors determine whether transmission will take place between the infective and the susceptible population; those are the survival lifetime of the agent in the environmental conditions and the number of contacts between the infected and susceptible population.

Various mathematical models describing infection transmission by respiratory tracts and proximate contact have been used to correlate human interventional behavior to disease transmission (Heesterbeek et al., 2015). Knowing that reducing contact between people during an outbreak can restrain the disease, analyzing the mixing pattern allows a better understanding of the disease dynamics (Barrat et al., 2010).

In the context of analyzing the effectiveness of alternate pedestrian mixing pattern policies to reduce infection spread in crowded environments through the proposed multiscale model, numerical simulations are performed to mimic the actual behavior of pedestrians in real life using a molecular dynamics self-propelled entity-based approach. The difficulty in modeling pedestrian movement lies in predicting pedestrian behavior at a given location (e.g. airport), given the various discretionary activities people participate in. No two individuals behave exactly in an alike manner because of their fundamental stochastic response to environmental effects. However, it is essential to develop some framework to mimic, up to a certain extent, the movement of pedestrians in an environment. This helps to develop, for instance, evacuation strategies in emergency encounters by computationally and mathematically approaching the scenario. Also, modeling pedestrian movement is essential during viral outbreaks. The interaction between proximate individuals stimulates disease propagation among the crowd.

Pedestrian motion is mathematically modeled by means of force fields, but defining the used parameters' values is a strain. The proposed self-propelling momentum is based on the social force model. The intentional (attractive) term depends on a local position-based input. In other words, the navigation speed is a function of the free, desired speed (v_0) and the distance (δ) between the pedestrian and the very front person in the queue.

Also, the pedestrian model used in this study comprises a repulsive term, preventing collision with obstacles, which is inspired by the Lennard-Jones atomic repulsive term. The switch of use of this force field from molecular to pedestrian application requires calibrating its parameters to reflect the real behavior. Some experimental data is available in literature to estimate the range of certain parameters. For other parameters, parallel computing is required to vary the unknown model parameters over a large design space and validate the appropriate combination that communicates the observed behavior.

Also, at the early stage of an epidemic outbreak, there is no specific model that estimates the precise propagation rate and its direct impact on the population due to intrinsic uncertainties. The propagation rate (P_{inf}) and mechanism (coarse droplet or fine aerosol particle transmission) represented by the contact radius (R) vary accordingly for each disease and the infective individual's clinical condition creating a large two-dimensional space. Table 5.1 discussed later, shows the large parameter space generated by this problem.

In order to quantify the uncertainties related to the self-propelled entity dynamics model as well as the stochastic epidemic individual-based model, the sources of uncertainty are parametrized and a parameter sweep is carried out over the parameters' ensembles to evaluate the robustness of these parameters. The parameter sweep methodology is successfully used in three scenarios: deplaning and enplaning during air travel, matching density in pedestrian bottlenecks and pedestrian queues to mitigate infectious disease spread. From the evolution of pedestrian trajectories in the time and spatial frames, the contact data is obtained. The contact data is then combined with a

stochastic epidemic individual-based model to estimate the distribution of the newly infected individuals.

The uncertainties of the proposed multiscale model may be addressed using several parameters sweep approaches; those are the uniform and non-uniform sweeping methods. The lattice-based method is the commonly used uniform method whereas pseudo-random and quasi-random are non-uniform methods. Non-uniform domain partition methods are promising algorithms enabling faster convergence at lower number of simulations compared to the lattice method. Quasi-random sequences are deterministic alternatives to pseudo-random sequences, referred as Low Discrepancy Sequences (LDS). In the context of this chapter, it is proposed to use the Scrambled Halton LDS as a parameter sweep method.

Exploring the vast parameter space in the context of pedestrian dynamics and infection spread will help identify vulnerabilities in a given strategy with a specific objective. For example, in the previous chapter, using temporary walls is proven to be effective in suppressing disease spread; if a parameter sweep is conducted for this problem, it can be analyzed, under what conditions is this policy effective? Are there conditions when this policy is less effective than the alternative? In addition, the parameter sweep can help determine the modeling parameters that most effectively model a given problem. Two such instances of parameter sweep are presented and used to determine modeling parameters, before proceeding to discuss effective parameter sweep methods in the second half of the chapter.

5.1.1 Determining Model Parameters for Pedestrian Dynamics in an Airplane

This approach has been previously used by Namilae et al. (2017a) to determine

adequate movement strategies that mitigate intervention between travelers and can

potentially suppress infection propagation. Namilae et al. (2017a) determined the exact

values of the parameters of the social force model such as the pedestrian desired speed,

the cut-off distance and the repulsive potential constants based on the deplaning time

aboard airplanes (Figure 5.1). Namilae et al. (2017a) performed a three-dimensional

lattice-based parameter sweep over a space of $41^3 = 68921$ combinations assuming 41

equally spaced possibilities for each of the three parameters. To accelerate the

computational effort, the algorithm was parallelized and run on the Blue Waters system at

the National Center for Supercomputing Applications (NCSA). The same computational

effort would have consumed several thousand hours if the computations were sequential.

In continuation of this work, diseases spread during air travel are assessed for various

diseases assuming a range of transmission probabilities dependent on the evolution of the

virus in the blood serum and contact radii ranges. The multiscale framework combining

the social force approach and the epidemic model is applied to airplane boarding and

deplaning for different carrier capacities and configurations ranging between 50 and 240

seats (Namilae et al., 2017b; Derjany et al., 2017; Derjany et al., 2018).
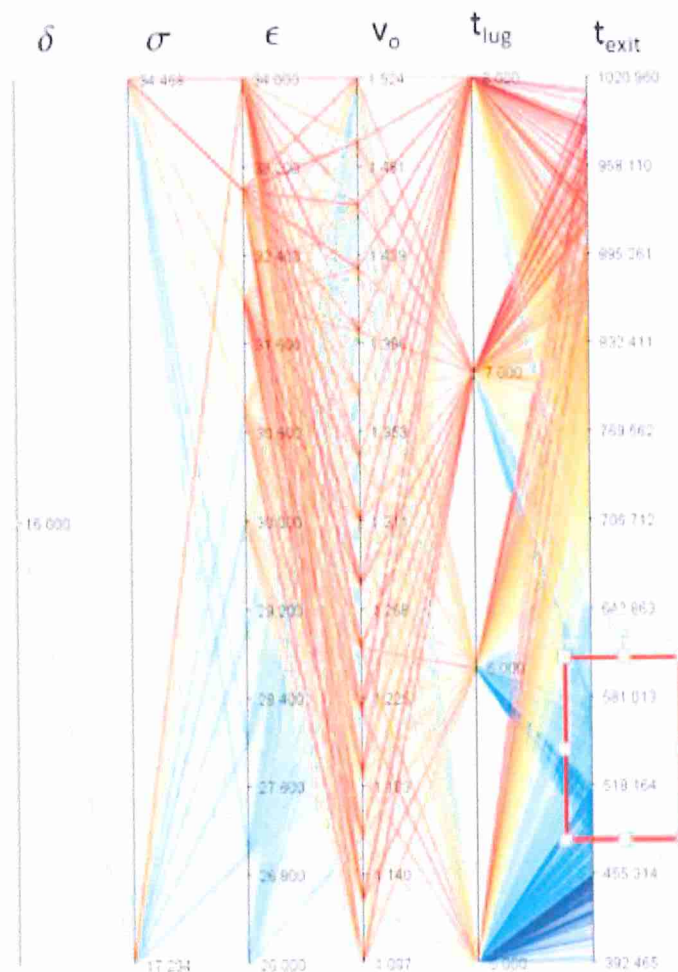
Figure 5.1. Parallel coordinate plot of model parameters sweep leading to different exit times (Namilae et al., 2017a).

5.1.2 Matching Density in Pedestrian Bottlenecks

Here, an application of a lattice-based parameter sweep to determine the correlation between pedestrian speed and density is presented. There is significant experimental evidence for reduction of pedestrian speed with increase in pedestrian density with studies dating back from 1935 (Greenshields et al., 1935). Crowd density is one of the primary factors affecting the movement of pedestrians. This is expected to be more important during emergency and high-crowd density situations. A crowd density is defined as the ratio of neighboring pedestrians over the area within a cut-off distance

from the targeted pedestrian navigating towards his destination. In this field, there is

significant experimental evidence for reduction of pedestrian speed with increase in

density. The reduction in the speed of the overall pedestrian group as a function of

density has been curve-fitted to experimental data and is expressed either in linear,

exponential or polynomial forms (Greenshields et al., 1935; Older, 1968; Navin &

Wheeler, 1969; Fruin, 1970; Pushkarev, 1975; Tregenza, 1976; Polus et al.,, 1983;

Tanaboriboon et al., 1986; Tanaboriboon & Guyano, 1989; Weidmann, 1993; Lam et al.,

1995; Tewarson, 2002; Al-Azzawi & Raeside, 2007; Bruno & Venuti, 2008; Jia et al.,

2009; Laxman, Rastogi & Chandra, 2010; Chen, Ye & Jian, 2010; Rahman et al., 2013;

Rastogi & Chandra, 2013; Das et al., 2015; Kretz et al., 2016; Nikolić et al., 2016;

Kawsar et al., 2017) by various researchers. This behavior is often termed as fundamental

diagram of pedestrian motion. The table in Appendix A tabulates the previous research

on density-speed relation found in literature.

A theoretical model is proposed to reflect the comportment of pedestrians in a crowd

by implementing the effect of density on the individual's behavior and decision making

within the framework of the social force pedestrian dynamics model. The speed-density

diagram is confined by two essential boundary conditions that control the motion of

pedestrians. Those are achieved at a minimum surrounding crowd density (ρ_{min}) where

the pedestrian is not impeded by adjacent pedestrian and he is free to move at his desired

speed ($V_{ped_{max}}$), and a highly packed crowd (ρ_{max}) where the herd accumulates and

forms a cluster exiting at a sedate footpath ($V_{crowd_{min}}$) towards a narrow congested

single-directional exit.

The model is implemented in an evacuation simulation of pedestrians from a room with a single exit (Figure 5.2) to replicate the controlled experiment (Figure 5.3) performed by Daamen and Hoogendoorn (2003). In their experiment, volunteers were required to walk through a bottleneck of 1m opening. The scene was recorded and the density-speed data were collected from visual interpretation by Nikolić et al. (2016) within a rectangular area labeled in blue in Figure 5.3. Nikolić et al. (2016) then plotted the speed-density relationship using a probabilistic method for 119,156 observations. The mean values of their findings were compared to speed-density models suggested by Tragenza (1976), Weidmann (1993) and Rastogi et al. (2013). In this study, the experiment is replicated by means of three models (1) without implementing the density term to the speed equation, by implementing (2) a linear density-dependent relation (Polus, 1983; Tanaboriboon, 1986; Tanaboriboon, 1989) and (3) a non-linear density-dependent expression (Das et al., 2015 & Kawsar et al., 2017). The evolution of the particles, representing pedestrians, in the MD model is shown in Figure 5.2.

The speed expression comprises some unknown parameters such as the minimum pedestrian speed V_A, the pedestrian speed constant V_B, the maximum crowd density ρ_{max}, and the minimum crowd speed $V_{crowd,min}$. Setting the parameters (Table 5.1) the exact values were estimated using parameter sweep on 27,000 processors on National Center for Supercomputing Applications (NCSA) Bluewaters supercomputer. The best-fitting mean speed-density curve is obtained with their attributed parameters' values, then compared to the work of Nikolić et al. (2016). A qualitative match is found between speed-density plots from simulations (Figure 5.4) and the experimental observations

(Figure 5.5). This example shows another use of parameter sweeps in engineering

problems related to pedestrian dynamics.
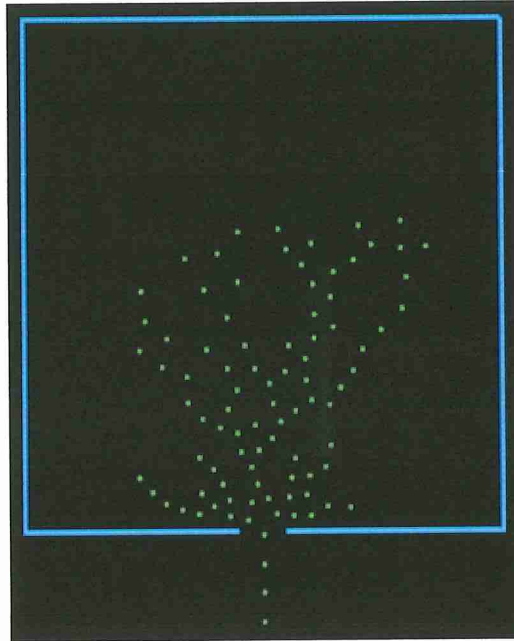
Figure 5.2. Simulation of an evacuation scenario from a room with a single exit.
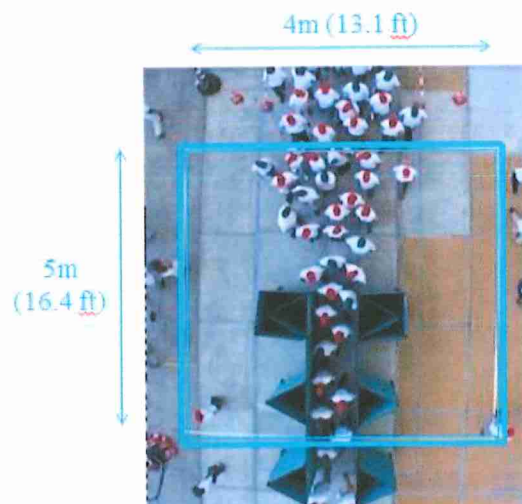
Figure 5.3. A controlled experiment of a crowd passing through a bottleneck (Daamen & Hoogendoorn, 2003).

Table 5.1

Parameters range of the pedestrian speed-density formulation.

Description	Parameter	Range	Increment	Array length
Minimum pedestrian speed [ft/s]	V_A	[3,5]	0.5	5
Pedestrian speed constant [ft/s]	V_B	[16,20]	1	5
Maximum crowd density [ped/m^2]	ρ_{max}	[3,7]	1	5
Minimum crowd speed [ft/s]	$V_{crowd,min}$	[3,8]	1	6
Pedestrian distribution pattern				12
Desired speed formulation				3
Total number of combinations				27,000
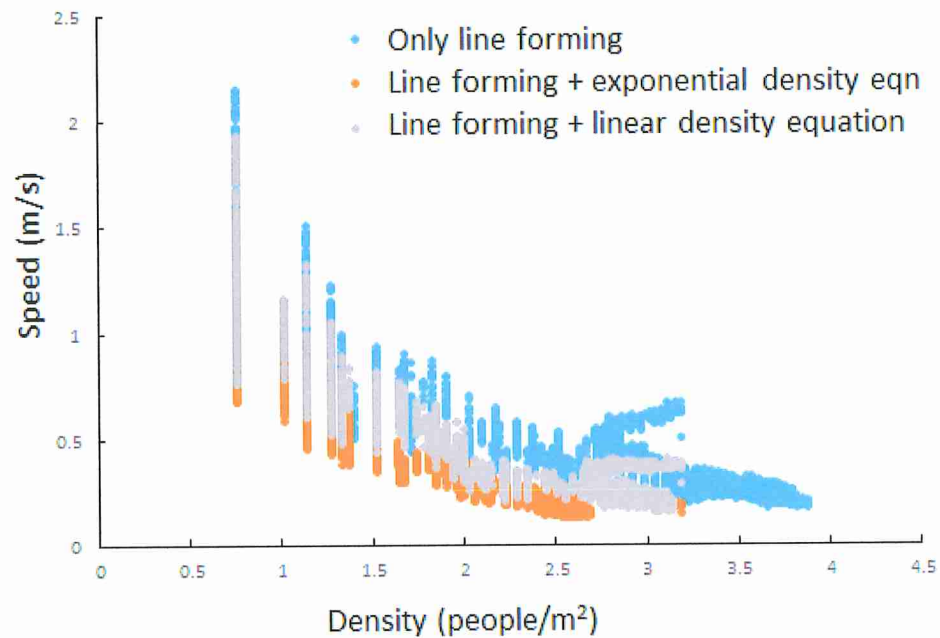
Figure 5.4. Speed-density plot for various speed formulations.
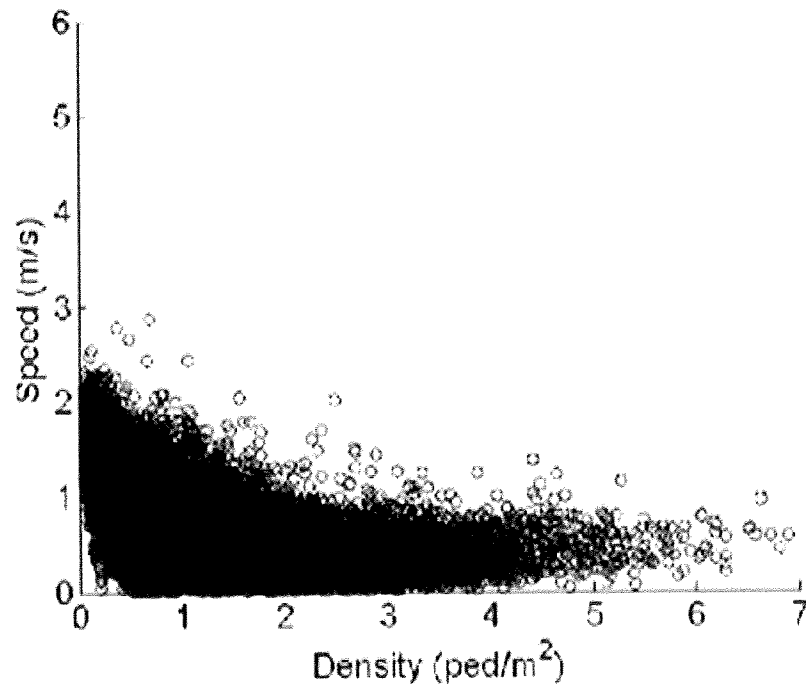
Figure 5.5. Speed-density plot from the controlled experiment (Nikolić et al., 2016).

5.2 Methodology

The multiscale model characterizing infection spread through the pedestrian movement model has included many new features compared to its predecessors. The potentially introduced features comprise parameters that create a significant challenge for tuning especially that the human behavior is stochastic by nature and some factors of infection propagation are not identifiable. Using one-at-a-time tuning of parameters may degrade the other parameters. A better adjustment of these variables over their large domain of definition requires permuting simultaneously all the variables.

The lattice-based algorithm applied in Namilae et al. (2017a) to the pedestrian model is re-applied here for the set of parameters under investigation. In Namilae et al. (2017a), the pedestrian model parameters are swept over their ranges of definition. Here, the framework consists of applying the parameter sweep for the pedestrian parameters first,

generate a set of trajectories output files to which the infection parameter sweep

algorithm is then applied as the workflow in Srinivasan et al. (2016). The time

consumption and the necessity to detect convergence more precisely do not make the

lattice algorithm a good parameter sweep method and urge to apply a novel Scrambled

Halton Low Discrepancy Sequence (LDS) method for the parameter sweep as in

Chunduri et al. (2018). Another significant advantage of LDS is that if additional

variables are added later to the multi-scale model, the scrambled Halton sequence enables

re-using previous output files. This facilitates 'restart' of parameter sweep problems. In

Chunduri et al. (2018), LDS is only applied to the pedestrian model. Here, LDS is applied

interchangeably for the pedestrian and infection models with their parameter ranges

shown in Table 5.2. The results are then compared to the lattice method to prove the

efficiency of LDS in terms of faster convergence and execution time.

Table 5.2

Parameters range of the pedestrian-infection model formulation.

Parameter	V_0	δ_1	δ_2	R	P_{inf}
Range	3.2-5.4 ft/s	15-25 in	25-40 in	36-84 in	0.025-0.225

For Lattice and LDS sweeping algorithms, a coarse mesh is initiated then refined until

convergence is attained. At each mesh size, a histogram with the targeted variable (the

mean number of newly infected pedestrians) versus the frequency of occurrence is

plotted. For each histogram, four descriptive moments of the probability distribution are

determined. As the statistical moments are of different scales, a relative difference is used

to check for convergence. Once the relative differences converge within an approximated

tolerance allowed from zero value, no more refinement of the parameter space is

required. The four descriptive moments used are the mean, standard deviation, skewness and kurtosis. The mean is given by the relation:

$$\bar{x} = \frac{\sum_{i=1}^{N} p_i x_i}{\sum_{i=1}^{N} p_i} \tag{22}$$

Where x_i is the variable evaluated in the histogram (on the x-axis, and p_i is the frequency or probability of repetition.

The standard deviation from the mean expressed in equation (22), for the number of newly infected pedestrians considered as a discrete variable and obtained from various mesh elements is the square root of the variance:

$$s = \sqrt{\frac{\sum (x-\bar{x})^2}{N}} \tag{23}$$

Skewness is the degree of distortion, asymmetry or shift from the mean in a symmetrical bell curve or a normal distribution. Skewness is expressed by:

$$Skewness = \frac{3.(\bar{x}-median)}{s} \tag{24}$$

Where the median is the value of the $\left(\frac{N+1}{2}\right)^{th}$ term in the cumulative data distribution.

Kurtosis, also used to describe the distribution, defines the sharpness, or tailedness of the peak of a frequency distribution curve. Kurtosis defines the difference heaviness between the normal and the evaluated distribution. Kurtosis is obtained from:

$$Kurtosis = \frac{\sum (x-\bar{x})^4}{N.s^4} \tag{25}$$

The convergence criterion between two successive runs (run "i" and run "i+1") of different mesh sizes is validated by the percentage difference relation:

$$\frac{V_i - V_{i+1}}{\left[\frac{V_i + V_{i+1}}{2}\right]} \leq \varepsilon \tag{26}$$

Where V is a statistical variable and ε is a tolerance value ($0 \leq \varepsilon \leq 1$). The selection of the tolerance order depends on the statistical moment. For instance, for the relative mean, ε is of the order of 10^{-3} compared to 10^{-1} for the root of standard deviation, skewness and kurtosis. The abrupt drop of the relative kurtosis from a value greater than unity to a value of order 10^{-1} indicates that the histogram distribution is invariant between the runs. When all these conditions are met, then, convergence is attained.

In the previous chapter, different queue configurations are evaluated in terms of contact generation and infection propagation among neighboring pedestrians. These queues vary in shape and aisle arrangement but the floor area is kept constant. Four different aspects of the queue are varied; those are (1) the aisles layered in a vertical or horizontal pattern, (2) the waiting area portioned into two zones or kept as one zone, (3) pedestrians distributed in a single file or abreast side-by-side pattern and (4) the floor plan shaped in a rectangular or square manner. The different combinations of pedestrian queues aspects generate a large qualitative and quantitative parameter space. In addition, with every queue scenario, an infective walker is introduced to the population assuming various probabilities of transmission and contact radii. The queue and infection parameter sweep generating different numbers of newly infected individuals is shown in Figure 5.6. Among the different evaluated combinations, configuration 3 with a two-zone floor plan is suitable to mitigate disease spread due to the distribution of its aisles and corners within the zones.

In this chapter, the study focuses on the abreast rectangular queue configuration 3 with a rope separator and the various pedestrian and infection parameters are evaluated by means of a novel low discrepancy parameter sweep that is expected to lead to

convergence faster and more effectively than the conventional lattice-based method used previously to match parameters in airplanes.
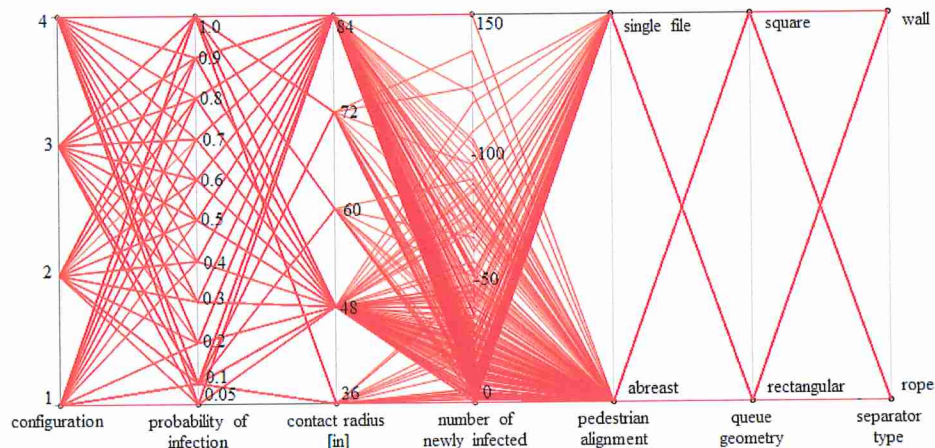
Figure 5.6. Parallel coordinate plot of a 6D parameters combinations and their corresponding infection generation.

5.3 Results

Lattice and Low Discrepancy Sequence (LDS) parameter sweeps are performed at various mesh sizes. The objective of these simulations is to determine the computationally most efficient sweeping method. Four different algorithms are applied in the search of infection transmission rates among a crowd in the queue. First, 5D lattice (3D pedestrian and 2D infection models) simulations are executed. Then, a combined LDS and lattice are then applied for the 3D pedestrian and 2D infection parameters space interchangeably. Finally, a 5D LDS is used for the entire multiscale model.

5.3.1 5D Lattice (3D Lattice pedestrian parameters x 2D Lattice infection) Parameters Sweep

Exploring the parameter space of the multiscale model, a lattice-based parameter sweep is applied first on the parameters of both models separately. The trajectories are obtained from the social force based pedestrian model at different pedestrian speeds and

allowable proximate pedestrian-pedestrian distance. The contact data is then generated

from the instantaneous position data of every pedestrian at various distance and

transmission probability. Looking for the sensitive parameters mostly contributing to

infection transmission, a parameter sweep is achieved at various mesh sizes, starting from

a coarse mesh and refining the space repartition successively until convergence is

reached. The ranges of the parameters as well as the different space repartitions are

shown in Table 5.3.

Table 5.3

5D Parameter space exploration using the lattice-based algorithm.

Parameter	Range	Mesh type	Mesh sizes					
			Mesh 1	Mesh 2	Mesh 3	Mesh 4	Mesh 5	Mesh 6
V_0	3.2-5.4 ft/s	Lattice	12 (0.2)	12 (0.2)	23 (0.1)	23 (0.1)	23 (0.1)	23 (0.1)
δ_1	15-25 in	Lattice	3 (5)	3 (5)	3 (5)	11 (1)	11 (1)	11 (1)
δ_2	25-40 in	Lattice	4 (5)	4 (5)	4 (5)	16 (1)	16 (1)	16 (1)
R	36-84 in	Lattice	5 (12)	9 (6)	25 (2)	25 (2)	49 (1)	97 (0.5)
P_{inf}	0.025-0.225	Lattice	9 (0.025)	9 (0.025)	21 (0.01)	21 (0.01)	21 (0.01)	21 (0.01)
Number of grid points			6,480	11,664	144,900	2,125,000	4,165,392	8,245,776

Note: For the different mesh dimensions, the numbers between parentheses represent the increment size of each parameter.

After running all the simulations with a different number of grid points, the

histograms, in Figure 5.7 (a-f), plot the mean number of newly infected pedestrians

versus their frequency of occurrence at each parameter combination. Note that

convergence can be visually ascertained when the shape of the histogram remains

proportionally the same while increasing the number of simulations. With running more

simulations, the histograms gradually start to alter in shape until convergence is reached

and the overall shape remains unchanged (for instance, starting from mesh 4 in Figure 5.7d here). The convergence is then validated theoretically by statistical variables.

MESH 1

(a)

MESH 2

(b)

MESH 3

(c)

MESH 4

(d)

MESH 5

(e)

MESH 6

(f)
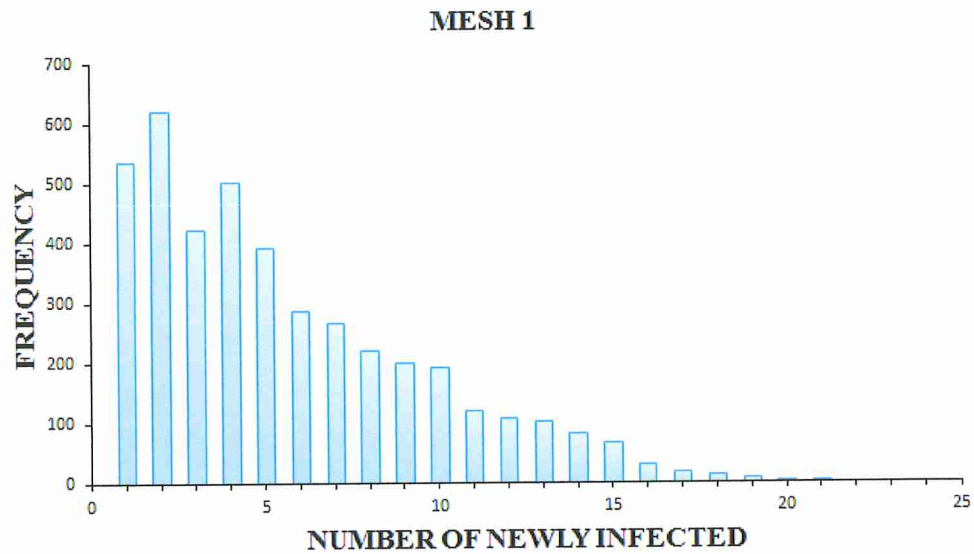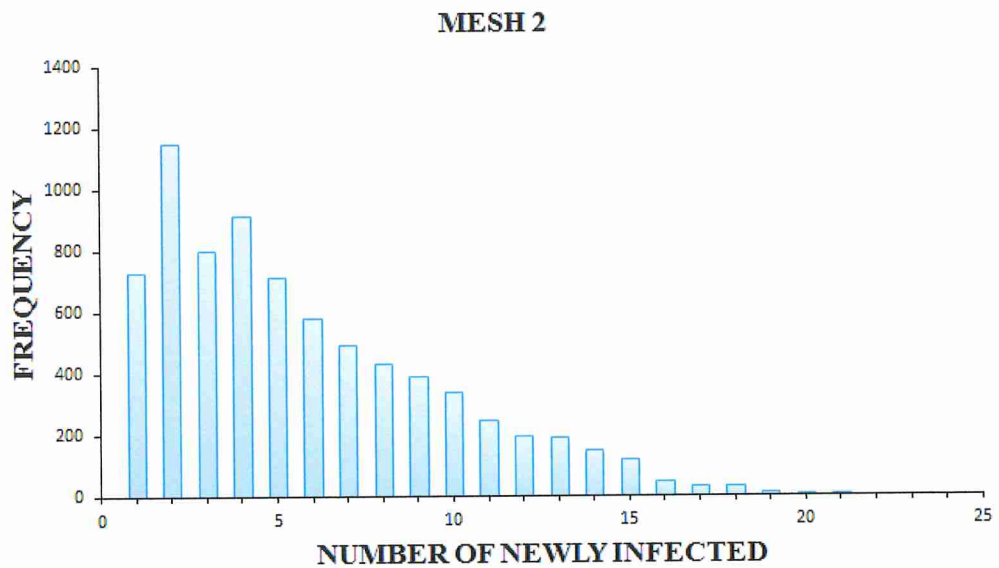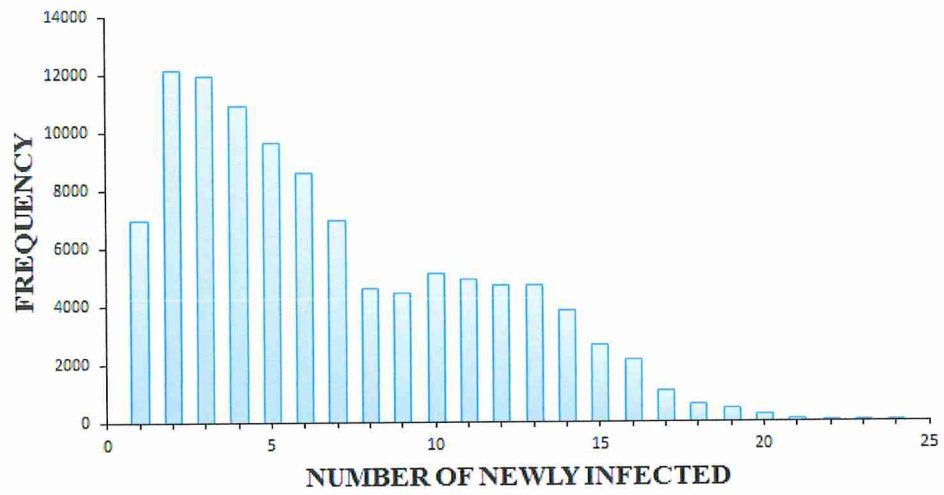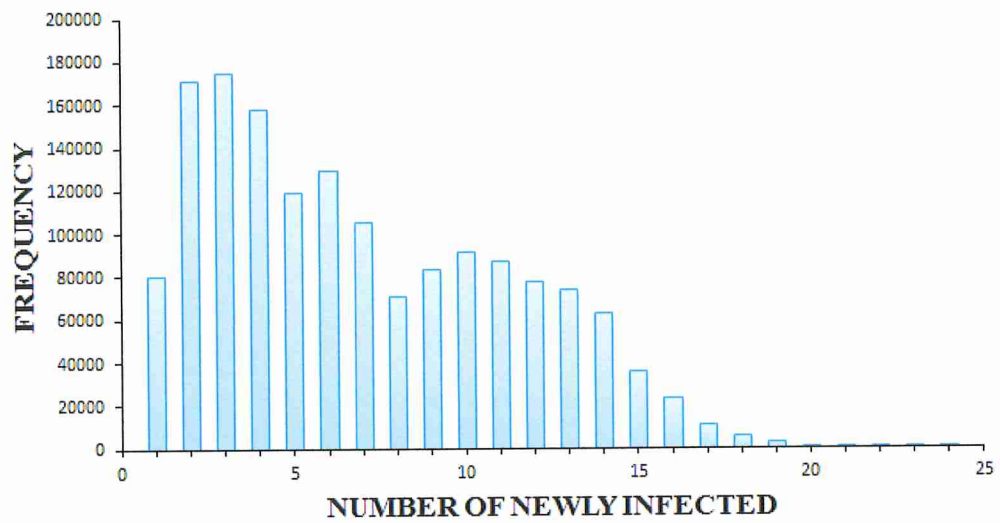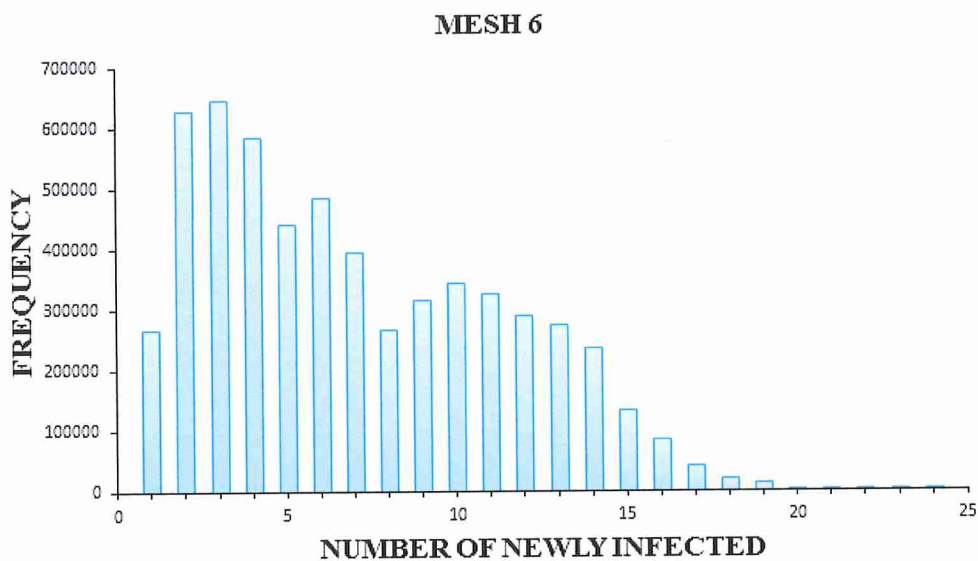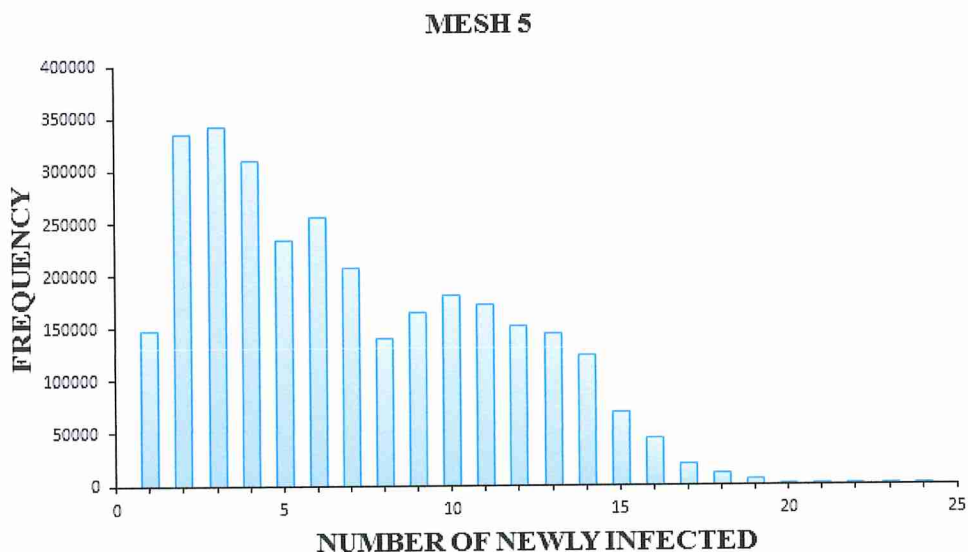
Figure 5.7. Infection distribution histograms for (a) 6480, (b) 11,664, (c) 144,900, (d) 2,125,000, (e) 4,165,392 and (f) 8,245,776 grid points using 5D Lattice method.

Having obtained the histograms from the lattice parameter sweep algorithm, the data is compared to the LDS algorithm implemented for the two-dimensional infection parameters sweep as in section 5.4.2, then the same process is repeated but for the three-dimensional pedestrian parameters sweep, shown in section 5.4.3. It is expected that the

convergence takes place earlier (with a coarser mesh size compared to that of lattice) when implementing LDS. Also, comparing the LDS algorithms applied for the 3D pedestrian and 2D infection models, LDS is expected to converge more efficiently at the higher 3D order of dimensionality compared to that of 2D.

5.3.2 3D Lattice Pedestrian Parameters x 2D LDS Infection Parameters

Different parameter space partitions are simulated using a lattice of uniformly distributed sequences to evaluate the parameters related to the social force model, while LDS is used for the infection parameters. Following the same parameter sweep methodology as before for the speed and cut-off distances variables, an LDS algorithm is adopted to sweep the infection transmission variables over their ranges. Predicting a better performance when implementing the LDS algorithm, lower numbers of simulations are used here, compared to the 5D lattice method, previously shown. Also, seeking for the influence of the parameters' increments on the outcomes, each parameter's ensemble is evaluated to determine whether the pedestrian trajectory or the transmission mechanism has a greater effect on the outcomes. Accordingly, in Table 5.4, the first three meshes (Mesh 1, 2 and 3) are coarsely partitioned for the social force model related parameters and finely distributed using large low discrepancy sequences for infection related terms. For the remaining three meshes (Mesh 4, 5 and 6), an inverse process is applied using fine 2D LDS and coarse 3D Lattice algorithms. The outcomes of this algorithm are plotted in histograms in Figure 5.8 (a-f).

Table 5.4

5D Parameter space exploration using the 3D lattice and 2D LDS based algorithms for the social force and infection models respectively.

Parameter	Range	Mesh type	Mesh sizes					
			Mesh 1	Mesh 2	Mesh 3	Mesh 4	Mesh 5	Mesh 6
V_0	3.2-5.4 ft/s	Lattice	12 (0.2)	12 (0.2)	12 (0.2)	23 (0.1)	23 (0.1)	23 (0.1)
δ_1	15-25 in	Lattice	3 (5)	3 (5)	3 (5)	11 (1)	11 (1)	11 (1)
δ_2	25-40 in	Lattice	4 (5)	4 (5)	4 (5)	16 (1)	16 (1)	16 (1)
R	36-84 in	LDS	750	1000	2000	200	250	300
P_{inf}	0.025-0.225	LDS						
Number of grid points			108,000	144,000	288,000	809,600	1,012,000	1,214,400

Note: For the different mesh dimensions, the numbers between parentheses represent the increment size of each parameter.

MESH 1

(a)

MESH 2

(b)

MESH 3

(c)

MESH 4

(d)

MESH 5

(e)

MESH 6
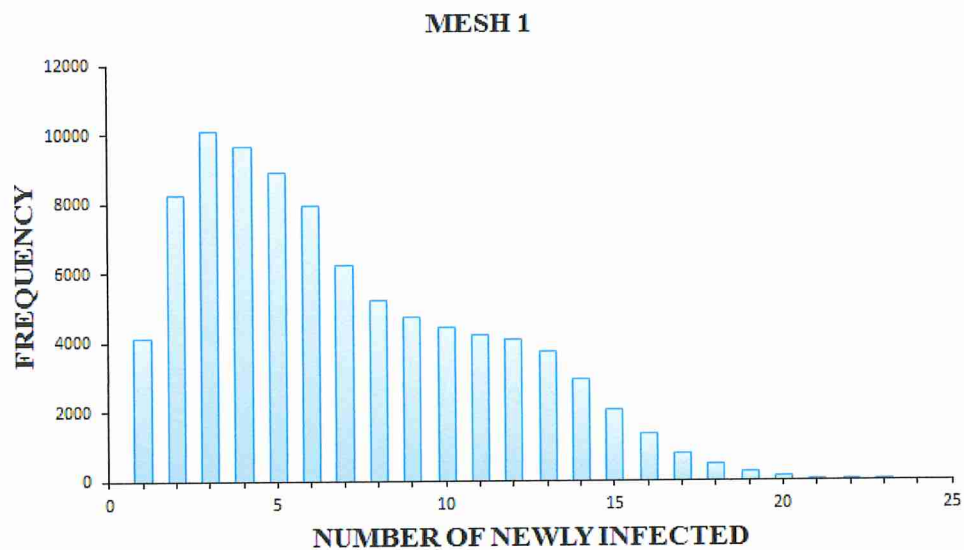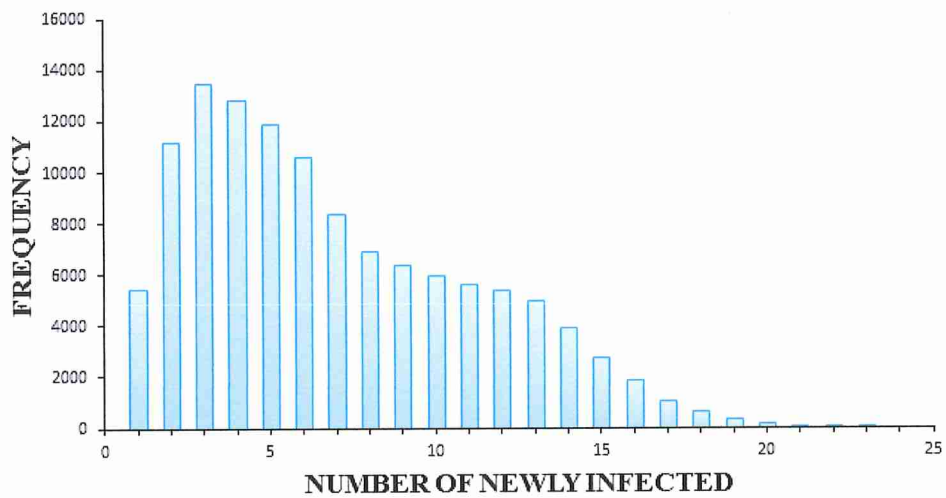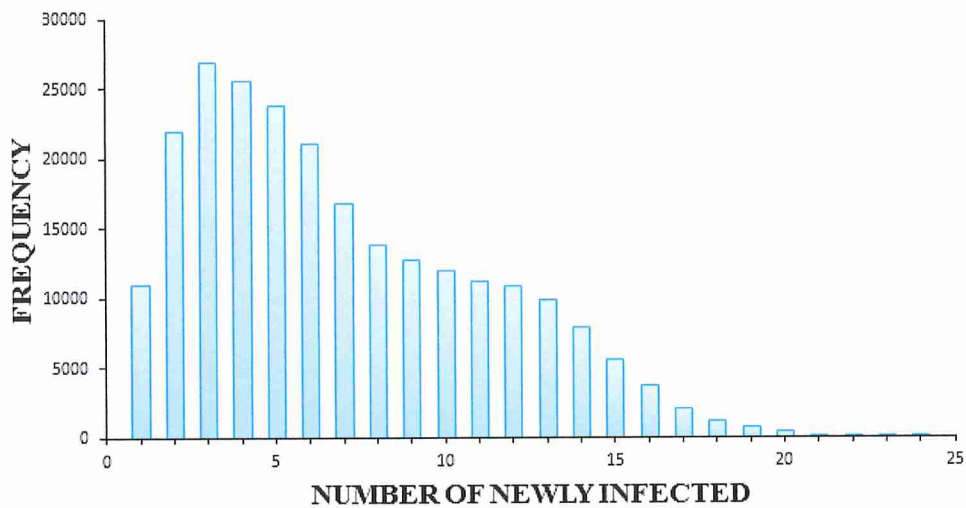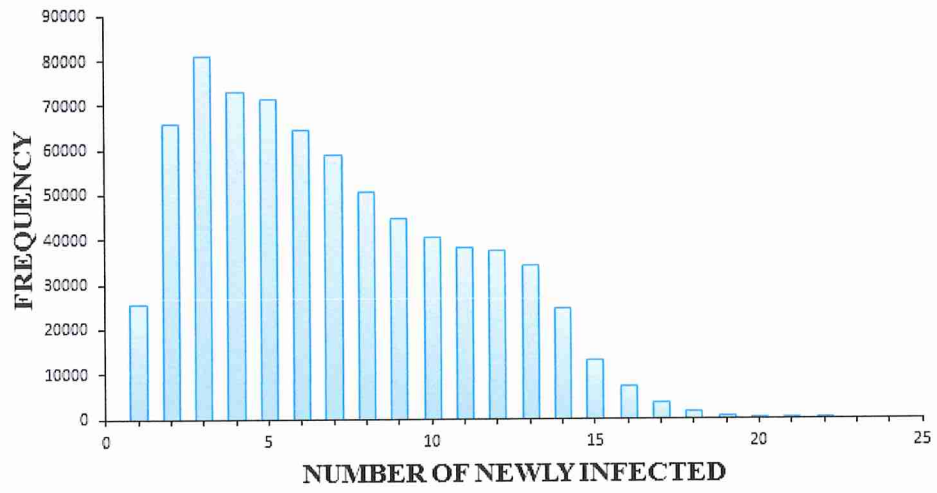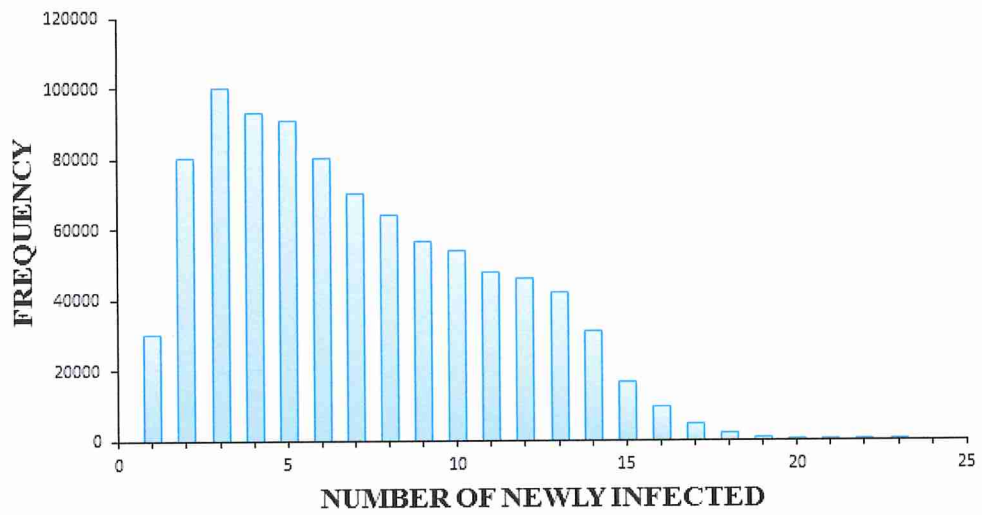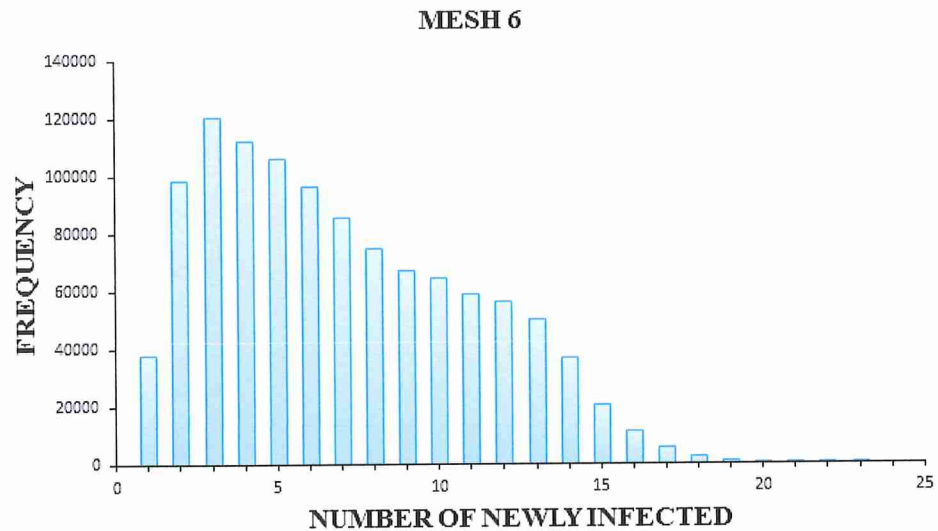
(f)

Figure 5.8. Infection distribution histograms for (a) 108,000, (b) 144,000, (c) 288,000, (d) 809,600, (e) 1,012,000 and (f) 1,214,400 grid points using 3D pedestrian Lattice combined with 2D LDS method.

5.3.3   3D LDS Pedestrian Parameters x 2D Lattice Infection Parameters

In this section, LDS is applied for the pedestrian parameters space having higher

dimensionality and greater ranges compared to those of the infection parameters. Aiming

to obtain faster convergence than with the 3D lattice-2D LDS method, the mesh sizes are

again reduced for the 3D LDS-2D lattice method. After estimating the required mesh

increment of the infection parameters from the 5D lattice sweep for convergence, the

pedestrian model variables' increments are the main focus. In Table 5.5, a coarser starting

mesh is selected for the 3D space compared to Table 5.4 since convergence is expected to

be attained at lower simulations number compared to that of the previous section. In

addition, finer mesh sizes are selected for the 3D space (pedestrian parameter space) to

confirm the convergence whereas the mesh size of the infection parameters is kept the

same from mesh 2 to mesh 6. Re-running the simulations for both the pedestrian and

infection algorithms successively, the results are recorded in Figure 5.9 (a-f) for the

various mesh sizes. With a low sequence of 50 combinations for the speed and distance parameters and at a coarse mesh for the infection parameters (Mesh 1 and 2), the histograms of Figure 5.9 (a & b) cannot capture the distribution of the newly infected at high numbers. Therefore, a better refinement is performed and the number of simulations is increased to achieve higher precision.

Table 5.5

5D Parameter space exploration using the 3D LDS and 2D lattice-based algorithms for the social force and infection models respectively.

| Parameter	Range	Mesh type	Mesh sizes					
			Mesh 1	Mesh 2	Mesh 3	Mesh 4	Mesh 5	Mesh 6
V_0	3.2-5.4 ft/s	LDS	50	50	100	300	1000	1500
δ_1	15-25 in	LDS						
δ_2	25-40 in	LDS						
R	36-84 in	Lattice	9 (6)	25 (2)	25 (2)	25 (2)	25 (2)	25 (2)
P_{inf}	0.025-0.225	Lattice	9 (0.025)	9 (0.025)	21 (0.01)	21 (0.01)	21 (0.01)	21 (0.01)
Number of grid points			4,050	11,250	52,500	157,500	525,000	787,500

Note: For the different mesh dimensions, the numbers between parentheses represent the increment size of each parameter.

MESH 1

(a)

MESH 2

(b)

MESH 3

(c)

MESH 4

(d)

MESH 5

(e)

MESH 6
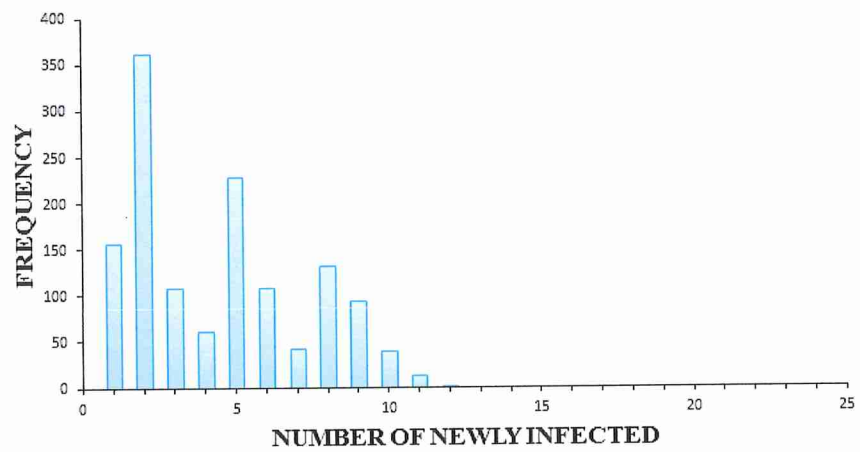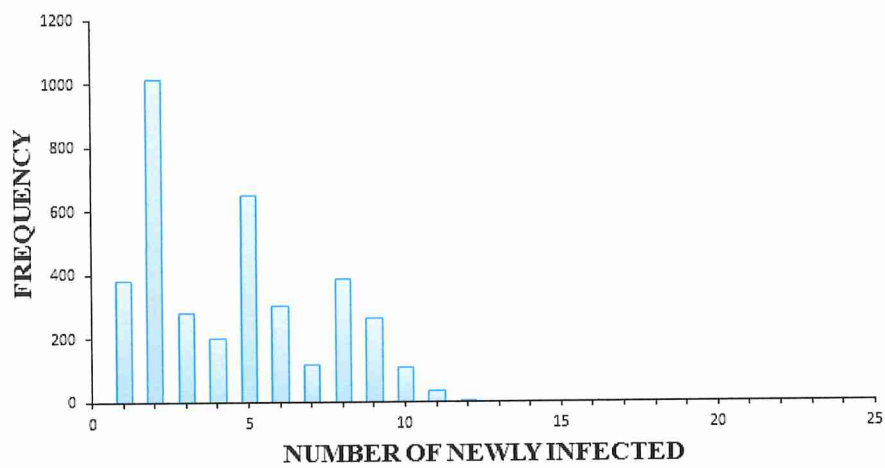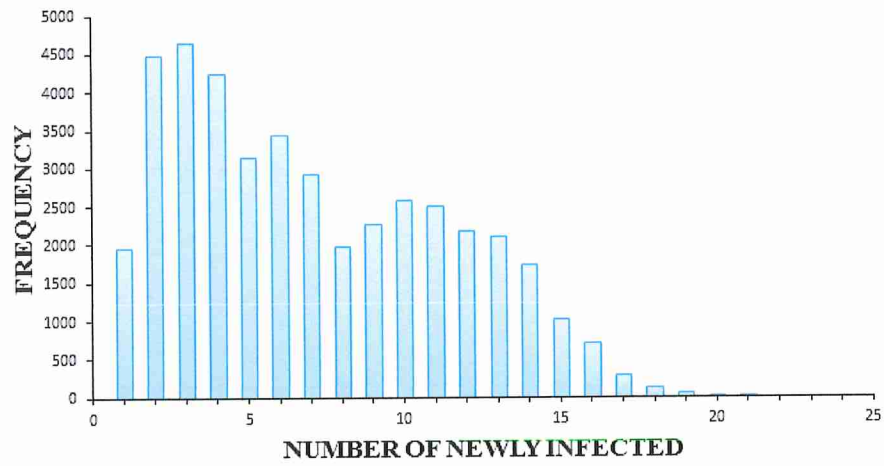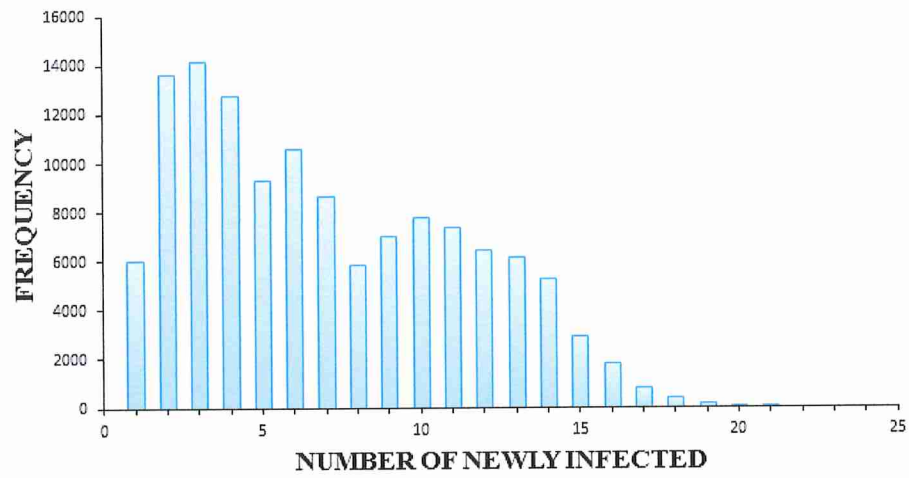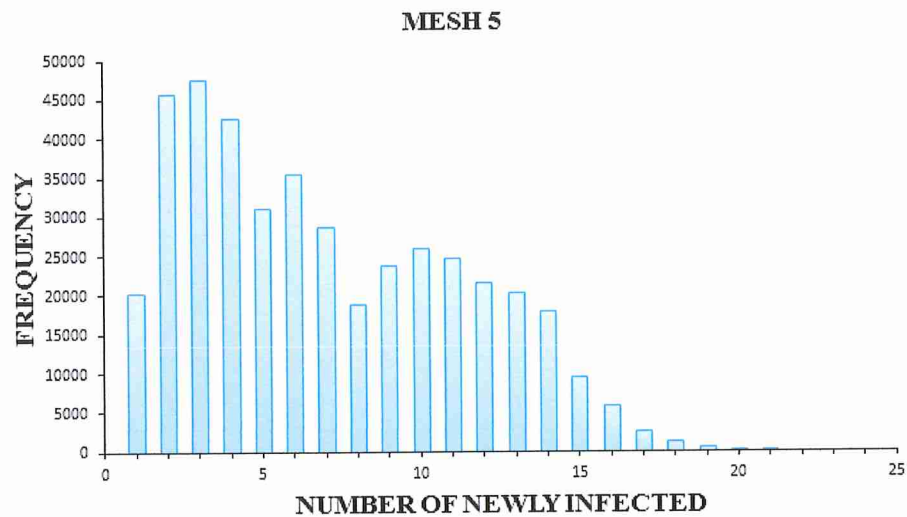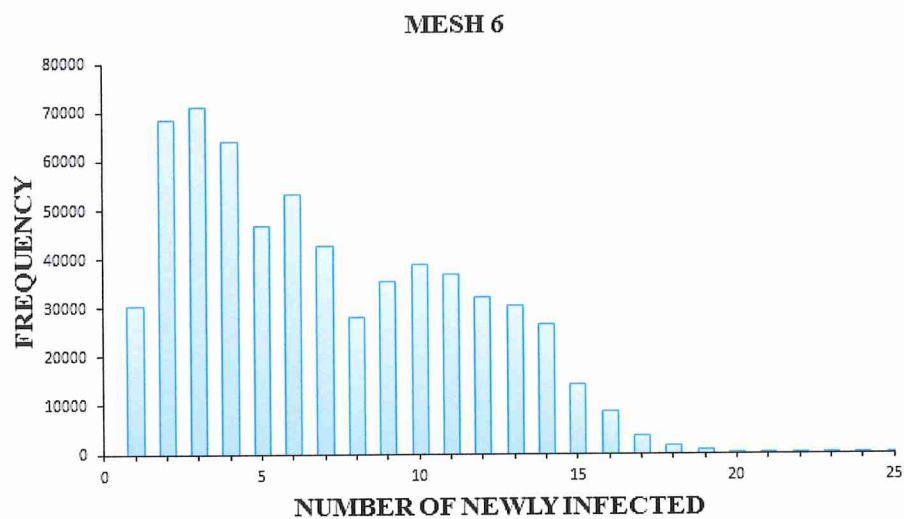
(f)

Figure 5.9. Infection distribution histograms for (a) 4,050, (b) 11,250, (c) 52,500, (d) 157,500, (e) 525,000 and (f) 787,500 grid points using 3D pedestrian LDS combined with 2D Lattice method.

5.3.4   3D LDS Pedestrian Parameters x 2D LDS Infection Parameters

Having proven the efficiency of implementing the LDS method in the models

especially at higher dimensionality order, 5D LDS simulations are performed to deduce

the overall reduction ratio of the required computational effort between 5D lattice and 5D

LDS. Recall that the low discrepancy method generates sequences of different parameter

variations aiming to approach faster to the outcomes. Accordingly, with a pure LDS

sequence a very coarse mesh will lead to convergence faster than a very fine 5D lattice

mesh. Here, the parameter space is meshed in only four different patterns to deduce

convergence as shown in Table 5.6. Here the 5D sequences are first generated. The first

three terms of each sequence are applied to the pedestrian model and the two remaining

terms are used for the infection parameters. In a 5D dimensional space, the possible

combinations of parameters leading to convergence are located more precisely in the

space of study, thus, with reduced grid points, the rate to achieve convergence is faster.

The increase of dimensionality places more constraints on the space of study and

localizes more accurately each coordinate with respect to its domain of definition. This

statement is validated by Figure 5.10 (a-d), where no major alteration of the overall

histogram distribution can be noticed with the increase of the simulations' number.

Table 5.6

5D LDS Parameter space exploration algorithm for the multiscale model.

Parameter	Range	Mesh type	Mesh sizes			
			Mesh 1	Mesh 2	Mesh 3	Mesh4
V_0	3.2-5.4 ft/s	LDS				
δ_1	15-25 in	LDS	50	100	150	200
δ_2	25-40 in	LDS				
R	36-84 in	LDS	50	100	100	150
P_{inf}	0.025-0.225	LDS				
Number of grid points			2,500	10,000	15,000	30,000

MESH 1

(a)

MESH 2

(b)

MESH 3

(c)

MESH 4
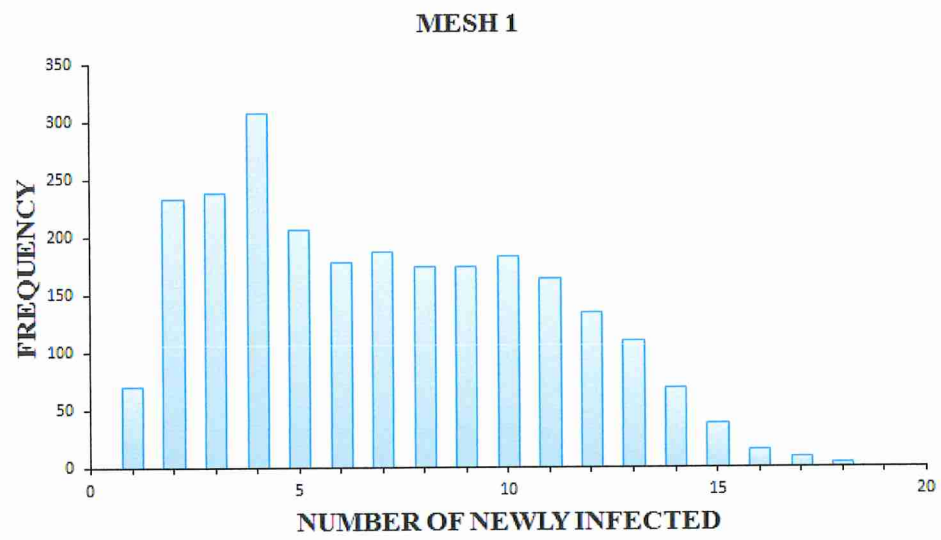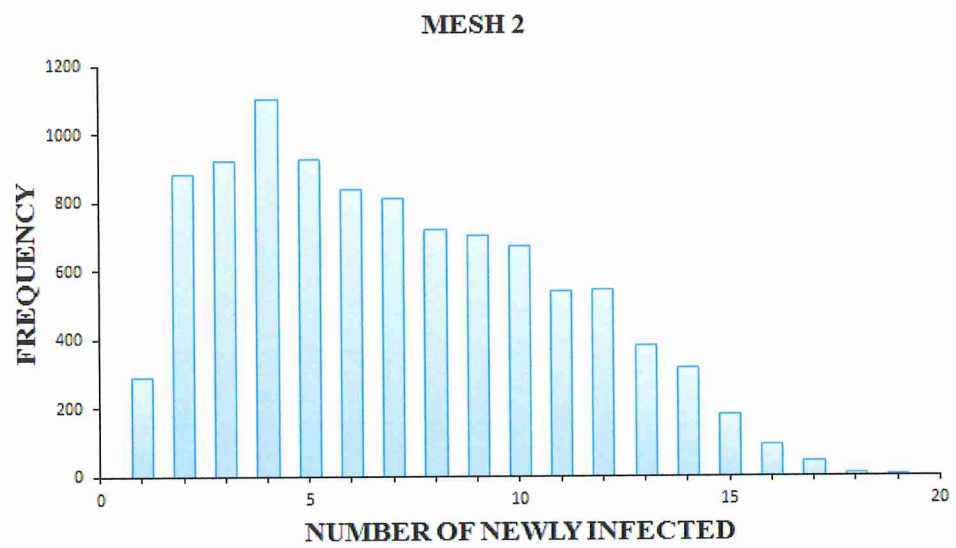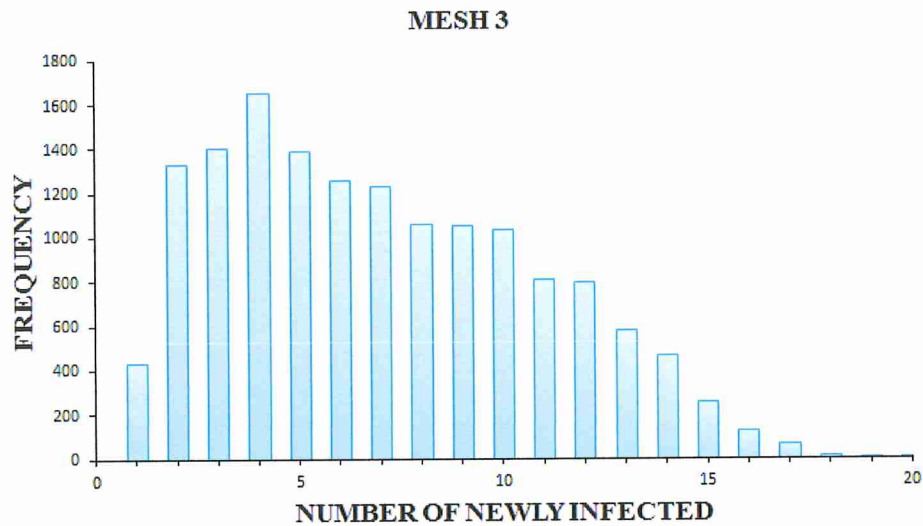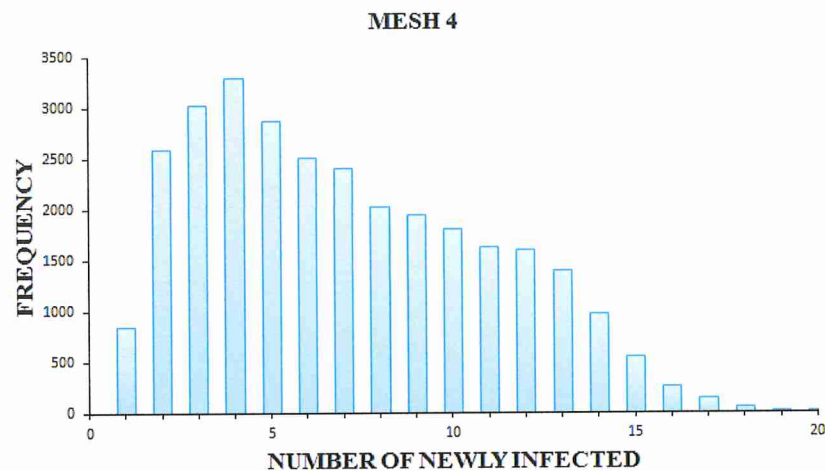
(d)

Figure 5.10. Infection distribution histograms for (a) 2,500, (b) 10,000, (c) 15,000, and (d) 30,000 grid points using 5D LDS method.

5.4   Analysis of Convergence Measures

In the previous section, the mesh resizing of each algorithm is visually dependent on the overall shape of the biased histogram where the distribution of the frequencies remains proportional with the mesh refinement. However, validating the convergence by means of the relative differences of statistical variables (mean, standard deviation,

skewness and kurtosis) is required. Statistical analysis is attributed to each of the algorithms to confirm its effectiveness to reach convergence at a different space repartition. The statistical analysis also tells when no more refinement is required. Recall that with mesh refinement of the 5D domain, used here, the simulation time and computational efforts increase. Below the convergence bases are discussed for the different parameter sweep algorithms.

5.4.1 5D Lattice

In the 5D lattice method, the parameter sweep is performed using six different meshes starting by a mesh size in the order of thousands and increased to become in the order of millions. With a 5D lattice sweep method, a lower number of simulations cannot cover effectively the parameter space with the large increment between the points, thus, convergence could not be captured precisely. Convergence is attained at mesh 4 with 2,125,000 simulations. A 0.1 ft/s, 1in, 1in, 2in and 0.01 increments are used for V_0, δ_1, δ_2, R and P_{inf} respectively as shown previously in Table 5.1. As the contact radius R increment is reduced 1in then to 0.5 in, the relative difference of the mean, standard deviation, skewness and kurtosis values have not changed as shown in Figure 5.11.

Looking at the evolution of same statistical variables in Table 5.7, the values of the mean and standard deviation are slightly varying in the order of hundredth whereas the skewness and kurtosis kept increasing which indicated the biasing of the histograms toward a high-frequency value of three newly infected pedestrians. The distribution of the histogram in bell shape around the peak accounts for the stochasticity of the model. However, in decision making, the preventive plan should account for the worst-case scenario. The histogram's peak is attained at three newly infected members (highest

probability) and extends to twenty-four possible infection cases with a mean of

approximately 7 new infections.

Table 5.7

Statistical data distribution for various mesh sizes using a 5D Lattice sweeping algorithm.

Statistical variables	Mesh 1	Mesh 2	Mesh 3	Mesh 4 (convergence)	Mesh 5	Mesh 6
Mean	5.60	5.76	6.88	6.98	7.02	7.03
Standard Deviation	0.57	0.422	0.13	3.46E-02	2.47E-02	1.75E-02
Skewness	8.389	12.51	42.25	172.07	245.38	348.44
Kurtosis	446.73	806.10	10026.76	147123	288386.7	570908.6
Simulations number	6,480	11,640	144,900	2,125,000	4,165,392	8,245,776
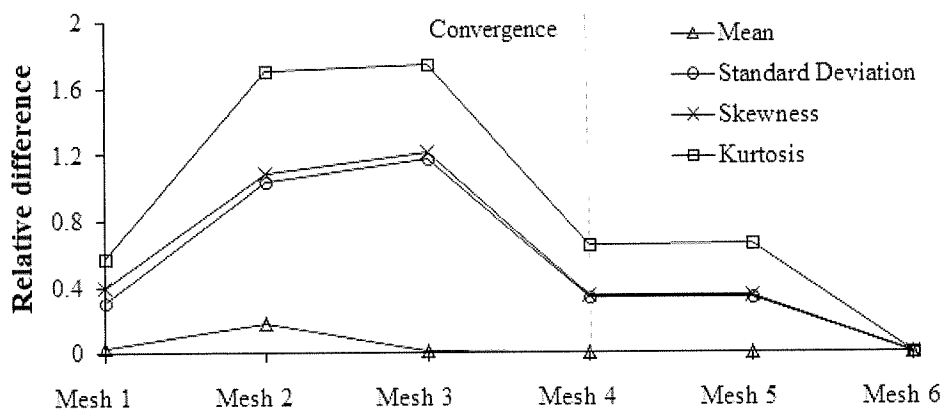
Figure 5.11. Statistical moments distribution with mesh refinement using a 5D Lattice sweeping algorithm.

5.4.2   3D Lattice, 2D LDS

Incorporating LDS to the parameter sweep process, the same mean of 6.98 with a

close standard deviation is obtained at mesh 4 with only 809,600 simulations (see Table

5.8) compared to 2,125,000 required for 5D Lattice. The convergence is reached with the

same increments used previously for the pedestrian model parameters and only 200 low

discrepancy sequences to cover the 2-Dimensional infection parameters space. The

computational efforts are dropped to less than 50% compared to that required for a 5D

lattice. The plot of Figure 5.12 representing the relative difference of the four statistical moments behaves in a similar manner as that of Figure 5.11 after convergence is reached showing almost constant values.

Table 5.8

Statistical data distribution for various mesh sizes implementing a 2D LDS sweeping algorithm.

Statistical variables	Mesh 1	Mesh 2	Mesh 3	Mesh 4 (convergence)	Mesh 5	Mesh 6
Mean	6.95	6.95	6.96	6.98	7.02	7.00
Standard Deviation	0.13	0.12	8.86E-02	4.25E-02	4.14E-02	3.78E-02
Skewness	43.90	50.71	66.42	139.52	146.30	159.02
Kurtosis	8796.40	11728.52	22477.07	75371.34	90290.05	108353.80
Simulations number	108,000	144,000	288,000	809,600	1,012,000	1,214,400
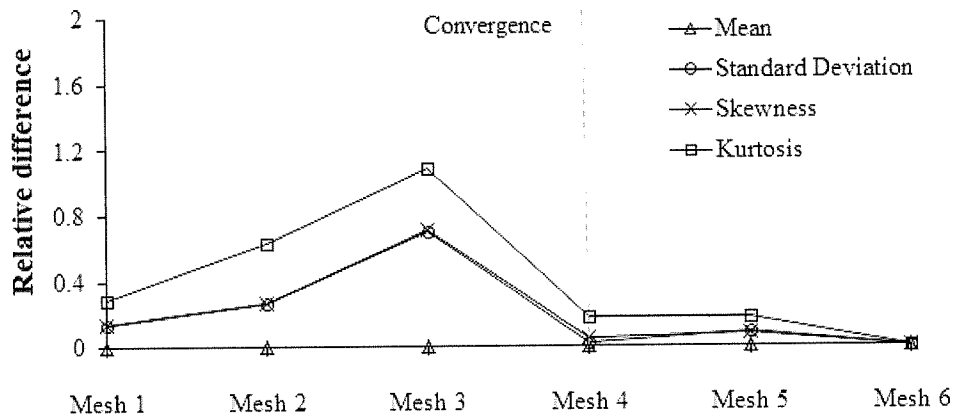
Figure 5.12. Statistical moments distribution with mesh refinement implementing a 2D LDS sweeping algorithm.

5.4.3   3D LDS, 2D Lattice

Higher-order low discrepancy sequences are applied here for the pedestrian model parameter instead of the infection parameters as of section 5.4.2. With the application of LDS at a higher order of dimensionality, convergence is attained faster at 157,500 simulations with a mean of 7.04 compared to 6.98 previously (Table 5.9). This slight shift

of the mean is resultant of the greater precision of the 3D LDS method applied to the

pedestrian parameters compared to the 2D LDS method in the previous section. Again, at

mesh 4, the relative differences of the statistical moments converge toward a zero value

as shown in Figure 5.13.

Table 5.9

Statistical data distribution for various mesh sizes implementing a 3D LDS sweeping algorithm.

Statistical variables	Mesh 1	Mesh 2	Mesh 3	Mesh 4 (convergence)	Mesh 5	Mesh 6
Mean	4.45	4.51	7.11	7.04	7.02	7.02
Standard Deviation	0.39	0.23	0.16	9.29E-02	5.09E-02	5.87E-02
Skewness	11.49	20.17	39.58	65.91	118.83	103.29
Kurtosis	247.40	684.19	4503.48	13533.93	45135.96	57254.43
Simulations number	4,050	11,250	52,500	157,500	525,000	787,500
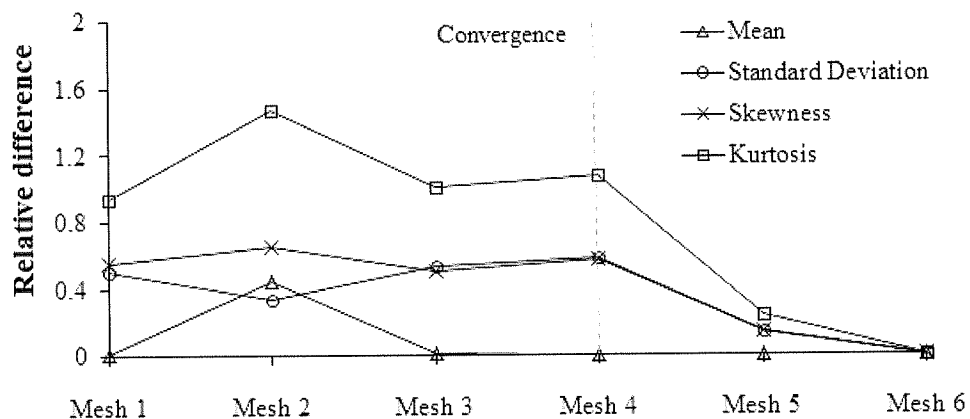
Figure 5.13. Statistical moments distribution with mesh refinement implementing a 3D LDS sweeping algorithm.

5.4.4 3D LDS, 2D LDS

As LDS has proven greater efficiency at higher orders, a 5D LDS is applied to the

whole parameter space. In the previous three algorithms, with the increase of the number

of simulations, the precision of the mean variable increases accordingly. Here, with 5D

LDS, a fluctuation of the mean is noticed in Table 5.10. This is explained by the fact that the LDS simulations are performed successively starting with a 3D LDS for the pedestrian model, then combined with a 2D LDS for the infection model. For instance, mesh 2 and mesh 4 have the same mean. This happens when the appropriate combination of the whole 5D sequence is obtained. In other words, convergence occurred when the 5 elements of the permuted sequence are matching in the simulations. The standard deviation between mesh 2 and 3 varies slightly in the order of a hundredth indicating convergence labeled in Figure 5.14 at 15,000 simulations.

Table 5.10

Statistical data distribution for various mesh sizes implementing a 3D LDS sweeping algorithm.

Statistical variables	Mesh 1	Mesh 2	Mesh 3 (convergence)	Mesh 4
Mean	7.028	7.058	7.039	7.058
Standard Deviation	0.488	0.271	0.246	0.173
Skewness	6.322	11.712	12.692	35.608
Kurtosis	295.782	1143.650	1655.944	3309.564
Simulations number	2,500	10,000	15,000	30,000
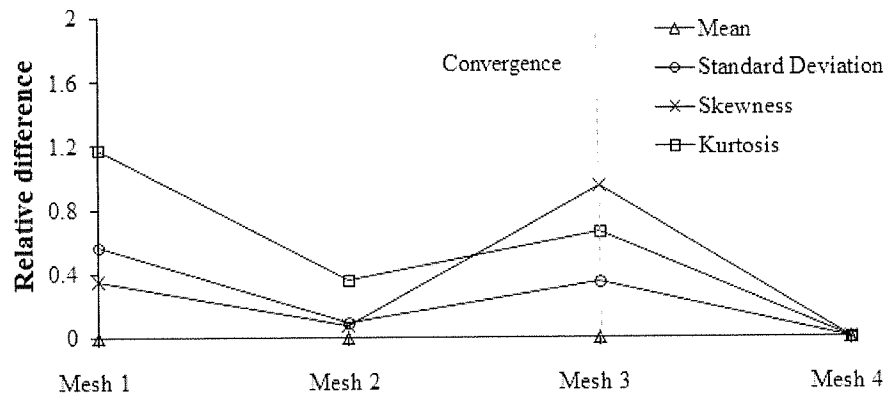
Figure 5.14. Statistical moments distribution with mesh refinement implementing a 5D LDS sweeping algorithm.

5.5   Discussion

Sequences have found various applications such as mathematics (Caflisch &

Moskowitz, 1995), physics (Binder et al., 2012) and finance (Joy et al., 1996). For

instance, multi-dimensional integrals are evaluated by means of a (quasi) stochastic

Monte Carlo method. A major issue with these pseudo-random finite sequences is that

they are not equidistributed over the domain of integration which grants poor results. The

usage of increased equidistributed sequences with more random number improves

accuracy, but requires longer simulation time (Zaremba, 1968). The lattice-based space

repartition is a uniform distribution method that partitions the domain uniformly. This

method requires even higher computational simulations that are time-costly compared to

the pseudo-random sequences. Low discrepancy sequences using quasi-random numbers

are introduced to solve the high computation time problem on parallel clusters.

Sequences generated using Low-discrepancy (quasi-random) in a unit domain are better

"equidistributed" than pseudo-random numbers. The Halton sequence, a multi-

dimensional digital arithmetic version of the Van der Corput sequence converts the

integer numbers into numbers of base "b" (Halton, 1960). These digital sequences

constructed on binary bases enable better implementation in computer programs

(L'Ecuyer & Lemieux, 2005).

In a multidisciplinary model, low discrepancy sequences can be used to sweep the

parameters over their large domain of definition. For instance, consider the case of

analysis of a pedestrian winding queue in a security checkpoint of an airport. Knowing

that proximate interactions between pedestrians enable disease transmission, the contact

pattern between the travelers should be obtained. Pedestrian trajectories are traced by

means of a molecular dynamics-like approach using a social force model. From the trajectories data, the contact pattern is mapped. This contact pattern is then combined with a stochastic individualistic mathematical epidemiological model to assess the transmission rate among the crowd. Here, the framework is of a multi-disciplinary nature. Both models are inter-connected and the contact data outputted from the social force model is inputted to the infection model.

In both, the pedestrian and epidemiological models, certain parameters cannot be exactly defined due to the inherent stochasticity in human behavior and the uncertainty of disease propagation manner. The low discrepancy sequence method can be used in at least one disciplinary branch to reduce the simulations effort (Figure 5.15). Applying LDS to the whole model becomes more efficient provided that the whole sequence is simultaneously applied to both models. In other words, in the model, the social force model comprised three uncertain terms compared to two terms for the infection model. Assuming a sequence of five elements using LDS, the first three terms should be attributed to the first model, whereas the remaining two are used for the infection model.
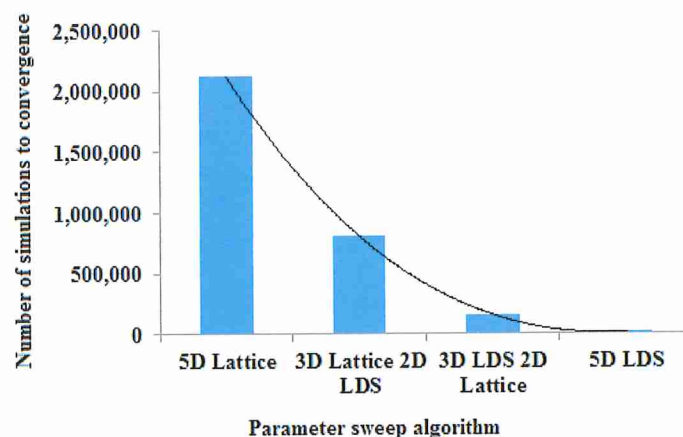
Figure 5.15. Number of simulations required for each parameter sweep algorithm.

5.6   Summary and Conclusions

In this chapter, the aim is to evaluate the disease propagation among a crowd in an optimum abreast rectangular winding queue with 2 zones configuration (Rectangular configuration 3 of chapter 4). The same multiscale model combining a pedestrian model, evolving in a molecular dynamics-like approach and generating movement trajectories, with an individualistic, stochastic epidemiological model that defines contact and infection contraction based on a certain transmission probability is used. Due to the stochastic nature and inherent uncertainty of the model's parameters, a parameter sweep is performed over the domain of definition of these parameters. In the pedestrian model, the focus is on the pedestrian's free speed, the cut-off distances between pedestrians of the same group (family members, friends) and that of different groups. The mathematical epidemiological model also relies on the contact radius and transmissibility probability. Consequently, a domain of definition of five dimensions is generated and every element of this domain corresponds to a certain scenario. Running each scenario separately generates a certain number of infections assuming a single infective member in the queue.

At first, a Lattice-based sweeping method is applied to the large parameter space to generate the parameter combinations to be evaluated. In each dimension, the increment is taken to be constant, generating a uniformly distributed vector of values within the range of definitions of each parameter. The uniform partition of the parameters vectors may leave some combinations uncovered, which in turn can lead to deficiencies in the results. Also, simulating all the different combinations of parameters may be computationally exhaustive and time-consuming, even on massively parallel computers. This occurrence

is undesirable especially during decision making to come up with preventive strategies to inhibit the propagation of a certain disease during its outbreak. Instead, an innovative Low Discrepancy Sequence method is proposed and the application to the multiscale model is demonstrated. This LDS method requires fewer simulations and has the ability to cover the parameter space more efficiently.

A conventional five dimensions lattice-based parameter sweep is applied at various mesh sizes leading to convergence at 2,125,000 simulations ran on a multi-processor cluster. The results are plotted in a histogram and statistical moments are used to indicate convergence where no refinement of the mesh is required. Aiming to reduce the computational enormous efforts, the LDS method is applied to the two-dimensional infection parameters domain. At a lower number of 809,600 simulations the same mean of 6.98 newly infected individuals is obtained. The number of infections may extend up to 24 cases with a higher probability to obtain only 3 cases.

Increasing the dimensionality of the low discrepancy sequence and applying it to the pedestrian model parameters three- dimensional domain, LDS has again proven to be very efficient to deliver the same results with only 157,500 runs. Note that with the application of LDS to a 3D domain, more sequences are required compared to a 2D domain to localize more precisely the candidate parameter combinations leading to convergence. Further, a fourth LDS algorithm is used to sweep the entire 5D domain granting convergence at only 15,000 simulations. Therefore, LDS sweeping method was able to reduce the simulations from an order of millions to the order of ten thousand. In a multidisciplinary model requiring parameter sweep, LDS can be applied at least in one discipline in order to reduce drastically the computational efforts.

6. Summary and Conclusions

There is a direct evidence of disease contraction in publicly crowded environments.

Air travel forums (airports and airplanes) have been identified as a location for several

infectious diseases spread such as influenza, severe acute respiratory syndrome,

tuberculosis, measles, etc. Inhibiting air travel during an outbreak can be economically

harmful and carry considerable human costs. Instead, producing science-based public

policies is an option that mitigates the disease spread without disturbing travelers in

airports. In addition, there is no appropriate fast scanning equipment that may determine

the infection of a traveler with an infectious disease especially at the early stage before

appearance of clinical symptoms. This dissertation presents a formulation of certain

pedestrian walking strategies that reduce the proximate interaction between the travelers,

thus, reducing the occurrence of infection propagation among the travelers.

A multiscale approach combining a social force model that generates the walking

trajectories of each pedestrian during enplaning from an airport lounge and deplaning

from aircraft of different sizes and seating configurations is used. Contact data between

travelers is obtained and combined with a stochastic individualistic Susceptible-Infected

(SI) model to map the propagation pattern via a Poisson distribution. Different enplaning

and deplaning strategies are evaluated. It is noticed that a two-section boarding disperses

the travelers aboard the airplane and reduces contact. Boarding by sections is commonly

used by airlines to facilitate the flow of travelers to the airplane and reduce the turn time in airports. However, airlines do not account for the possibility of disease propagation when the travelers congregate in narrow areas during boarding due to economic considerations. On the other hand, deplaning has no major effect and no strategy is prioritized over the others. This is explained by the jamming of the aisles during luggage unloading from their compartments along the aisle expanding from the entrance door to the most rear economy section. Deplaning usually occurs from front to back where travelers exit their seats and align in the aisle using common sense as the flow is ongoing.

Knowing that in crowded public places pedestrians stay in proximate contact for an extended time, the winding queues that have various applications to organize the pedestrians' flow in waiting zones are studied. Winding queues found usefulness in air travel at security and boarding gates. They are also observed in theme parks and entertainment centers. Winding queues come in different geometries and configurations. Some winding queues allow for a single file or abreast (side-by-side) flow of pedestrians. Aisles of winding queues can be arranged in vertical or horizontal pattern, in one or multiple zones, over a rectangular or square floor plan. Four different winding queues with single and abreast pedestrians flow are evaluated. Ropes are compared to temporary shading walls separators used to reduce interactions between pedestrians of adjacent aisles.

The multiscale approach used previously is extended for this problem and studied the effect of contact radii and infection probabilities on disease spread. The variation of the contact radius represents the possibility of transmission mechanism via fine aerosols or coarse droplets. Fine aerosols remain suspended for a longer duration and travel a longer distance than coarse droplets before depositing and contaminating a surface. The different infection probabilities represent the degree of infectiousness of the disease and its chance of survival and transmission in an appropriate environment. It can be concluded that in a rectangular layout with abreast pedestrian queue, short aisles are favorable in coarse droplets propagation mechanism with rope separator.

Using rope separator, interaction occurs between pedestrians of neighboring aisles and between the two zones. With aerosols able to travel farther, aisles configuration has no major role. The two-zone configurations reduce contact as the pedestrian exits faster compared to one-zone configuration. Placing temporary walls between the aisles reduces drastically the interaction between pedestrians, as pedestrians interact with others only within the same aisle. In this case, configurations with short aisles are suitable assuming coarse droplets transmission mechanism. At the corners, with long aerosol travel range, more pedestrians are involved within the circle of contact.

In a square layout with very short aisles, congestion occurs at the corners. With rope separators and droplet mechanism, frequent turning corners cause the same contact

pattern as long aisles for abreast queues. With aerosols dispersing farther, no square

configuration has priority over the others. Again, for aerosols higher contact rate is

detected at corners. Single-file motion is also addressed in a rectangular floor plan.

Pedestrians are more dispersed within the queue compared to side-by-side walking

arrangement. Using ropes, the transmission rate is independent of the exiting time,

depending on the number of zones, and remains invariable with the disease propagation

mechanism. For wall separators, all four configurations behave in the same manner with

higher contact at the corners.

Evaluating the four different configurations comprised many parameters in the social

force model and the infection model that have a direct influence on the outcomes of the

simulations. In order to quantify the uncertainty of these parameters, a parameter sweep

is performed and the optimal (configuration 3) rectangular with abreast pedestrian

alignment and rope separator is chosen for analysis. The aim of applying the proposed

multiscale model is to expect the distribution of the number of newly infected individuals

when infective members are among a crowd. The focus concentrated on the free

pedestrian speed and cut-off distances in the social force model, and on the contact radius

and infection probability in the epidemiological model, leading in total to a five-

dimensional space.

Due to the large space of definition of parameters, the probabilistic distribution of the

newly infected individuals varied based on the values of the chosen parameters. The entire parameter space is covered using a conventional lattice-based algorithm. This method sections each parameter domain uniformly using the same increment between the terms. This lattice method is applied separately for each model and the mean number of infections is obtained under various infection scenarios in a 5D domain. Running all the possible permutations of variables values is computationally expensive especially when more variables are added to the model. In addition, not knowing the appropriate increment requires refining the mesh sequentially until convergence is attained. The results are plotted in a histogram and convergence is monitored by statistical moments. With the increase of simulations, the run time increased exponentially. Therefore, there is a necessity for an innovative shortcut method that can reduce the simulations time and grant similar results of high accuracy during decision meetings.

A parallel low discrepancy parameter sweep implementing Halton sequences, used previously by the VIPRA team (Chunduri et al., 2018, May), is used separately in a multi model setting. The LDS method is first introduced for the infection model in the 2D domain with a 3D lattice sweep for the social force model. The convergence is attained at a much lower number of simulations compared to the 5D lattice. LDS is then used at higher 3D order for the social force model combined with a 2D lattice for the infection model. A higher number of sequences was required for the 3D LDS algorithm, to cover

accurately the entire domain, with overall lower number of simulations compared to the

2D LDS model. Finally, a 5D LDS algorithm is applied to the parameters of the entire

multiscale model reducing drastically the required simulations in the entire space and

granting similar results. Accordingly, LDS has proven to be highly efficient when used in

the proposed multidisciplinary model either in one discipline or in all disciplines. These

computational aspects could be easily extended to parameter sweep problems in multi-

model setting in other research areas.

7. Recommendations for Future Research

In this study, a detailed insight into how to predict disease outbreak in a crowded environment is provided by mimicking pedestrian behavior using a multiscale model. In the pedestrian social force model, some empirical data was used to calibrate the force fields. In addition, pedestrians were projected to their destination using an agent-based model defining the motion direction. Concerning the infection epidemiological model, the formulation could be applied to any directly transmitted disease. Computational aspects of large scale parameter sweeps in a multiscale formulation are also investigated. Several future research directions could be built on this framework.

The extension of this research may take four different routes. In the social force model, more precise empirical data can be obtained from more updated sources and newly available virtual and social-media data sources. Pedestrians can also be guided towards their destination by means of domain adaptation, a subfield of machine learning. The speed-density model can be enhanced by the use of the Voronoi diagram. In the epidemiological model, an immunized category can be added to the susceptible and infected categories.

7.1 Novel Empirical Data Sources

In this study, some parameters in the social force model were obtained from empirical data found in the literature. This data is obtained from set-up experiments where pedestrians are informed in advance about their assigned tasks (Zhang & Seyfried, 2013; Seyfried et al., 2009; Liu et al., 2014; Schadschneider & Seyfried, 2011; Timmermans, 2009; Seyfried et al., 2010; Zhang et al., 2011). Other data was obtained from analyzing videos recorded at certain locations (Han et al., 2019; Davidich & Köster, 2013; Zhu et

al., 2019; Guo, 2018; Ellis et al., 2009; Mansouri et al., 2018; Dridi, 2014). The social force model is also calibrated in the queue application by extracting actual data from theme parks. However, this data is narrow and insufficient as several factors affect pedestrians' motion. For instance, at theme parks, the flow depends on the time (regular or rush time). Accordingly, updated data in time frame is required. Recently, developed approaches, such as Location-Based Services (LBS) data enables tracking pedestrian motion in certain public locations (i.e. airports, theme parks, entertainment centers, etc.) as a function of time. Such data will be more appropriate for use in calibrating the model.

LBS are smartphone applications offering services based on the device's geographical location (Quercia et al., 2010, December; Steiniger et al., 2006; GSM Association, 2003; Wang et al., 2008, May). LBS track the geographical location of the user if allowed, through a global positioning system (GPS) to provide information under a variety of contexts (Guo et al., 2008; Guo et al., 2012; Deuker, 2008). These services allow users to check-in at places and events. Collecting and analyzing trajectories data from the service provider offer better insight into the natural pedestrian behavior without directly interfering with these pedestrians via planned experiments for data collection.

7.2 Voronoi Diagram-Based Pedestrian Density Model

The use of image processing to measure pedestrian density from experimental data (video tracking) or counting the particles representing the pedestrians within a control area (circle, rectangle, square, etc.) in simulations leads to data scatter. This data scatter arises from the application of the classical density definition applied in materials science and fluid mechanics to the limit of infinite particles on the macroscale to locally finite particles (pedestrians) on the microscale. The classical definition of density is given by

the relation D = N/A, where N represents the number of particles within a control area A. Averaging the densities over space and time domains of study reduces the possibility to accurately estimate the density. This calculates the average density of pedestrians over a floor plan instead of the density distribution over the specific area of the floor plan of interest. Also, the selection of the finite control area in which density is calculated is critical. The shape of the floor plan (size and boundaries) is of great influence. Another error arises from the calculation of density at each time step whereas the average speed is obtained from a time interval (Hankin & Wright, 1958; Navin & Wheeler, 1969).

A concept to measure the microscopic characteristics of pedestrian movement based on individuals' trajectories is introduced by Steffen and Seyfried (2009). In their contribution, Steffen and Seyfried (2009) introduced the concept of the Voronoi diagram (Voronoi, 1908) that reduces the density scatter. This method computes the density distribution by means of the Voronoi diagram at an exact position in a cell area A_i attributed to each person, integrates the distribution in the direction of motion, and divides it by the total area A. Likewise, the principle of the Voronoi diagram can also be applied to calculate the average motion speed and direction from position transformations evolving in the time frame in a quasi-static flow through a bottleneck (Steffen & Seyfried, 2009). The difference between this method and the conventional density method is the computation of the density distribution instead of counting the number of particles in a control area.

7.3 Domain Adaptation and Reinforced Learning

Various mathematical models have been developed to understand crowd behavior. The social force model is a popular model developed by Helbing and his coworkers and has

been extensively used in the simulation of crowds (Helbing & Molnar, 1995; Helbing et al., 2000; Helbing et al., 2002). Despite the accuracy of the results to replicate pedestrian motion, various factors such as the surrounding context (normal or emergency situation, newly explored or common place) affect the pedestrian behavior. Accordingly, crowd behavior models should account for the diversity of the context and the difference in pedestrians' behavior with the variation of this context (Curtis & Manocha, 2014). In pedestrian models, the motion of each individual is guided as it is previously almost predicted with slight deviations allowed. In other words, the surrounding context on which the pedestrian response is based is already implemented. This limitation in the model could be disentangled using deep learning (Pan & Yang, 2010).

Deep learning is a subfield of machine learning, a subset of artificial intelligence. Artificial intelligence is the implementation of human-like intelligence to machines using algorithms. Accordingly, these machines will have the capability to learn, analyze and plan by means of programmed reasoning. Machine learning is the science of developing algorithms that rely on statistical data to perform independently a certain task without any explicit intervention. The algorithm will analyze and classify the task based on a previously introduced training data set. Domain adaptation uses knowledge from a source domain to model a different target domain (Pan & Yang, 2010; Bruzzone & Marconcini, 2010; Venkateswara et al., 2017). In pedestrian motion, domain adaptation relies on data from the source domains to predict human behavior in another domain. The data sources can be pedestrian dynamics, empirical data, observations from cameras, data from media applications, etc. These could be used to predict pedestrian behavior and movement in

unknown domains e.g. emergency evacuation. Combining pedestrian dynamics with domain adaptation has great potential for improving pedestrian models.

7.4   Accounting for Immunized Individuals in the Model

In the context of this dissertation, it is referred to infection probability charts for Ebola, SARS and H1N1 during the incubation period post-onset of the symptoms. The incubation period extends from the latent to the infectious period. It is assumed that infection transmission is based on the contact time threshold and occurs once this time duration is met. However, during the latent period a susceptible individual exposed to an infective may not become infected. A modification to the used SI model can be done by implementing the exposed category. In this category, it is assumed that an infected individual is not yet infectious. Another issue to address is the resistance of certain individuals to the infection due to their immunity. The vaccination should be implemented in the model by introducing a vaccinated category of subjects with a certain probability since vaccination cannot eradicate the disease contraction or propagation.

REFERENCES

Abell, G. C. (1985). Empirical chemical pseudopotential theory of molecular and metallic bonding. *Physical Review B, 31*(10), 6184.

Abramson, D., Cope, M., & McKenzie, R. (1994). Modelling photochemical pollution using parallel and distributed computing platforms. In *International Conference on Parallel Architectures and Languages Europe, 4-8 July; Athens, Greece* (pp. 478-489). Springer, Berlin Heidelberg, Germany.

Ajelli, M., Gonçalves, B., Balcan, D., Colizza, V., Hu, H., Ramasco, J.J., Merler, S., & Vespignani, A. (2010). Comparing large-scale computational approaches to epidemic modeling: agent-based versus structured metapopulation models. *BMC infectious diseases, 10*(1), 190.

Al-Azzawi, M., & Raeside, R. (2007). Modeling pedestrian walking speeds on sidewalks. *Journal of Urban Planning and Development, 133*(3), 211-219.

Allen, L. J. (2008). An introduction to stochastic epidemic models. In *Mathematical epidemiology* (pp. 81-130). Springer, Berlin Heidelberg, Germany.

Allen, M. P. (2004). Introduction to molecular dynamics simulation. *Computational soft matter: from synthetic polymers to proteins, 23,* 1-28.NIC series.

Alonso-Marroquin, F., Busch, J., Chiew, C., Lozano, C., & Ramírez-Gómez, Á. (2014). Simulation of counterflow pedestrian dynamics using spheropolygons. *Physical Review E, 90*(6), 063305.

Anderson, R. M., Anderson, B., & May, R. M. (1992). *Infectious diseases of humans: dynamics and control.* Oxford University Press. New York, USA.

Andersson, H., & Britton, T. (2012). *Stochastic epidemic models and their statistical analysis* (Vol. 151). Springer Science & Business Media.

Leach, A. R., & Leach, A. R. (2001). *Molecular modelling: principles and applications.* Pearson education.

Baker, M.G., Thornley, C.N., Mills, C., Roberts, S., Perera, S., Peters, J., Kelso, A., Barr, I., & Wilson, N. (2010). Transmission of pandemic A/H1N1 2009 influenza on passenger aircraft: retrospective cohort study. *BMJ, 340,* c2424.

Bansal, S., Read, J., Pourbohloul, B., & Meyers, L. A. (2010). The dynamic nature of contact networks in infectious disease epidemiology. *Journal of Biological Dynamics, 4*(5), 478-489.

Barrat, A., Cattuto, C., Tozzi, A. E., Vanhems, P., & Voirin, N. (2014). Measuring contact patterns with wearable sensors: methods, data characteristics and applications to data-driven simulations of infectious diseases. *Clinical Microbiology and Infection, 20*(1), 10-16.

Barreto, M. L., Teixeira, M. G., & Carmo, E. H. (2006). Infectious diseases epidemiology. *Journal of Epidemiology & Community Health, 60*(3), 192-195.

Barrett, C. L., Bisset, K. R., Eubank, S. G., Feng, X., & Marathe, M. V. (2008). EpiSimdemics: an efficient algorithm for simulating the spread of infectious disease over large realistic social networks. In *SC'08: Proceedings of the 2008 ACM/IEEE Conference on Supercomputing, 15-21 November; Austin, Texas, USA* (pp. 1-12). IEEE.

Basney, J., Livny, M., & Mazzanti, P. (2000). Harnessing the capacity of computational grids for high energy physics. In *Conference on Computing in High Energy and Nuclear Physics, 7-11 February; Padova, Italy* (pp. 610-613).

Baydin, A. G. (2008). Dissipative Particle Dynamics and Coarse-Graining. Chalmers University of Technology (Master's Thesis).

Beeman, D. (1976). Some multistep methods for use in molecular dynamics calculations. *Journal of Computational Physics, 20*(2), 130-139.

Bellomo, N., & Dogbe, C. (2008). On the modelling crowd dynamics from scaling to hyperbolic macroscopic models. *Mathematical Models and Methods in Applied Sciences, 18 (Suppl.* 1), 1317-1345.

Bender, G. (2016). Airport Terminal Security Screening Checkpoints: Still an Industrial Engineering Problem. Retrieved from https://www.arenasimulation.com/blog/post/airport-terminal-security-screening-checkpoints-still-an-industrial-enginee

Berman, F., Wolski, R., Figueira, S., Schopf, J., & Shao, G. (1996). Application-level scheduling on distributed heterogeneous networks. In *Supercomputing'96: Proceedings of the 1996 ACM/IEEE Conference on Supercomputing, 01 January; Pittsburgh, Pennsylvania, USA* (pp. 39-39). IEEE.

Binder, K., Ceperley, D.M., Hansen, J.P., Kalos, M.H., Landau, D.P., Levesque, D., Mueller-Krumbhaar, H., Stauffer, D., & Weis, J. J. (2012). *Monte Carlo methods in statistical physics* (Vol. 7). Springer Science & Business Media, Berlin Heidelberg, Germany.

Bobashev, G. V., Goedecke, D. M., Yu, F., & Epstein, J. M. (2007). A hybrid epidemic model: combining the advantages of agent-based and equation-based approaches. In *2007 Winter Simulation Conference, 9-12 December; Washington, DC, USA* (pp. 1532-1537). IEEE.

Bogoch, I.I., Creatore, M.I., Cetron, M.S., Brownstein, J.S., Pesik, N., Miniota, J., Tam, T., Hu, W., Nicolucci, A., Ahmed, S. & Yoon, J.W. (2015). Assessment of the potential for international dissemination of Ebola virus via commercial air travel during the 2014 west African outbreak. *The Lancet, 385*(9962), 29-35.

Bosmans, S., Maricaux, G., & Van der Schueren, F. (2016). Predictive algorithms for scheduling parameter sweep calculations in a cloud environment. In *International Conference on P2P, Parallel, Grid, Cloud and Internet Computing, 5-7 November; Asan, South Korea* (pp. 789-798). Springer, Cham, Switzerland.

Botelho-Nevers, E., Gautret, P., Benarous, L., Charrel, R., Felkai, P., & Parola, P. (2010). Travel-Related Influenza A/H1N1 Infection at a Rock Festival in Hungary: One Virus May Hide Another One. *Journal of Travel Medicine, 17*(3), 197-198.

Bourouiba, L., Dehandschoewercker, E., & Bush, J. W. (2014). Violent expiratory events: on coughing and sneezing. *Journal of Fluid Mechanics, 745*, 537-563.

Brauer, F., & Castillo-Chavez, C. (1995). Basic models in epidemiology. In *Ecological Time Series* (pp. 410-447). Springer, Boston, MA.

Brenner, D. W. (1990). Empirical potential for hydrocarbons for use in simulating the chemical vapor deposition of diamond films. *Physical Review B, 42*(15), 9458.

Britton, T. (2010). Stochastic epidemic models: a survey. *Mathematical Biosciences, 225*(1), 24-35.

Brookes, D. W., Miah, S., Lackenby, A., Hartgroves, L., & Barclay, W. S. (2010). Pandemic H1N1 2009 influenza virus with the H275Y oseltamivir resistance neuraminidase mutation shows a small compromise in enzyme activity and viral fitness. *Journal of Antimicrobial Chemotherapy, 66*(3), 466-470.

Bruno, L., & Venuti, F. (2008). The pedestrian speed-density relation: modelling and application. *Proceedings of the Third International Conference on Footbridges, 2-4 July; Porto, Portugal* (pp. 255-256). Universidade do Porto, Faculdade de Engenharia, Portugal.

Bruzzone, L., & Marconcini, M. (2009). Domain adaptation problems: A DASVM classification technique and a circular validation strategy. *IEEE transactions on Pattern Analysis and Machine Intelligence, 32*(5), 770-787.

Burke, D. S., Epstein, J. M., Cummings, D. A., Parker, J. I., Cline, K. C., Singa, R. M., & Chakravarty, S. (2006). Individual-based computational modeling of smallpox epidemic control strategies. *Academic Emergency Medicine, 13*(11), 1142-1149.

Burstedde, C., Klauck, K., Schadschneider, A., & Zittartz, J. (2001). Simulation of pedestrian dynamics using a two-dimensional cellular automaton. *Physica A: Statistical Mechanics and its Applications, 295*(3), 507-525.

Caflisch, R. E., & Moskowitz, B. (1995). Modified Monte Carlo methods using quasi-random sequences. In *Monte Carlo and Quasi-Monte Carlo Methods in Scientific Computing* (pp. 1-16). Springer, New York, USA.

Casanova, H., Berman, F., Obertelli, G., & Wolski, R. (2000a). The AppLeS parameter sweep template: User-level middleware for the grid. In *SC'00: Proceedings of the 2000 ACM/IEEE Conference on Supercomputing, 4 - 10 November; Washington, DC, USA* (pp. 60-60). IEEE.

Casanova, H., Legrand, A., Zagorodnov, D., & Berman, F. (2000b). Heuristics for scheduling parameter sweep applications in grid environments. In *Proceedings 9th Heterogeneous Computing Workshop (HCW 2000)(Cat. No. PR00556), 1May; Cancun, Mexico* (pp. 349-363). IEEE.

Epidemiologic Notes and Reports Interstate Importation of Measles Following Transmission in an Airport--California, Washington, 1982. (1983). Retrieved from https://www.cdc.gov/mmwr/preview/mmwrhtml/00000070.htm.

Review of human-to-human transmission of Ebola virus. (2014). Retrieved from http://www. cdc. gov/vhf/ebola/transmission/human-transmission. html.

Ceperley, D. M. (1999). Microscopic simulations in physics. In More Things in Heaven and Earth (pp. 741-751). Springer, New York, NY.

Chandra, S., & Bharti, A. K. (2013). Speed distribution curves for pedestrians during walking and crossing. *Procedia-Social and Behavioral Sciences, 104*, 660-667.

Chattaraj, U., Seyfried, A., & Chakroborty, P. (2009). Comparison of pedestrian fundamental diagram across cultures. *Advances in Complex Systems, 12*(03), 393-405.

Chen, X., Ye, J., & Jian, N. (2010). Relationships and characteristics of pedestrian traffic flow in confined passageways. *Transportation Research Record, 2198*(1), 32-40.

Cheng, L. (2014). Modelling airport passenger group dynamics using an agent-based method. Queensland University of Technology (Doctoral Dissertation).

Chevalier, A., Silva, D.A., Rocklin, G.J., Hicks, D.R., Vergara, R., Murapa, P., Bernard, S.M., Zhang, L., Lam, K.H., Yao, G., & Bahl, C. D. (2017). Massively parallel de novo protein design for targeted therapeutics. *Nature, 550*(7674), 74.

Chopard, B., Dupuis, A., Masselot, A., & Luthi, P. (2002). Cellular automata and lattice Boltzmann techniques: An approach to model and simulate complex systems. *Advances in Complex Systems, 5*(2), 103-246.

Chraibi, M., Seyfried, A., & Schadschneider, A. (2010). Generalized centrifugal-force model for pedestrian dynamics. *Physical Review E, 82*(4), 046111.

Chunduri, S., Ghaffari, M., Lahijani, M. S., Srinivasan, A., & Namilae, S. (2018). Parallel low discrepancy parameter sweep for public health policy. In *2018 18th IEEE/ACM International Symposium on Cluster, Cloud and Grid Computing (CCGRID), 1-4 May; Washington, DC, USA* (pp. 291-300). IEEE.

Clark, R. P., & de Calcina-Goff, M. L. (2009). Some aspects of the airborne transmission of infection. *Journal of the Royal Society Interface, 6* (*Suppl.* 6), S767-S782.

Cook, B. K., & Jensen, R. P. (2002). Discrete element methods: numerical modeling of discontinua. In *Proceedings 3rd International Conference on Discrete Element Method, 23-25 September; Santa Fe, New Mexico* (pp. 355-360). ASCE.

Curtis, S., & Manocha, D. (2014). Pedestrian simulation using geometric reasoning in velocity space. In *Pedestrian and Evacuation Dynamics 2012* (pp. 875-890). Springer, Cham, Switzerland.

Daamen, W., & Hoogendoorn, S. P. (2003). Experimental research of pedestrian walking behavior. *Transportation Research Record, 1828*(1), 20-30.

Das, P., Parida, M., & Katiyar, V. K. (2015). Analysis of interrelationship between pedestrian flow parameters using artificial neural network. *Journal of Modern Transportation*, 23(4), 298-309.

Davidich, M., & Köster, G. (2013). Predicting pedestrian flow: A methodology and a proof of concept based on real-life data. *PloS one, 8*(12), e83355.

Daw, M. S., & Baskes, M. I. (1984). Embedded-atom method: Derivation and application to impurities, surfaces, and other defects in metals. *Physical Review B, 29*(12), 6443.

De Cao, E., Zagheni, E., Manfredi, P., & Melegaro, A. (2014). The relative importance of frequency of contacts and duration of exposure for the spread of directly transmitted infections. *Biostatistics, 15*(3), 470-483.

del Solar, M. R., Boton-Fernandez, M., & Herrero, G. D. (2015). Energetic island design optimization. A case study using sweep parameter search and variable neighborhood search techniques. In *2015 IEEE International Conference on Industrial Technology (ICIT), 17-19 March; Seville, Spain* (pp. 3108-3113). IEEE.

Derjany, P., & Namilae, S. (2017). Effect of pedestrian movement on the spread of infectious diseases during air. In 2017 *Transportation Research Forum, 20-12 April; Chicago, Illinois, USA*.

Derjany, P., & Namilae, S. (2018). Computational Model for Pedestrian Movement and Infectious Diseases Spread During Air Travel. In 2018 *AIAA Modeling and Simulation Technologies Conference, 8-12 January, Kissimmee, Florida* (p. 0419).

Deuker, A. (2008). Del 11.2: Mobility and LBS. *FIDIS Deliverables, 11*(2).

Diekmann, O., & Heesterbeek, J. A. P. (2000). Mathematical epidemiology of infectious diseases: model building, analysis and interpretation (Vol. 5). John Wiley & Sons.

Dingreville, R., Karnesky, R. A., Puel, G., & Schmitt, J. H. (2016). Review of the synergies between computational modeling and experimental characterization of materials across length scales. *Journal of Materials Science, 51*(3), 1178-1203.

Dong, H., Gao, X., Gao, T., Sun, X., & Wang, Q. (2014). Crowd Evacuation Optimization by Leader-follower Model. IFAC Proceedings Volumes, 47(3), 12116-12121.

Dridi, M. H. (2014). Tracking individual targets in high density crowd scenes analysis of a video recording in hajj 2009. *arXiv preprint arXiv:1407.2044*.

Dridi, M. H. (2015). Simulation of high density pedestrian flow: Microscopic model. arXiv preprint arXiv:1501.06496.

Eichner, M., Dowell, S. F., & Firese, N. (2011). Incubation period of Ebola hemorrhagic virus subtype Zaire. *Osong public health and research perspectives, 2*(1), 3-7.

Ellis, D., Sommerlade, E., & Reid, I. (2009). Visual analysis of pedestrian motion. *Technical Report*, 419. University of Oxford, England.

Espanol, P. (2004). Dissipative Particle Dynamics and Other Fluid Particle Models. In Micromechanics and Nanoscale Effects (pp. 213-235). Springer, Dordrecht.

Evans, M. R., Meldrum, R., Lane, W., Gardner, D., Ribeiro, C. D., Gallimore, C. I., & Westmoreland, D. (2002). An outbreak of viral gastroenteritis following environmental contamination at a concert hall. *Epidemiology & Infection, 129*(2), 355-360.

Feig, M., Nawrocki, G., Yu, I., Wang, P. H., & Sugita, Y. (2018, June). Challenges and opportunities in connecting simulations with experiments via molecular dynamics of cellular environments. In *Journal of Physics: Conference Series, International Meeting on "High-Dimensional Data-Driven Science" (HD3-2017)10-13 September, Mielparque Kyoto, Japan* (Vol. 1036, No. 1, p. 012010). IOP Publishing.

Ferguson, N. M., Cummings, D. A., Fraser, C., Cajka, J. C., Cooley, P. C., & Burke, D. S. (2006). Strategies for mitigating an influenza pandemic. *Nature, 442*(7101), 448.

Fishman, G. (2013). *Monte Carlo: concepts, algorithms, and applications*. Springer Science & Business Media.

Foo, H., Blyth, C.C., Van Hal, S., McPhie, K., Ratnamohan, M., Fennell, M., Alawi, F.B., Rawlinson, W., Adamson, S., Armstrong, P., & Dwyer, D. E. (2009). Laboratory test performance in young adults during influenza outbreaks at World Youth Day 2008. *Journal of Clinical Virology*, 46(4), 384-386.

Ford, R. L., & Nelson, W. R. (1978). *EGS code system: computer programs for the Monte Carlo simulation of electromagnetic cascade showers. Version 3* (No. SLAC-R-210). Stanford Linear Accelerator Center, CA (USA).

Fruin, J. J. (1970). Designing for Pedestrians. A Level of Service Concept. Polytechnical Institute of Brooklyn (Doctoral Dissertation).

Fruin, J. J. (1993). The causes and prevention of crowd disasters. *Engineering for crowd safety, 1*(10), 99-108.

Gautret, P., & Steffen, R. (2016). Communicable diseases as health risks at mass gatherings other than Hajj: what is the evidence?. *International Journal of Infectious Diseases, 47*, 46-52.

Germann, T. C., Kadau, K., Longini, I. M., & Macken, C. A. (2006). Mitigation strategies for pandemic influenza in the United States. *Proceedings of the National Academy of Sciences, 103*(15), 5935-5940.

Giesecke, J. (2017). *Modern infectious disease epidemiology*. CRC Press, Boca Raton, Florida, USA.

Goncu, A. (2009). *Monte Carlo and quasi-Monte Carlo methods in financial derivativepricing*. The Florida State University (Doctoral Dissertation).

Greenshields, B. D., Channing, W., & Miller, H. (1935). A study of traffic capacity. In *Highway research board proceedings* (Vol. 1935). National Research Council (USA), Highway Research Board.

GSM Association. (2003). Permanent Reference Document SE. 23: Location Based Services. *Website: http://www. gsmworld. com/documents/lbs/se23. pdf.*

Gundlapalli, A.V., Rubin, M.A., Samore, M.H., Lopansri, B., Lahey, T., McGuire, H.L., Winthrop, K.L., Dunn, J.J., Willick, S.E., Vosters, R.L., & Waeckerle, J.F. (2006). Influenza, winter olympiad, 2002. *Emerging Infectious Diseases, 12*(1), 144.

Guo, B., Fujimura, R., Zhang, D., & Imai, M. (2012). Design-in-play: improving the variability of indoor pervasive games. *Multimedia Tools and Applications, 59*(1), 259-277.

Guo, B., Satake, S., & Imai, M. (2008). Home-Explorer: Ontology-based physical artifact search and hidden object detection system. *Mobile Information Systems, 4*(2), 81-103.

Guo, J. (2018). Accuracy Improvement of Pedestrian Trajectory Prediction by an Extended Kalman Filter and Pedestrian Behavior Classification. Rose-Hulman Institute of Technology (Master's thesis).

Gupta, J. K., Lin, C. H., & Chen, Q. (2009). Flow dynamics and characterization of a cough. *Indoor Air, 19*(6), 517-525.

Halton, J. H. (1960). On the efficiency of certain quasi-random sequences of points in evaluating multi-dimensional integrals. *Numerische Mathematik, 2*(1), 84-90.

Halton, J. H. (1964). Algorithm 247: Radical-inverse quasi-random point sequence. *Communications of the ACM, 7*(12), 701-702.

Han, Y., Li, Q., Wang, F., Wang, B., Mizuno, K., & Zhou, Q. (2019). Analysis of pedestrian kinematics and ground impact in traffic accidents using video records. *International Journal of Crashworthiness, 24*(2), 211-220.

Hankin, B. D., & Wright, R. A. (1958). Passenger flow in subways. *Journal of the Operational Research Society, 9*(2), 81-88.

Healthcare worker who tested positive for Ebola flew on Frontier flight day before getting sick. Sky Talk. 2014. Retrieved from http://blogs.star-telegram.com/sky_talk/2014/10/healthcare-worker-who-tested-positive-for-ebola-flew-on-frontier-flight-day-before-getting-sick.html

Heesterbeek, H., Anderson, R.M., Andreasen, V., Bansal, S., De Angelis, D., Dye, C., Eames, K.T., Edmunds, W.J., Frost, S.D., Funk, S., & Hollingsworth, T. D. (2015). Modeling infectious disease dynamics in the complex landscape of global health. *Science, 347*(6227), aaa4339.

Helbing, D., & Molnar, P. (1995). Social force model for pedestrian dynamics. *Physical Review E, 51*(5), 4282.

Helbing, D., Farkas, I. J., Molnar, P., & Vicsek, T. (2002). Simulation of pedestrian crowds in normal and evacuation situations. *Pedestrian and Evacuation Dynamics, 21*(2), 21-58.

Helbing, D., Farkas, I., & Vicsek, T. (2000). Simulating dynamical features of escape panic. *Nature, 407*(6803), 487.

Henderson, L. F. (1971). The statistics of crowd fluids. *Nature, 229*(5284), 381-383.

Hethcote, H. W. (1989). Three basic epidemiological models. In *Applied Mathematical Ecology* (pp. 119-144). Springer, Berlin, Heidelberg, Germany.

Hollingsworth, S. A., & Dror, R. O. (2018). Molecular dynamics simulation for all. *Neuron*, 99(6), 1129-1143.

Hou, T., Wang, J., Li, Y., & Wang, W. (2010). Assessing the performance of the MM/PBSA and MM/GBSA methods. 1. The accuracy of binding free energy calculations based on molecular dynamics simulations. *Journal of Chemical Information and Modeling, 51*(1), 69-82.

Hyman, J. M., Li, J., & Stanley, E. A. (2003). Modeling the impact of random screening and contact tracing in reducing the spread of HIV. *Mathematical Biosciences, 181*(1), 17-54.

Jaax, N., Jahrling, P., Geisbert, T., Geisbert, J., Steele, K., McKee, K., Nagley, D., Johnson, E., Jaax, G., & Peters, C. (1995). Transmission of Ebola virus (Zaire strain) to uninfected control monkeys in a biocontainment laboratory. *The Lancet, 346*(8991-8992), 1669-1671.

Jia, H., Yang, L., & Tang, M. (2009). Pedestrian Flow Characteristics Analysis and Model Parameter Calibration in Comprehensive Transport Terminal. *Journal of Transportation Systems Engineering and Information Technology*, 9(5), 117-123. doi:10.1016/s1570-6672(08)60082-3.

Jones, R. M., & Brosseau, L. M. (2014). Ebola virus transmission via contact and aerosol—a new paradigm. Center for Infectious Disease Research and Policy, University of Minnesota, Minneapolis, MN. Retrieved from http://www. cidrap. umn. edu/news-perspective/2014/11/commentary-ebolavirus-transmission-contact-and-aerosol-new-paradigm.

Joy, C., Boyle, P. P., & Tan, K. S. (1996). Quasi-Monte Carlo methods in numerical finance. *Management Science*, *42*(6), 926-938.

Judson, S., Prescott, J., & Munster, V. (2015). Understanding ebola virus transmission. *Viruses*, 7(2), 511-521.

Kalakou, S., Moura, F., & Medeiros, V. (2015). Analysis of airport configuration and passenger behaviour. In *Proceedings of the 10th International Space Syntax Symposium, 13-17 July; London, England.*

Kawsar, L. A., Ghani, N. A., Kamil, A. A., & Mustafa, A. (2017). An Improved Speed-Density Relationship Model for Pedestrian Flow. *American Journal of Applied Sciences*, 14(1), 184-203. doi:10.3844/ajassp.2017.184.203.

Keeling, M. J. (1999). The effects of local spatial structure on epidemiological invasions. *Proceedings of the Royal Society of London. Series B: Biological Sciences*, *266*(1421), 859-867.

Keeling, M. J. (2005). Models of foot-and-mouth disease. *Proceedings of the Royal Society B: Biological Sciences*, *272*(1569), 1195-1202.

Keeling, M. J., & Rohani, P. (2008). Modeling infectious diseases in humans and animals. Princeton University Press.

Kenyon, T. A., Valway, S. E., Ihle, W. W., Onorato, I. M., & Castro, K. G. (1996). Transmission of multidrug-resistant Mycobacterium tuberculosis during a long airplane flight. *New England Journal of Medicine*, 334(15), 933-938.

Kermack, W. O., & McKendrick, A. G. (1927). A contribution to the mathematical theory of epidemics. *Proceedings of the royal society of london. Series A, Containing papers of a mathematical and physical character, 115*(772), 700-721.

Kim, E. H., Park, S. J., Kwon, H. I., Kim, S. M., Kim, Y. I., Song, M. S., & Choi, Y. K. (2015). Mouse adaptation of influenza B virus increases replication in the upper respiratory tract and results in droplet transmissibility in ferrets. *Scientific Reports*, 5, 15940.

Kiss, T., Greenwell, P., Heindl, H., Terstyanszky, G., & Weingarten, N. (2010). Parameter sweep workflows for modelling carbohydrate recognition. *Journal of Grid Computing*, 8(4), 587-601.

Knoblauch, R. L., Pietrucha, M. T., & Nitzburg, M. (1996). Field studies of pedestrian walking speed and start-up time. *Transportation Research Record, 1538*(1), 27-38.

Kraal, B., Popovic, V., & Kirk, P. J. (2009). Passengers in the airport: artefacts and activities. In *Proceedings of the 21st Annual Conference of the Australian Computer-Human Interaction Special Interest Group: Design: Open 24/7, 23-27 November; Melbourne, Australia* (pp. 349-352). ACM.

Kretz, T., Lohmiller, J., & Schlaich, J. (2016). The Inflection Point of the Speed-Density Relation and the Social Force Model. In *Traffic and Granular Flow'15* (pp. 145-152). Springer, Cham, Switzerland.

L'Ecuyer, P., & Lemieux, C. (2005). Recent advances in randomized quasi-Monte Carlo methods. In *Modeling uncertainty* (pp. 419-474). Springer, Boston, MA, USA.

Lakoba, T. I., Kaup, D. J., & Finkelstein, N. M. (2005). Modifications of the Helbing-Molnar-Farkas-Vicsek social force model for pedestrian evolution. *Simulation, 81*(5), 339-352.

Lam, W. H., Morrall, J. F., & Ho, H. (1995). Pedestrian flow characteristics in Hong Kong. *Transportation Research Record,* (1487), 56-62.

Lämmel, G., & Plaue, M. (2014). Getting out of the way: Collision-avoiding pedestrian models compared to the realworld. In *Pedestrian and Evacuation Dynamics 2012* (pp. 1275-1289). Springer, Cham, Switzerland.

Last, J. M. (Ed.). (1988). *A dictionary of epidemiology*. Oxford University Press, USA.

Laxman, K. K., Rastogi, R., & Chandra, S. (2010). Pedestrian flow characteristics in mixed traffic conditions. *Journal of Urban Planning and Development, 136*(1), 23-33.

Lennard-Jones, J. E. (1924). On the determination of molecular fields II. From the equation of state of a gas. *Proceedings of the Royal Society of London. Series A, Containing Papers of a Mathematical and Physical Character, 106*(738), 463-477.

Li, Z., & Jiang, Y. (2014). Friction based social force model for social foraging of sheep flock. *Ecological Modelling, 273,* 55-62.

Lin, Y. H., & Chen, C. F. (2013). Passengers' shopping motivations and commercial activities at airports–The moderating effects of time pressure and impulse buying tendency. *Tourism Management, 36,* 426-434.

Lipsitch, M., Cohen, T., Cooper, B., Robins, J. M., Ma, S., James, L., & Fisman, D. (2003). Transmission dynamics and control of severe acute respiratory syndrome. *Science*, 300(5627), 1966-1970.

Liu, X. D., Song, W. G., & Lv, W. (2014). Empirical data for pedestrian counterflow through bottlenecks in the channel. *Transportation Research Procedia, 2*, 34-42.

Ma, W. (2013). Agent-based model of passenger flows in airport terminals. Queensland University of Technology (Doctoral dissertation).

Maheshwaran, M., Ali, S., Siegel, H. J., Hengsen, D., & Freund, R. F. (1999). Dynamic matching and scheduling of a class of independent tasks onto heterogeneous computing systems. In *8th Heterogeneous Computing Systems Workshop (HCW'99)*.

Mangili, A., & Gendreau, M. A. (2005). Transmission of infectious diseases during commercial air travel. *The Lancet*, 365(9463), 989-996.

Mansouri, N., Watelain, E., Jemaa, Y. B., & Motamed, C. (2018). Video-processing-based system for automated pedestrian data collection and analysis when crossing the street. *Journal of Electronic Imaging, 27*(2), 023016.

Marelli, S., Mattocks, G., & Merry, R. (1998). The role of computer simulation in reducing airplane turn time. *Aero Magazine, 1*(1). Retrieved from https://www.boeing.com/commercial/aeromagazine/aero_01/textonly/t01txt.html

Matsuda, H., Ogita, N., Sasaki, A., & Satō, K. (1992). Statistical mechanics of population: the lattice Lotka-Volterra model. *Progress of theoretical Physics, 88*(6), 1035-1049.

Matthews, L., & Woolhouse, M. (2005). New approaches to quantifying the spread of infection. *Nature Reviews Microbiology, 3*(7), 529.

McCarthy, M. (2015). Measles outbreak linked to Disney theme parks reaches five states and Mexico. *BMJ: British Medical Journal (Online)*, 350:h436. doi: https://doi.org/10.1136/bmj.h436

Mehran, R., Oyama, A., & Shah, M. (2009). Abnormal crowd behavior detection using social force model. In *2009 IEEE Conference on Computer Vision and Pattern Recognition, 25 June; Miami Beach, Florida, USA* (pp. 935-942). IEEE.

Mollison, D. (1977). Spatial contact models for ecological and epidemic spread. *Journal of the Royal Statistical Society: Series B (Methodological), 39*(3), 283-313.

Monge, D. A., Pacini, E., Mateos, C., & Garino, C. G. (2018). Meta-heuristic based autoscaling of cloud-based parameter sweep experiments with unreliable virtual machines instances. *Computers & Electrical Engineering, 69,* 364-377.

Morawska, L.J.G.R., Johnson, G.R., Ristovski, Z.D., Hargreaves, M., Mengersen, K., Corbett, S., Chao, C.Y.H., Li, Y., & Katoshevski, D. (2009). Size distribution and sites of origin of droplets expelled from the human respiratory tract during expiratory activities. *Journal of Aerosol Science, 40*(3), 256-269.

Morokoff, W. J., & Caflisch, R. E. (1994). Quasi-random sequences and their discrepancies. *SIAM Journal on Scientific Computing,* 15(6), 1251-1279.

Moser, M. R., Bender, T. R., Margolis, H. S., Noble, G. R., Kendal, A. P., & Ritter, D. G. (1979). An outbreak of influenza aboard a commercial airliner. *American Journal of Epidemiology, 110*(1), 1-6.

Moussaïd, M., Perozo, N., Garnier, S., Helbing, D., & Theraulaz, G. (2010). The walking behaviour of pedestrian social groups and its impact on crowd dynamics. PloS One, 5(4), e10047.

Mustapha, N. A. C., Alam, A. Z., Khan, S., & Azman, A. W. (2015, December). Parametric sweep analysis of medium voltage range boost converter for energy harvester application. In *2015 IEEE International WIE Conference on Electrical and Computer Engineering, 19-20 December; Buet, Dhaka, Bangladesh (WIECON-ECE)* (pp. 1-4). IEEE.

Nagel, K. (1996). Particle hopping models and traffic flow theory. *Physical Review E,* 53(5), 4655.

Naito, Y., Taguchi, M., & Yoden, S. (2003). A parameter sweep experiment on the effects of the equatorial QBO on stratospheric sudden warming events. *Journal of the Atmospheric Sciences, 60*(11), 1380-1394.

Namilae, S., Derjany, P., Mubayi, A., Scotch, M., & Srinivasan, A. (2017b). Multiscale model for pedestrian and infection dynamics during air travel. *Physical Review E,* 95(5), 052320.

Namilae, S., Srinivasan, A., Mubayi, A., Scotch, M., & Pahle, R. (2017a). Self-propelled pedestrian dynamics model: Application to passenger movement and infection propagation in airplanes. *Physica A: Statistical Mechanics and its Applications,* 465, 248-260.

Navin, F. P., & Wheeler, R. J. (1969). Pedestrian flow characteristics. *Traffic Engineering and Control,* 39(9), 30-36.

Nelson, K., Marienau, K., Schembri, C., & Redd, S. (2013). Measles transmission during air travel, United States, December 1, 2008–December 31, 2011. *Travel Medicine and Infectious Disease, 11(2),* 81-89.

Nelson, W. R., Rogers, D. W., & Hirayama, H. (1985). *The EGS4 code system* (No. SLAC-0265).

Nikolić, M., Bierlaire, M., Farooq, B., & de Lapparent, M. (2016). Probabilistic speed–density relationship for pedestrian traffic. *Transportation Research Part B: Methodological,* 89, 58-81.

Nordlund, K., Runeberg, N., & Sundholm, D. (1997). Repulsive interatomic potentials calculated using Hartree-Fock and density-functional theory methods. *Nuclear Instruments and Methods in Physics Research Section B: Beam Interactions with Materials and Atoms, 132*(1), 45-54.

Older, S. J. (1968). Movement of pedestrians on footways in shopping streets. *Traffic Engineering and Control,* 10(4), 160-163.

Olsen, S.J., Chang, H.L., Cheung, T.Y.Y., Tang, A.F.Y., Fisk, T.L., Ooi, S.P.L., Kuo, H.W., Jiang, D.D.S., Chen, K.T., Lando, J., & Hsu, K.H. (2003). Transmission of the severe acute respiratory syndrome on aircraft. *New England Journal of Medicine,* 349(25), 2416-2422.

Osterholm, M. T., Moore, K. A., Kelley, N. S., Brosseau, L. M., Wong, G., Murphy, F. A., & Kapetshi, J. (2015). Transmission of Ebola viruses: what we know and what we do not know. *MBio,* 6(2), 1-9.

Pan, S. J., & Yang, Q. (2010). A survey on transfer learning. *IEEE Transaction on Knowledge Discovery and Data Engineering,* 22 (10), 1-15.

Papineni, R. S., & Rosenthal, F. S. (1997). The size distribution of droplets in the exhaled breath of healthy human subjects. *Journal of Aerosol Medicine,* 10(2), 105-116.

Paquette, S. G., Banner, D., Huang, S. S., Almansa, R., Leon, A., Xu, L., & Kelvin, A. A. (2015). Influenza transmission in the mother-infant dyad leads to severe disease, mammary gland infection, and pathogenesis by regulating host responses. *PLoS Pathogens,* 11(10), e1005173.

Pelechano, N., Allbeck, J. M., & Badler, N. I. (2007). Controlling individual agents in high-density crowd simulation. *In Proceedings of the 2007 ACM SIGGRAPH/Eurographics Symposium on Computer Animation, 2-4 August; San Diego, California, USA (*pp. 99-108). Eurographics Association.

Perez, L., & Dragicevic, S. (2009). An agent-based approach for modeling dynamics of contagious disease spread. *International Journal of Health Geographics, 8*(1), 50.

Pfaff, G., Lohr, D., Santibanez, S., Mankertz, A., Treeck, U. V., Schönberger, K., & Hautmann, W. (2010). Spotlight on measles 2010: Measles outbreak among travellers returning from a mass gathering, Germany, September to October 2010. Retrieved from https://www.eurosurveillance.org/content/10.2807/ese.15.50.19750-en

Pharaon, J., & Bauch, C. T. (2018). The influence of social behaviour on competition between virulent pathogen strains. *Journal of Theoretical Biology*, 455, 47-53.

Polus, A., Schofer, J. L., & Ushpiz, A. (1983). Pedestrian flow and level of service. *Journal of Transportation Engineering*, 109(1), 46-56.

Popovic, V., Kraal, B., & Kirk, P. J. (2010). Towards airport passenger experience models. *In Proceedings of 7th international conference on design & emotion, 4-7 October; Chicago, Illinois, USA.*

Pushkarev, B. (1975). Urban Space for Pedestrians: A Report of the Regional Plan Association: With Jeffrey M. Zupan. MIT Press.

Quercia, D., Lathia, N., Calabrese, F., Di Lorenzo, G., & Crowcroft, J. (2010, December). Recommending social events from mobile phone location data. In *2010 IEEE International Conference on Data Mining, 13-17 December; Sydney, Australia* (pp. 971-976). IEEE.

Rahman, A. (1964). Correlations in the motion of atoms in liquid argon. *Physical Review*, 136(2A), A405.

Rahman, K., Ghani, N. A., Kamil, A. A., & Mustafa, A. (2013). Weighted regression method for the study of pedestrian flow characteristics in Dhaka, Bangladesh. *Modern Applied Science*, 7(4), 17.

Rakowski, F., Gruziel, M., Bieniasz-Krzywiec, Ł., & Radomski, J. P. (2010). Influenza epidemic spread simulation for Poland—a large scale, individual based model study. *Physica A: Statistical Mechanics and its Applications, 389*(16), 3149-3165.

Rand, D. A. (1999). Correlation equations and pair approximations for spatial ecologies. *Advanced Ecological Theory: Principles and Applications*, 100-142. (Online ISBN: 9781444311501)

Rapaport, D. C., & Rapaport, D. C. R. (2004). The art of molecular dynamics simulation. Cambridge University Press.

Rastogi, R., & Chandra, S. (2013). Pedestrian flow characteristics for different pedestrian facilities and situations. *European Transport,* 53(6):1-21.

Regan, J.J., Jungerman, R., Montiel, S.H., Newsome, K., Objio, T., Washburn, F., Roland, E., Petersen, E., Twentyman, E., Olaiya, O., & Naughton, M. (2015). Public health response to commercial airline travel of a person with Ebola virus infection-United States, 2014. MMWR. *Morbidity and mortality weekly report*, 64(3), 63-66.

Riley, R. L., & O'Grady, F. (1961). *Airborne infection: transmission and control*. The Macmillan Company, New York.

Rivers, C. M., Lofgren, E. T., Marathe, M., Eubank, S., & Lewis, B. L. (2014). Modeling the impact of interventions on an epidemic of Ebola in Sierra Leone and Liberia. PLoS Currents, 6. doi: 10.1371/currents.outbreaks.4d41fe5d6c05e9df30ddce33c66d084c

Rocha, L. E., & Masuda, N. (2016). Individual-based approach to epidemic processes on arbitrary dynamic contact networks. *Scientific Reports*, *6*, 31456.

Satō, K., Matsuda, H., & Sasaki, A. (1994). Pathogen invasion and host extinction in lattice structured populations. *Journal of Mathematical Biology*, *32*(3), 251-268.

Satoh, A. (2010). Introduction to practice of molecular simulation: molecular dynamics, Monte Carlo, Brownian dynamics, Lattice Boltzmann and dissipative particle dynamics. Elsevier, London, UK.

Sawyer, W. G., & Tichy, J. A. (2001). Lubrication with granular flow: Continuum theory, particle simulations, comparison with experiment. *Journal of Tribology*, 123(4), 777-784.

Schadschneider, A., & Seyfried, A. (2011). Empirical results for pedestrian dynamics and their implications for modeling. *Networks & Heterogeneous Media*, *6*(3), 545-560.

Schultz, M., Lehmann, S., & Fricke, H. (2006). Pedestrian dynamics in airport terminals considering emergency cases. *Proceedings of 25th International Congress of Aeronautical Sciences (ICAS),3-8 September 2006; Hamburg, Germany.*

Schuss, Z. (2015). *Brownian dynamics at boundaries and interfaces*. Springer-Verlag, New York.

Security Checkpoint Layout Design and Reconfiguration Guide. (2006). Retrieved from https://www.aci-na.org/static/entransit/Checkpoint_Layout_Design_Guide_v1r0-0.pdf

Seyfried, A., Boltes, M., Kähler, J., Klingsch, W., Portz, A., Rupprecht, T., Schadschneider, A., Steffen, B., & Winkens, A. (2010). Enhanced empirical data for the fundamental diagram and the flow through bottlenecks. In *Pedestrian and Evacuation Dynamics 2008* (pp. 145-156). Springer, Berlin, Heidelberg, Germany.

Seyfried, A., Steffen, B., Winkens, A., Rupprecht, T., Boltes, M., & Klingsch, W. (2009). Empirical data for pedestrian flow through bottlenecks. In *Traffic and Granular Flow '07* (pp. 189-199). Springer, Berlin, Heidelberg, Germany.

Sharkey, K. J. (2008). Deterministic epidemiological models at the individual level. *Journal of Mathematical Biology*, 57(3), 311-331.

Sharkey, K. J., Bowers, R. G., Morgan, K. L., Robinson, S. E., & Christley, R. M. (2007). Epidemiological consequences of an incursion of highly pathogenic H5N1 avian influenza into the British poultry flock. *Proceedings of the Royal Society B: Biological Sciences*, 275(1630), 19-28.

Sharkey, K. J., Fernandez, C., Morgan, K. L., Peeler, E., Thrush, M., Turnbull, J. F., & Bowers, R. G. (2006). Pair-level approximations to the spatio-temporal dynamics of epidemics on asymmetric contact networks. *Journal of Mathematical Biology*, 53(1), 61-85.

Shuaib, F., Gunnala, R., Musa, E.O., Mahoney, F.J., Oguntimehin, O., Nguku, P.M., Nyanti, S.B., Knight, N., Gwarzo, N.S., Idigbe, O., & Nasidi, A. (2014). Ebola virus disease outbreak-Nigeria, July–September 2014. *MMWR. Morbidity and Mortality Weekly Report*, 63(39), 867.

Sime, J. D. (1995). Crowd psychology and engineering. *Safety Science*, 21(1), 1-14.

Smieszek, T. (2009). A mechanistic model of infection: why duration and intensity of contacts should be included in models of disease spread. *Theoretical Biology and Medical Modelling*, 6(1), 25.

Smieszek, T., Balmer, M., Hattendorf, J., Axhausen, K. W., Zinsstag, J., & Scholz, R. W. (2011). Reconstructing the 2003/2004 H3N2 influenza epidemic in Switzerland with a spatially explicit, individual-based model. *BMC Infectious Diseases*, 11(1), 115.

Sokolowski, J. A., & Banks, C. M. (Eds.). (2011). Principles of modeling and simulation: a multidisciplinary approach. John Wiley & Sons. Hoboken, New Jersey, USA.

Srinivasan, A., Sudheer, C. D., & Namilae, S. (2016). Optimizing massively parallel simulations of infection spread through air-travel for policy analysis. In *2016 16th IEEE/ACM International Symposium on Cluster, Cloud and Grid Computing (CCGrid), 16-19 May; Cartagena, Columbia* (pp. 136-145). IEEE.

Steiniger, S., Neun, M., & Edwardes, A. (2006). Foundations of location based services. *Lecture Notes on LBS*, *1*(272), 2.

Stiles, J. R., Bartol, T. M., Salpeter, E. E., & Salpeter, M. M. (1998). Monte Carlo simulation of neuro-transmitter release using MCell, a general simulator of cellular physiological processes. In *Computational Neuroscience* (pp. 279-284). Springer, Boston, MA, USA.

Stillinger, F. H., & Weber, T. A. (1985). Computer simulation of local order in condensed phases of silicon. *Physical Review B*, *31*(8), 5262.

Succi, S. (2001). *The lattice Boltzmann equation: for fluid dynamics and beyond*. Oxford University Press. New York, USA.

Tadmor, E. B., & Miller, R. E. (2011). Modeling materials: continuum, atomistic and multiscale techniques. Cambridge University Press. United Kingdom.

Tanaboriboon, Y., & Guyano, J. A. (1989). Level of service standards for pedestrian facilities in Bangkok: A case study. *ITE Journal*, 59(11), 39-41.

Tanaboriboon, Y., Hwa, S. S., & Chor, C. H. (1986). Pedestrian Characteristics Study in Singapore. *Journal of Transportation Engineering*, *112*(3), 229–235. doi: 10.1061/(asce)0733-947x(1986)112:3(229).

Tang, J. W., Li, Y., Eames, I., Chan, P. K. S., & Ridgway, G. L. (2006). Factors involved in the aerosol transmission of infection and control of ventilation in healthcare premises. *Journal of Hospital Infection*, 64(2), 100-114.

Tersoff, J. (1986). New empirical model for the structural properties of silicon. *Physical Review Letters*, *56*(6), 632.

Tersoff, J. (1988a). New empirical approach for the structure and energy of covalent systems. *Physical Review B*, *37*(12), 6991.

Tersoff, J. (1988b). Empirical interatomic potential for silicon with improved elastic properties. *Physical Review B*, *38*(14), 9902.

Tersoff, J. (1989). Modeling solid-state chemistry: Interatomic potentials for multicomponent systems. *Physical Review B*, *39*(8), 5566.

Teunis, P. F., Brienen, N., & Kretzschmar, M. E. (2010). High infectivity and pathogenicity of influenza A virus via aerosol and droplet transmission. *Epidemics*, 2(4), 215-222.

Teunis, P. F., Moe, C. L., Liu, P., E. Miller, S., Lindesmith, L., Baric, R. S., & Calderon, R. L. (2008). Norwalk virus: how infectious is it?. *Journal of Medical Virology*, 80(8), 1468-1476.

Tewarson, A. (2002). Generation of heat and chemical compounds in fires. *SFPE handbook of fire protection engineering*, 3, 83-161. Quincy, Massachusetts.

Thagard, P. (1998a). Ulcers and bacteria I: Discovery and acceptance. *Studies in History and Philosophy of Biological and Biomedical Sciences*, 29, 107-136.

Thagard, P. (1998b). Ulcers and bacteria II: Instruments, experiments, and social interactions. *Studies in History and Philosophy of Biological and Biomedical Sciences*, 29, 317-342.

Timmermans, H. (Ed.). (2009). *Pedestrian behavior: models, data collection and applications*. Emerald Group Publishing Limited. United Kingdom.

Towner, J. S., Rollin, P. E., Bausch, D. G., Sanchez, A., Crary, S. M., Vincent, M., & Kaducu, F. (2004). Rapid diagnosis of Ebola hemorrhagic fever by reverse transcription-PCR in an outbreak setting and assessment of patient viral load as a predictor of outcome. *Journal of Virology*, 78(8), 4330-4341.

Tregenza, P. (1976). The design of interior circulation. Van Nostrand Reinhold. London, United Kingdom.

Treiber, M., Hennecke, A., & Helbing, D. (1999). Derivation, properties, and simulation of a gas-kinetic-based, nonlocal traffic model. *Physical Review E*, 59(1), 239.

Van Landeghem, H., & Beuselinck, A. (2002). Reducing passenger boarding time in airplanes: A simulation based approach. *European Journal of Operational Research*, 142(2), 294-308.

Venkateswara, H., Chakraborty, S., & Panchanathan, S. (2017). Deep-learning systems for domain adaptation in computer vision: Learning transferable feature representations. *IEEE Signal Processing Magazine*, 34(6), 117-129.

Verhoef, L., Duizer, E., Vennema, H., Siebenga, J., Swaan, C., Isken, L., Koopmans, M., Balay, K., Pothier, P., McKeown, P., & Van Dijk, G. (2008). Import of norovirus infections in the Netherlands and Ireland following pilgrimages to Lourdes, 2008–preliminary report. *Eurosurveillance*, 13(44), 19025.

Verlet, L. (1967). Computer" experiments" on classical fluids. I. Thermodynamical properties of Lennard-Jones molecules. *Physical Review*, 159(1), 98.

von Sivers, I., Templeton, A., Künzner, F., Köster, G., Drury, J., Philippides, A., Neckel, T., & Bungartz, H.J. (2016). Modelling social identification and helping in evacuation simulation. *Safety Science*, 89, 288-300.

Voronoi, G. (1908). Nouvelles applications des paramètres continus à la théorie des formes quadratiques. Premier mémoire. Sur quelques propriétés des formes quadratiques positives parfaites. *Journal Für die Reine und Angewandte Mathematik, 133*, 97-178.

Vynnycky, E., & White, R. (2010). *An introduction to infectious disease modelling.* Oxford University Press. New York, USA.

Wald, A., Harmon, M., & Klabjan, D. (2014). Structured deplaning via simulation and optimization. *Journal of Air Transport Management, 36*, 101-109.

Wang, B., Zhang, A., Sun, J. L., Liu, H., Hu, J., & Xu, L. X. (2005). Study of SARS transmission via liquid droplets in air. *Transactions of the ASME-K-Journal of Biomechanical Engineering*, 127(1), 32-38.

Wang, L., Wu, Y., Deng, Y., Kim, B., Pierce, L., Krilov, G., Lupyan, D., Robinson, S., Dahlgren, M.K., Greenwood, J., & Romero, D.L. (2015). Accurate and reliable prediction of relative ligand binding potency in prospective drug discovery by way of a modern free-energy calculation protocol and force field. *Journal of the American Chemical Society, 137*(7), 2695-2703.

Wang, S., Min, J., & Yi, B. K. (2008). Location based services for mobiles: Technologies and standards. In *IEEE International Conference on Communication (ICC, 19-23 May;* Beijing, China (Vol. 19).

Weidmann, U. (1993). Transporttechnik der Fußgänger-Transporttechnische Eigenschaften des Fußgängerverkehrs (Literaturauswertung)(Schriftenreihe des IVT No. 90). *ETH Zürich.(Second Edition, in German).*

Wei-Guo, S., Yan-Fei, Y., Bing-Hong, W., & Wei-Cheng, F. (2006). Evacuation behaviors at exit in CA model with force essentials: A comparison with social force model. *Physica A: Statistical Mechanics and its Applications*, 371(2), 658-666.

Widdowson, M. A., Glass, R., Monroe, S., Beard, R. S., Bateman, J. W., Lurie, P., & Johnson, C. (2005). Probable transmission of norovirus on an airplane. *JAMA, 293*(15), 1855-1860.

Wiersma, L. C., Kreijtz, J. H., Vogelzang-van Trierum, S. E., van Amerongen, G., van Run, P., Ladwig, M., & Osterhaus, A. D. (2015). Virus replication kinetics and pathogenesis of infection with H7N9 influenza virus in isogenic guinea pigs upon intratracheal inoculation. *Vaccine*, 33(49), 6983-6987.

Wilson, M. E. (1995). Travel and the emergence of infectious diseases. *Emerging Infectious Diseases*, *1*(2), 39-46.

Yang, B. (2005). Stress, strain, and structural dynamics: an interactive handbook of formulas, solutions, and MATLAB toolboxes. Academic Press. United Kingdom.

Youn, C., & Kaiser, T. (2010). Management of a parameter sweep for scientific applications on cluster environments. *Concurrency and Computation: Practice and Experience*, *22*(18), 2381-2400.

Yu, H., Liao, Q., Yuan, Y., Zhou, L., Xiang, N., Huai, Y., & Gao, Z. (2010). Effectiveness of oseltamivir on disease progression and viral RNA shedding in patients with mild pandemic 2009 influenza A H1N1: opportunistic retrospective study of medical charts in China. *BMJ*, 341, c4779.

Yuen, K. Y., & Wong, S. S. Y. (2005). Human infection by avian influenza A H5N1. *Hong Kong Medical Journal*. 11, 189-199.

Zanlungo, F., Ikeda, T., & Kanda, T. (2011). Social force model with explicit collision prediction. EPL (Europhysics Letters), 93(6), 68005.

Zaremba, S. K. (1968). The mathematical basis of Monte Carlo and quasi-Monte Carlo methods. *SIAM Review*, *10*(3), 303-314.

Zębala, J., Ciępka, P., & RezA, A. (2012). Pedestrian acceleration and speeds. *Probl. Forensic Sci.*, *91*, 227-234.

Zhang, J., & Seyfried, A. (2013). Empirical characteristics of different types of pedestrian streams. *Procedia Engineering*, *62*, 655-662.

Zhang, J., Klingsch, W., Rupprecht, T., Schadschneider, A., & Seyfried, A. (2011). Empirical study of turning and merging of pedestrian streams in T-junction. *arXiv preprint arXiv:1112.5299*.

Zhao, G. P. (2007). SARS molecular epidemiology: a Chinese fairy tale of controlling an emerging zoonotic disease in the genomics era. *Philosophical Transactions of the Royal Society B: Biological Sciences*, *362*(1482), 1063-1081.

Zhu, J., Chen, S., Tu, W., & Sun, K. (2019). Tracking and Simulating Pedestrian Movements at Intersections Using Unmanned Aerial Vehicles. *Remote Sensing*, *11*(8), 925.

Ziegler, J. F., & Biersack, J. P. (1985). The stopping and range of ions in matter. In *Treatise on heavy-ion science* (pp. 93-129). Springer, Boston, MA, USA.

Zieliński, A. (2009). Evidence for excessive incidence of infectious diseases at mass gatherings with special reference to sporting events. *Przegląd Epidemiologiczny*, 63(3):343-351.

APPENDICES

Literature survey of pedestrian density vs speed data and equation descriptions

References	Speed-density relation	Notes
Greenshields (1935)	$S = -a.D' + b$ where: D': density a, b: constants for the fitting line	Data collected by photographic method on a roadway section to monitor the traffic capacity.
Older (1968)	$v(k) = v_f - \theta.k$	
Navin (1969)	$v(k) = v_f - \theta.k$ where: v_f: free flow speed k: density θ: parameter	
Fruin (1970)	$S = \dfrac{a.M - b}{M}$ where: $M = 1/\rho$, ρ : density a, b: constants for the fitting curve	Uses level Of service (LOS) concept.
Pushkarev (1975)	$v = -\alpha.k + \beta$	The author incorporates previous work for the various pedestrian types.
Tregenza (1976)	$v_e = v_f \cdot \exp\left(-\left(\dfrac{k}{\theta}\right)^\gamma\right)$	
Polus (1983)	$v = -\alpha.k + \beta$	Video Data collected in the central business district of Haifa, Israel.
Tanaboriboon (1986)	$v(k) = v_f - \theta.k$	Bidirectional pedestrian data from sidewalks in Singapore using a photographic technique.
Tanaboriboon (1989)	$v = -\alpha.k + \beta$	Videographic data on pedestrian traffic in four walkways in Central Bangkok. The linear model represented the best fit.
Weidmann (1993)	$v = v_m \left[1 - e^{-\gamma\left(\frac{1}{u} - \frac{1}{u_M}\right)}\right]$ Where: v_m: free pedestrian speed γ : fitting free parameter U_M : maximum admissible density	

Lam (1995)	$v(k) = v_f - \theta.k$ where: v_f: free flow speed k: density θ: parameter	
Tewarson (2002)	$v(k) = v_f - \theta.k$	
Al-Azzawi (2007)	$\ln S = \alpha \ln V - \beta \ln D + \varepsilon$ Where: S: speed V: volume or flow D: density ε : random noise (constant) α, β: constants	Pedestrian movement on sidewalks in the United Kingdom. to develop speed, flow, and density relationships.
Bruno (2008)	Kladek non-linear formula Weidman (1993): $v = v_m \left[1 - e^{-\gamma \left(\frac{1}{u} - \frac{1}{u_M} \right)} \right]$	The study estimates the v_m, γ and u_M in Kladek formula taking into account various factors that have influence on the density-velocity relation such as age, culture, gender, travel purpose, type of infrastructure, walking direction represented in parameters α and β
Hongfei (2009)	$v = -\alpha.k + \beta$	Data collected in Chinese passenger transport terminal-Xizhimen underground station using video recording.
Laxman (2010)	$v = -\alpha.k + \beta$	Data collected at four locations in a medium-sized city of India and a metropolitan city in India.
Chen (2010)	Level passageway: $v = 75.267.D.e^{-\frac{1}{2}\left(\frac{D}{1.534}\right)^2}$ Ascending stairway: $v = -0.917D^3 - 1.234D^2 + 36.166D$ Descending stairway: $v = -0.12D^3 - 7.74D^2 + 46.754D$ Two-way stairway: $v = -0.161D^3 - 9.113D^2 + 46.698D$	Confined level passageways, ascending stairways, descending stairways, and two-way stairways in Shanghai, China, Metro stations with massive passenger volumes were observed.

Rahman (2013)	$v = \alpha - \beta.k + e$ Linear formula with addition of e, a random error term due to stochastic variations.	Data collected from three different locations in Dhaka. Pedestrian speed-flow-density relationships are predicted using a weighted regression method.
Rastogi (2013)	$v(k) = v_f .\exp\left(-\frac{k}{\theta}\right)$	Data collected from five cities in India.
Das (2015)	$U = U_f - \left(\frac{U_f}{k_j}\right) k$ $U = U_f\, e^{\frac{-k}{k_m}}$ where: U_f: free flow speed k_j: jam density k_m: optimum density	From speed-density relation, the Greenshield (1935) and Underwood (1961) models were fitted to determine the parameters U_f, k_j and k_m. The study describes bidirectional flow characteristics on sidewalks and carriageways around transport terminals in India.
Kretz (2016)	$v(\rho) = v_0 - (1 - \lambda)\,\dfrac{\tau A}{e^{\frac{1}{B\rho}}-1}$ where: v_0: the desired speed of pedestrian (the same for all pedestrians) $A>0$, $B>0$, $0\leq\lambda\leq1$, $\tau>0$ are appropriately chosen values	Derived from the Social Force Model for Steady-States in Single-File Movement.
Nikolić (2016)	$v_e = v_f .e^{-\left(\frac{k}{\theta}\right)^{\gamma}}$ where: v_e : equilibrium speed v_f : desired velocity θ, γ: pedestrian specific parameters k: density	Derived from the microscopic social force model proposed by Helbing and Molnar (1995). Tragenza model (1976) Two datasets: Pedestrian underpass at Lausanne train station and a controlled experiment at the Technical University of Delft.

Journal Publications

1. Derjany, P., Namilae, S., Liu, D., & Srinivasan, A. Parameter space exploration and uncertainty quantification of viral outbreak. *(In preparation)*.

2. Derjany, P., Namilae, S., Liu, D., & Srinivasan, A. Multiscale Model for Optimal Design of Pedestrian Queues to Mitigate Infectious Disease Spread. *Plos One (In Review)*.

3. Namilae, S., Derjany, P., Mubayi, A., Scotch, M., & Srinivasan, A. (2017). Multiscale model for pedestrian and infection dynamics during air travel. *Physical Review E, 95*(5), 052320.

Conference Publications

4. Pugh, N., Derjany, P., Namilae, S., Liu, D., & Park, H. Deep Adaptive Learning for Safe and Efficient Navigation of Pedestrian Dynamics – Airport Evacuation. *Transportation Research Board, 2020 (Submitted)*.

5. Derjany, P., Namilae, S., & Liu, D. (2019). Multiscale Pedestrian Dynamics and Infection Spread Model for Policy Analysis. *CATM University Transportation Center Symposium, 4 November; Daytona Beach, Florida, USA*.

6. Derjany, P., Namilae, S., Liu, D., & Srinivasan, A. Computational Modeling Framework for the Study of Infectious Disease Spread through Commercial Air-Travel. *2020 IEEE Aero Conference, 7-14 March; Big Sky. (Accepted)*.

7. Namilae, S., Mubayi, A., Srinivasan, A., & Derjany, P. (2018). Model Based Policy Analysis for Infection Spread during Air Transportation. *International Conference of Transportation and Health, 24-27 June; Michigan, USA*.

8. Namilae, S., Derjany, P., Liu, D., Mubayi, A., & Srinivasan, A. (2018). Multiscale Pedestrian Dynamics and Infection Spread Model for Policy Analysis. *Proceedings of the 9th International Conference on Pedestrian and Evacuation Dynamics (PED2018), 21-24 August; Lund, Sweden.*

9. Derjany, P., Namilae, S., Mubayi, A., & Srinivasan, A. (2018). Computational Model for Pedestrian Movement and Infectious Diseases Spread During Air Travel. *AIAA SciTech Forum and Exposition, 8-12 January; Kissimmee, Florida, USA.*

10. Derjany, P., Namilae, S., Seong, Y., & Liu, D. (2017). Modeling the Fundamental Diagram of Pedestrian Motion using Social Force Approach. *5th Annual UTC conference for the South Eastern Region, 16-17 November; Gainesville, Florida, USA.*

11. Derjany, P., Namilae, S., Seong, Y., & Liu, D. (2017). Modeling the Fundamental Diagram of Pedestrian Motion using Social Force Approach. *CATM University Transportation Center Symposium, 17 October; North Carolina, USA.*

12. Derjany, P., Namilae, S., Mubayi, A., Scotch, M., & Srinivasan, A. (2017). Molecular Dynamics Like Numerical Approach for Studying Infection Propagation. *International conference on composites Engineering ICCE, 16-22 July; Rome, Italy.*

13. Derjany, P., Namilae, S., Mubayi, A., Scotch, M., & Srinivasan, A. (2017). Multiscale pedestrian movement - infection dynamics model for transportation hubs. *Transportation Research Forum, 20-21 April, Chicago, Illinois, USA.*